GEORG-AUGUST-UNIVERSITÄT
GÖTTINGEN

Analysis of the organization and signaling capacity of the membrane IgE during its interaction with CD19 and CD23 in B lymphocytes

Dissertation
for the award of the degree
"Doctor rerum naturalium"
of the Georg-August-Universität Göttingen

within the doctoral program Molecular Medicine
of the Georg-August University School of Science (GAUSS)

submitted by
Christina Kerntke

from Aschaffenburg, Germany

Göttingen, 2021

Thesis Committee:

Prof. Dr. Jürgen Wienands
Institute for Cellular and Molecular Immunology, University Medical Center, Göttingen

Prof. Dr. Michael Thumm
Department of Cellular Biochemistry, University Medical Center, Göttingen

Prof. Dr. Matthias Dobbelstein
Institute of Molecular Oncology, University Medical Center, Göttingen

Dr. Niklas Engels
Institute for Cellular and Molecular Immunology, University Medical Center, Göttingen

Members of the Examination Board:
Referee: **Prof. Dr. Jürgen Wienands**
Institute for Cellular and Molecular Immunology, University Medical Center, Göttingen

2nd Referee: **Prof. Dr. Michael Thumm**
Department of Cellular Biochemistry, University Medical Center, Göttingen

Further members of the Examination Board

Prof. Dr. Matthias Dobbelstein
Institute of Molecular Oncology, University Medical Center, Göttingen

Prof. Dr. Lutz Walter
Department of Primate Genetics, German Primate Center Göttingen

Prof. Dr. Michael P. Schön
Clinic für Dermatology, Venerology und Allergology, University Medical Center Göttingen

Prof. Dr. mult. Thomas Meyer
Department of Hematology and Oncology, University Medical Center Göttingen

Date of oral examination: 21st of July 2021

Acknowledgements

First, I would like to sincerely thank Prof. Jürgen Wienands for giving me the opportunity to conduct my PhD in his lab and thus enabling my little journey through the cosmos of B cells. I would also like to thank Dr. Niklas Engels for the interesting project, being my supervisor and for proof-reading my dissertation.
Furthermore, I would like to acknowledge the members of my thesis committee, Prof. Michael Thumm and Prof. Matthias Dobbelstein for their valuable scientific feedback and advice during our committee meetings.

Special thanks to Ines Heine and Gabi Sonntag for their outstanding technical support, helpfulness, and the positivity, brightening up the days in the lab. Ines, you always offered me a helping hand with casting countless SDS-PAGEs or adding Doxycycline to my cells in the early hours. I could always count on you, thank you so much! My heartfelt thanks also to Anika Schindler, for her organizational support and patience.

Thanks to all former and current members of the Institute for Cellular and Molecular Immunology – you all made and make the daily lab-life as versatile, open and friendly as it is. Alina, Carolina, Florian, Jakob, Jan, Jens, Kristin, Matthias, Saed, Stela, Swantje and Vanessa, thank you for the great time throughout the years in and outside the lab, including barbecues, Flammkuchen all-you-can-eat or “Feierabend-Glühwein” at the Christmas market.
My special thanks to Matthias, Stela and Jens, who were my office and trusty bench mates introducing me to the lab and helping to figure out and get through the early stages of my PhD. Thank you for the fun, relaxed office hours, the helpful discussions and for sharing experiences in the lab. Carolina, it was a pleasure sharing the office with you. Thank you for sharing your chocolate supplies and I will miss the joyful talks with you.

Nadine, thank you for being a wonderful friend, for your never-ending encouragement and cheerfulness offering me relief and distraction especially in times I needed it the most. Thank you for your friendship!

Most of all, I would like to thank my parents and brother for their unconditional love, immeasurable faith and encouragement to do my best. You are my pillar of strength and made this possible. Christian, you are my King of the written word and I thank you so much for proof-reading my thesis. Thank you, Yuri, for being by my side throughout the last three years. You are my oasis of warmth and comfort.

Table of Contents

I Abstract

The predominant allergy type I (hypersensitivity reaction type I) poses an increasing health issue in industrialized countries over the last decades. A key mediator in the pathogenesis of hypersensitivity or allergic diseases is IgE and its interaction with the IgE-specific FcεRI. This makes IgE a promising target for the treatment of allergic disorders. Currently, immunotherapies of patients with severe allergies are based on neutralizing soluble IgE, which inhibits the IgE-FcεRI association. This strategy, however, does not target IgE that is already bound, which is why the therapy has to be performed on a regular basis. Therefore, studies about IgE synthesis and its regulation are of great importance. In vivo studies of the biology of IgE, however, are difficult not only because of the scarcity of IgE+ B cells but also due to the difficulty to identify IgE+ B cells, since serum IgE also binds to FcεRs expressed on all B cells. The development of transgenic mouse models in the last decade, though, enabled the identification of mIgE-expressing B cells and their further functional analysis. By analyzing murine and human mIgE-BCRs in B cell lines, this thesis focused on its interaction with the B cell co-receptor CD19 and the IgE-specific receptor CD23.

Previous studies, using murine in vitro B cell models, proposed that the murine mIgE-BCR appears to regulate the terminal differentiation of IgE-switched B cells into plasma cells in an autonomous way. In particular, CD19 appeared to play an essential role in this context, which implied a direct interaction with the murine mIgE-BCR. The first task of this thesis was to test this interaction. Despite the application of exactly the same affinity-purification approach, which was the base for the reported mIgE-CD19 interaction, such receptor interaction could not be revealed. The same could be observed through a more specified approach. The data presented herein hint to unspecific interactions between the used affinity-matrix and CD19, which might have falsified the reported interaction. Alternatively, the interaction between murine mIgE and CD19 may require additional, unknown intermediates not expressed in my cellular model system.

Studies about the regulation of IgE are essential especially in regard to the potentially life-threatening impact of IgE in anaphylactic reactions. A crucial factor in the regulation of IgE expression is CD23, as studies on transgenic mouse models lacking or overexpressing CD23 have shown. This study reveals an association between the human mIgE-BCR isoforms and CD23, which appears to significantly inhibit the surface expression of the mIgE isoform, mIgE-S. In particular, basis for the inefficient surface expression of mIgE-S appears to be an impaired assembly of the Igα/Igβ heterodimer with mIgE as a result from the mIgE-CD23 assocation. The reduced surface expression of mIgE-BCR was accompanied by significantly hampered Ca^{2+} signaling, observed in co-expression of CD23. Similar observations could be made in a human B cell model, expressing IgE in more physiological amounts by using its endogenous IgE heavy chain promotor.

II Introduction

II.1 The Immune system at a glance

During the immune system of vertebrates has developed to a complex defense system that provides reliable protection of the host from a variety of pathogens in the environment. Pathogenic microbes themselves are constantly evolving and threaten the host with a broad range of pathologic mechanisms [1]. Thus, a multitude of defense mechanisms is needed to efficiently recognize and eliminate such invading organisms. These mechanisms are based on a broad range of innate and adaptive defense reactions. Their common feature is the discrimination between self and nonself, which is essential for the subsequent elimination of the respective pathogen without injuring own tissue, also referred to as self-tolerance [1],[2]. Any failure in this ability can result in variants of autoimmune diseases, a subject that has been extensively worked on over the past decades. Thus, the innate as well as the adaptive immune system have developed specific procedures to avoid false reactions against the host's own cells and tissues [3].

II.1.1 The innate immune system

When it comes to host-pathogen interaction it is the innate immune system that is the earliest and most prevailing defense against pathogens [4]. It comprises physical barriers to provide an effective immune border between the internal and external environment. Such barriers are the epidermal surface of the skin with its sweat and sebaceous glands as well as the lysozyme rich saliva in the oral cavity. Additionally, the secreted mucus overlaying the epithelium in the respiratory and gastrointestinal tract, reproductive tract as well as the ears and nose traps dirt particles and microorganisms and support their removal [5].

Besides the physical barrier there are also effective defenses built up by a variety of proteins. These may be either soluble and permanently expressed in endogenous fluids like complement proteins, defensins or ficolins [6],[7],[8]. Alternatively, they may be released by cells upon activation (e.g. cytokines and chemokines) which induce the inflammation and attract leukocytes to the site of infection [3],[4].

An essential property of the innate immune system is the recognition and binding of pathogen typical patterns also referred to as pathogen-associated molecular patterns (PAMPs) [9]. These are, for instance, bacterial and fungal cell-wall structures like lipopolysaccharides (LPS), glycolipids, peptidoglycan (PGN), lipoteichoic acids (LTA) [10],[11] or viral nucleic acids [12]. The detection of PAMPs is mediated by pattern-recognition receptors (PRRs) that are encoded in the host's germline DNA. They are present on a large variety of cells and induce inflammatory responses as part of the innate but also adaptive host defense [2],[13],[14],[12]. Due to this dominant presence, an immediate

defense reaction can be initiated by the innate immune system after the encounter of infiltrating pathogens [3].

II.1.2 The Adaptive Immunity

In contrast to the innate immune system, the adaptive immune system has developed a high specificity for individual pathogenic molecules, collectively termed antigens. Main cellular components of the adaptive immune system are lymphocytes, which can be separated into two main lineages. T lymphocytes, whose maturation site is the thymus [15],[16], and B lymphocytes, which emerge in the bone marrow from hematopoietic stem cells and constitute the source of antibody producing plasma cells [17]. After completion of their developing processes in the primary lymphoid organs, i.e. the thymus and bone marrow, B and T cells migrate to secondary lymphoid organs like the lymph nodes or the spleen, where the actual adaptive immune reactions take place [18]. Antigens, either circulating or bound by antigen - presenting cells (APC), are gathered there and recognized by the B and T cells. The antigen identification is based on antigen-specific receptors found on the cell surface of lymphocytes known as T cell and B cell antigen receptors, respectively [3],[17]. They are the result of a precise selection from a large array of germline - encoded gene elements that have undergone rearrangement processes upon antigen encounter. This assembly of individual antigen receptors facilitates the setup of a broad and highly specific antigen repertoire [19].

Upon antigen encounter, B and T cells become activated and subsequently can differentiate to effector cells: B lymphocytes differentiate to antibody producing cells, called plasma cells, whereas T lymphocytes form subsets with regulatory or cytotoxic functions [15],[20]. Eventually, the effector T cells enter the circulation to reach the site of infection and implement their effector functions. The lymphocyte trafficking is enabled by a repertoire of chemokines and adhesion molecules [15], [21]. An exceptional feature of the adaptive immune system is its capability to develop an immunologic memory for pathogens that persists even after the pathogen has been cleared. This immunological memory is maintained by so-called memory lymphocytes, which develop in a primary response and subsequently remain in an inert state, ready to get re-activated after the reencounter of the same pathogen. This immunologic memory allows a more efficient defense in the event of re-infection with recurrent pathogens [18],[22],[23].

The innate and adaptive immune systems are considered to be the two separate branches of the general, host's immune defense. However, it is their complementary interplay which results in an effective pathogen defense. The innate immune system as the first barrier

provides immediate defense measures against pathogenic agents, which are resumed after several days of clonal expansion of antigen specific B and T cells by the adaptive immune system [1],[3].

II.2 The little cosmos of B lymphocytes

II.2.1 The discovery of Immunoglobulins and B Lymphocytes

Since their discovery in the mid-1960s to early 1970s [24], [25], [26] , B lymphocytes have inspired and challenged the intellectual and experimental skills of natural scientists. B cells, also known as bursal or bone marrow derived lymphocytes can be defined as a cell population with a huge diversity of pathogen-specific antigen-receptors on their surface. In fact, their evolutionary history can be retraced back to the beginning of the development of the adaptive immune system in vertebrates, more than 500 million years ago [27],[28]. Behring and Kitasato et al. were the first to detect antitoxins (later known as Immunoglobulins) against diphtheria and tetanus [29]. It was the electrophoretic analysis of serum globulin [30] and the subsequent identification of antibodies as γ-globulins that marked the first milestone on the path of discovering antibody producing plasma cells [25]. This was further verified by Coons et al. [26] using immuno-fluorescence microscopy. At that point, the discovery of B lymphocytes was practically inevitable, resulting primarily from the almost coincidental discovery of the immunoglobulins (Igs).

By applying innovative approaches for cell surfaces analysis or animal model systems M. Cooper and R. Good were the first to discover T and B lymphocytes simultaneously [24], [25], [26]. Both identified the chicken bursa and the thymus as essential sources for the immunologic competence of two distinct cell populations (i.e. T and B cells) of the adaptive immune defense. Shortly after, studies were published that elucidated the circumstances for B cell differentiation to antibody producing plasma cells [30], [31], [32].

The structure and function of Igs have been investigated for more than a century. In general, Igs include two functions: first, they serve as cell-surface receptors for antigens on B cells, enabling cell survival, -signaling and –activation. Second, they exist as soluble molecules that can specifically recognize and bind an unlimited range of antigens. This capability of Igs to recognize individual antigen structures is based on a variety of complex processes, which modify or rearrange the DNA of developing B lymphocytes, a process termed somatic recombination or V(D)J recombination [33].

II.2.2 V(D)J-Recombination and Class - Switch - Recombination

About 15% of the leukocytes in the peripheral blood are B cells, which are characterized by the production of antigen-binding proteins i.e. Igs [3]. Typically, Igs have a heterodimeric structure and consist of two identical heavy (IgH) and two identical light (IgL) chains. The IgL locus encodes for both a κ or λ light chain, whereas the expressed IgL chain only expresses either chain type. The IgH and IgL chains can be further divided into a N-terminal variable (V) domain and a C-terminal constant (C) region [34].

Main function of the V domains of both IgH and IgL chains is the recognition and binding of antigens. The adaptability of the Ig V domains to the various antigen structures is based on a gene rearrangement process called V(D)J-recombination [35]. From the genetic point of view, the V domains of the IgH locus are composed of V(variable), D(diversity) and J(joining) gene segments, whereas the V domains of the IgL locus are only encoded by V and J segments. These gene segments exist as multiple copies on the chromosome and their incidental recombination to complete VDJ-segments (or VJ-segments respectively) is the basis for the huge repertoire of antigen specificities in Igs.

The V domains further contain three sequences of high variability; the so-called complementary-determining regions (CDRs), where these targeted mutation processes take place. Usually, the CDRs of the IgH and IgL form the antigen-binding portion and differ among Igs [33].

The C domains of the IgH chain determine the Ig specific effector functions like e.g. the interaction with Ig-specific receptors. In the mammalian IgH locus, the CH regions are encoded by various exon clusters located downstream of the V domain coding segments in the order Cμ, Cδ, Cγ, Cε and Cα (Fig. 1, upper panel) [32], These segments represent five distinct Ig isotypes: IgM, IgD, IgG, IgE and IgA [36] [37] [33]. Each of the indicated Ig variants has its own specific effector functions. Upon the first antigen-encounter, B cells mainly react with the production of IgM, which is important to combat the pathogen. In order to enable the immune system to accomplish defense responses, which are more specific for a pathogen, Ig class-switching recombination (CSR) takes place (Fig.1). This molecular process results in class-switching to a different Ig isotype. CSR is initiated by the enzyme activation-induced cytidine deaminase (AID), which is exclusively expressed in antigen-activated B cells [36],[31],[38],[37]. The AID is a single strand DNA (ssDNA) specific cytidine deaminase and belongs to the RNA/DNA editing enzyme family APOBEC. It converts cytosine (C) to uracil (U) by deamination [31],[39],[37]. This deamination reaction occurs at highly repetitive, GC-rich DNA segments, so-called switch (S) regions that are located upstream (2-10 kb) of each C_H gene segment (except for Cδ, that directly adjoins Cμ) [37].

The Cytosine deamination is recognized as base damage or U:G mismatch, therefore inducing either a base excision repair (BER) or a mismatch repair (MMR) process [36],[31]. During these repair mechanisms, double strand breaks are introduced between the S regions of Cμ and another selected C_H segment (Cγ, Cε or Cα). This is followed by the excision of intervening segments and NHEJ of the two target S regions, resulting in a “switch” of the expressed Ig isotype [31],[40],[41].

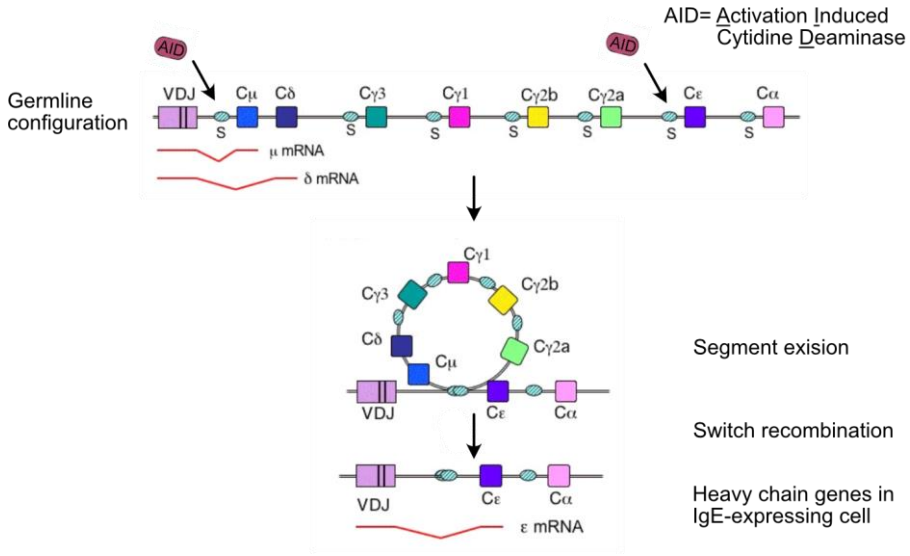

Figure 1: Schematic illustration of immunoglobulin class switch recombination (CSR) to the ε locus
DNA repair mechanisms are induced by introduction of base pair mismatches in the switch regions of the μ locus and ε locus by AID. These events culminate in double strand breaks followed by excision of intervening segments and non-homologous end-joining (NHEJ) of the two target switch regions. (adapted from [185])

In summary, V(D)J recombination and CSR both represent highly specific recombination processes, that extend the repertoire of Ig effector functions with enhanced antigen-specificities and -affinities and therefore increase the efficiency of the immune response [31],[40].

II.2.3 The B cell antigen receptor and its antigen-induced signaling

Igs also exist in a membrane-bound form (mIg) on the surface of B cells and serve as an indispensable part of the B cell antigen receptor (BCR), which ensures the positive selection of developing B cells as well as the survival and activation of mature B cells [42] [43] [44]. The existence of Igs as membrane anchored antitoxins had already been proposed by P. Ehrlich more than a hundred years ago [45],[46]. Referring to the findings of Behring and Kitasato et al. [29], he suggested that these antitoxins could be ascribed to cells carrying receptors specific for toxic antigens. He assumed that, upon binding to antigens, these cells

would produce more of these antitoxins carrying the same antigen specificity as the receptors on the respective cell [47] [41]. This idea was also addressed by Burnet in his clonal selection theory [48].

According to the prevalent model, the BCR is defined as a symmetric transmembrane multiprotein complex. It contains a mIg molecule that is non-covalently associated to a heterodimer of two subunits Igα and Igβ (also referred to as CD79a and CD79b) via its membrane – proximal CH domain and its transmembrane (TM) domain[49] [50] [43]. This is also important for the efficient transport of the BCR complex from the endoplasmic reticulum (ER) to the cell surface [50] [44] [51] [52]. B cells carry BCRs on their cell surfaces that recognize and bind the respective antigens subsequently inducing intracellular signaling pathways. How antigen-binding actually initiates these processes is still being discussed [53]. The cross-linking model (CLM) served as an initial explanation. According to this model, the BCRs are distributed as monomers on the surface on resting B cells and are cross-linked by multivalent antigens. This would lead to the activation of intracellular signaling pathways [54]. Yang and Reth however reported about an intrinsic ability of the BCR to form oligomers on the surface of resting B cells and that their opening to monomers resulted in B cell activation [55] [56]. Based on these observations, Yang and Reth proposed the dissociation activation model. Results gained with various methods like super resolution microscopy or Fab-based proximity ligation assay (Fab-PLA) supported this hypothesis [57],[58].

Whereas antigens are bound by the V domains of the BCR, the Igα/Igβ-heterodimer acts as an essential signaling subunit and initiates the subsequent intracellular pathways upon antigen-binding [39] [51] [59]. The cytoplasmic tail of Igα as well as Igβ contains an immunoreceptor tyrosine based activation motif (ITAM) with the consensus sequence $D/ExxD/Ex_7YxxI/Lx_7YxxI/L$ that plays an important role for BCR signaling [60] [61]. Profound analysis has shown that this motif is interacting with various signaling components [42] [62] [63]. The encounter and specific binding of an antigen by the BCRs lead to the activation of protein tyrosine kinases (PTKs) like the Src kinase Lyn and the spleen tyrosine kinase Syk. Lyn is responsible for the phosphorylation of the tyrosine residues of the ITAMs, which then form docking sites for the SH2 domains of Syk [64],[65]. This leads to Syk's subsequent recruitment to the BCR [53],[66],[67],[68]. Upon Syks' phosphorylation, it recruits the adapter protein SLP-65, also referred to as BLNK [66] [67] [69]. This, in turn induces the formation of the calcium Ca^{2+} initiation complex consisting of Bruton's tyrosine kinase (BTK) and phospholipase C-γ2 (PLCγ) [70]. Once activated PLCγ cleaves phosphatidylinositol-4, 5-bisphosphate (PIP2) into the second messengers inositol-1,4,5-trisphosphate (IP_3) and membrane-bound diacylglycerol (DAG). By binding of the IP_3 receptor (IP_3R) in the ER, IP_3 mediates the Ca^{2+} discharge into the cytosol. This leads to a rapid increase of the Ca^{2+}

concentration in the intracellular compartment and its binding to Calmodulin. Ca^{2+}-bound Calmodulin subsequently activates the phosphatase Calcineurin that dephosphorylates and therefore activates the transcription factor NFAT. Eventually, NFAT enters the nucleus inducing B cell activation and differentiation [71] [72] [53]. In contrast, the second messenger DAG remains at the plasma membrane and directly interacts with Ras guanine nucleotide release protein (RasGRP). Consequently, this leads to the activation of the ERK/MAPK pathway that induces several downstream signaling processes ending in the activation of another essential transcription factor nuclear factor kappa of activated B-cell (NF-κB). NF-κB subsequently translocates to the nucleus inducing the expression of BCL-2 or Cyclin D and contributing to the survival and proliferation of the cell [73] [74] [75].

Beside the described pathways, the network of all BCR signaling pathways comprises numerous other sub-processes that contribute to survival, cell death, proliferation or differentiation [56] [57] [76].

II.2.4 Examples of BCR co-receptors and their impact on the BCR signaling

Antigen-binding alone is not sufficient to induce B cell signaling. A combination of positive regulators, i.e. co-receptors such as CD19 or CD21 [77] [78] [79] and costimulatory receptors such as CD40, is required [80] [81].

CD19 is a B cell specific co-receptor that is expressed by B cells in various developmental stages and amplifies BCR signaling [27],[82]. For instance, cross-linking of CD19 with the BCR reduces the internalization of the BCR, which happens upon antigen uptake and B cell activation, and therefore reduces the BCR activation threshold [83] [84] [85]. This property could also be observed for CD19 when forming a multi-protein complex together with the complement receptor CD21 (CR2) and CD81 in the plasma membrane of B cells. This BCR co-receptor complex binds and responds to complement-tagged antigens, which has been shown to significantly enhance the BCR signaling [86] [85]. CD19 is the primary signaling component in this complex: it is phosphorylated and functions as an adapter protein recruiting effector molecules like Lyn and phosphoinositide-3 kinase (PI3K) [86] [75] [79] [87]. Moreover, analysis of CD19 deficient murine B cells showed a defective immune response to membrane-bound antigens and an impaired antibody production. This observation highlighted the importance of CD19 for B cell function [88].

Other co-stimulatory signals originate from the CD40 receptor that is expressed on the B cell surface. Its engagement with the CD40 ligand (CD40L), expressed on activated CD4 T cells, provides fundamental signals for the initiation of subsequent responses of B cells most protein antigens [81] [80].

II.2.5 Plasma-cell differentiation and antibody production

The majority of B cells circulate through the lymphatic system where they encounter antigens and become activated as the result of a combination of signals as outlined above. Upon activation, B cells can develop in two ways: either, they start to proliferate and develop into short-lived plasma cells that produce low-affinity antibodies, which are mostly of the isotype IgM, Alternatively, a fraction of the activated B cells enter lymphoid follicles of the spleen and lymph nodes and generate so called germinal centers (GC) [17] [27]. A GC is a transient microenvironment and is the main site where the humoral immune response occurs, that is, for instance, the constant increase of the Ig antigen specificity and affinity [89]. Those B cells develop into long-living antibody secreting plasma cells and memory B cells that maintain the protection against pathogens and also extend the antigen affinity of antibodies upon reinfection [90] [89] [91].

A process taking place in the GC is the CSR, which changes the production of IgM to other isotypes like IgG, IgE and IgA. Thus, this process enables an adaption of the Ig effector functions that are needed to eliminate the respective pathogen [92] [41]. For instance, IgG – as the predominant Ig isotype in the organism with the longest serum half-life among all Ig isotypes – performs essential tasks like the antibody-dependent cellular cytotoxicity (ADCC) during which IgG-coated antigens activate effector cells such as natural killer (NK) cells or monocytes. These cell types are responsible for the elimination of the IgG-bound targets.

IgA is mainly found in the mucosal tissue and its secretions. Its main function is the protection of this tissue segment from toxins, viruses and bacteria [93] [87] [94]. IgE, in contrast, shows the lowest serum concentration and the shortest half-life. Due to the low quantity of IgE^+ B cells in the circulation it is still challenging to analyze and visualize them, which is the reason why some of their cell-typical properties are still subject for research.

II.2.6 The discovery of the 5th Ig isotype and its role in allergy

C. Prausnitz and H. Küstner have first reported about the passive transfer of allergen-specific response in the skin via serum [95] [96]. Subsequently, K. Ishizaka, G. Johnsson and H. Bennich identified the allergy-responsible molecule in the late 60s as the 5th Ig isotype, IgE [97] [98]. From all known Ig classes, IgE is the least abundant one and is tightly regulated. Its average serum concentration is 50-200ng/ml and the serum half-life is about 2 days in humans (for comparison: IgG and IgA have a serum concentration of about 3-10 mg/ml on average with a serum half-life of 3 weeks for IgG and 6 days for IgA) [99] [100] [101]. In fact, the minute quantity of serum IgE reflects the amount of B cells, which have undergone the class switching to the Ig ε – HC locus.

Compared to other Igs, IgE is mainly restricted to tissues of the mucosa, alveoli or the gastrointestinal tract. It is likely that IgE has evolved in order to contribute to the first immune defense against parasitic infections like helminths or ambient substances such as venoms or toxins. Today IgE is best known for its role as a key mediator in the pathogenesis of hypersensitivity or allergic diseases (such as asthma or atopic dermatitis), especially with regard to the dramatic increase of allergic diseases over the last decades [102] [99] [103]. An IgE-mediated allergic reaction is complex and involves various cell types, different molecules and inflammatory mediators [104]. In regards to the first encounter of an allergen, activated B cells undergo CSR to IgE and develop to IgE-secreting plasma cells. Subsequently, the majority of secreted IgE is irreversibly bound to the high-affinity IgE-specific receptor FcεRI that is constitutively expressed on mast cells and basophils. In contrast to soluble IgE, FcεRI-bound IgE can persist for several weeks or months, which results in the sensitization of mast cells and basophiles [101] [105]. Upon second encounter of the same allergens the IgE-FcεRI complex binds to them, leading to mast cell activation. This quickly culminates in the degranulation of highly inflammatory mediators such as histamine and the de novo syntheses of other allergic mediators like leukotriene and prostaglandin. These mediators are responsible for immediate allergy symptoms [99] [104] [106].

Regarding the essential role of the IgE-FcεRI complex in mediating allergic responses, IgE represents a promising target for the treatment of allergic disorders. For quite some time, the only therapy against such diseases was the treatment with anti-histamines or cortisol, since it was difficult to identify therapeutics that could block IgE effects [96] [52] [107]. In vivo studies of IgE production and regulation were hampered not only because of the scarcity of IgE^+ B cells and plasma cells but also because of the difficulty to identify IgE^+ B cells, since serum IgE also binds to FcεRs expressed on all B cells [100]. To find suitable methods for the treatment of severe allergic disorders, the focus was on the neutralization of soluble IgE. This resulted in the clinical development of monoclonal humanized anti-IgE antibodies like Omalizumab [99] that binds and neutralizes serum IgE with high affinity and thus inhibits its interaction with FcεRI. To date, Omalizumab is applied in cases of allergic asthma and chronic spontaneous urticaria [108] [109] [107] [110].

While soluble IgE attracted more attention over the last decades, not in the least because of its central role in allergic disorders, many functions of the membrane-bound form of IgE (mIgE) still need further research.

II.2.7 The obscure IgE-switched B cell

The mIgE shows a molecular structure similar to other mIg isotypes and is part of the BCR complex together with the signaling subunits Igα and Igβ on the B cell surface [102] [44] [111]. In contrast to its soluble form, mIgE consists of two to three additional structural elements encoded by two additional exons termed M1 and M2. The transmembrane domain is stabilizing the receptor and is involved in the interaction with Igα/β. Of note is also the cytoplasmic domain and the extracellular membrane-proximal domain (EMPD) consisting of 52 amino acids and located between the transmembrane domain and the last constant Ig domain (CH4) [102]. The human mIgE-BCR, unlike the murine one, is expressed in two isoforms (Fig. 2) that result of alternative splicing events in the penultimate M1 exon in the ε heavy chain transcript [112] [113] [114]. The main difference between these two isoforms is the presence of the EMPD [115]. The resulting mIgE isoforms are referred below as the long (EMPD+) mIgE (mIgE-L) and short (EMPD-) mIgE (mIgE-S). The reasons for the benefits of two mIgE isoforms in the human organism are still unclear. For instance, Zhang et al. [112] and Peng et al. [113] reported a greater expression of mIgE-L in IgE^+ B cells, whereas Vanshylla et al. [116] described a greater abundancy of mIgE-S in comparison to the long isoform. In addition, according to the latter paper, the EMPD functions as an ER retention domain, restricting the surface expression of mIgE-L BCR in human B cells. Furthermore, the EMPD appears to function as a receptor intrinsic inhibitory domain that additionally hampers the intracellular signaling capacity of mIgE-L [116].

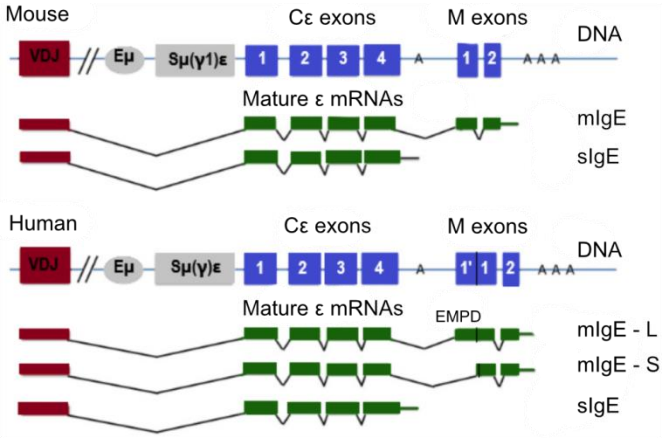

Figure 2: Model of the mouse and human mature IgE transcripts
The ε locus comprises four exons, each encoding an Ig-like domain. The transmembrane domain, the EMPD and the cytoplasmic tail are encoded by the two membrane (M1+ M2) exons. The M1 exon in humans carries additional 5′ DNA sequences (M1′) that encode for 52 extra amino acids in the EMPD. Alternative splicing events in this region result in a short or long EMPD, while mouse IgE has only a short EMPD. mIgE and secreted IgE are generated through the use of different polyadenylation sites (A) and alternative splicing. The internal polyadenylation site for secreted IgE has a consensus signal, while three atypical polyadenylation sites are located downstream of the M exons. Inefficiency in 3′ polyadenylation leads to preferential production of soluble IgE in IgE B cells. Eμ: enhancer of IgM; Sμ(γ1)ε and Sμ(γ)ε : switch (S) regions of the IgM, IgG or IgE gene locus ; (adapted from He et al. 2015)

The expression of IgE requires previous CSR to the ε locus. The switching to IgE happens during T cell-dependent immune responses and requires the cytokines IL-4 and IL-13 as well as CD40 [117]. IL-4 and IL-13 act through transcription factors like the signal transducer and activator of transcription 6 (STAT 6), which synergizes via the transcription factor NF-κB and promotes the Cε germline transcription [118] [119] [117]. Also the ligand for CD40 (CD40L), which is transiently expressed on antigen-stimulated T cells promotes the IgE class switching through NF-κB [120] .

However, how class switching to IgE occurs is still a subject of in-depth discussions. Currently, there are two pathways of CSR to IgE proposed in literature: the “direct” switching from IgM to IgE and the “sequential” or indirect pathway occurring from IgM to an IgG1 intermediate and eventually to IgE [117] [100]. Both pathways have been reported and discussed by several groups, but details regarding direct and indirect switching of the IgE isotype are not clear yet [121] [122] [123] [124]. For instance, according to Talay et al. [125], serum IgE originates from both IgE^+ memory cells that develop into plasma cells and $IgG1^+$ memory B cells, which undergo sequential CSR first, before differentiating to plasma cells. Similar findings were reported by He et al. [123]: IgE^+ GC B cells develop from direct switching, whereas IgE^+ plasma cells originate from sequential switching. Another hypothesis was presented by Erazo et al. [124]: studying immunized mice, they suggest that direct switching to IgE is connected to a very short GC phase with barely any interaction with the T-cell zone. The latter one is important for the support of B cell maturation and Ig affinity maturation. These switched IgE^+ B cells differentiate into plasma cells and rapidly leave the GC, displaying a minimal level of mutation with low allergen affinity. In contrast, the production of high-affinity IgE can be attributed to indirect switching through high-affinity $IgG1^+$ cells, which have already undergone affinity maturation in the GC [124] [126].

Whether a B cell switches directly or sequentially to IgE might be influenced by several factors [100]. For instance, the IgE switch region (Sε) is the shortest Ig switch region with the fewest nucleotide repeats [127] [128]. These usually form target motifs for the AID. The low number of these repeats likely hampers the binding of AID necessary for the induction of CSR [129] [32] [128]. For instance, Misaghi et al [130] could show that the replacement of the core Sε region by the larger Sμ region in mice resulted in an increased IgE production. This might be due to a preferential direct class switching to IgE rather than to IgG1. How the length of the Sε region exactly impacts direct class switching to IgE in physiological conditions remains to be clarified. Additionally, Sε is more distant from Sμ than Sγ1, which results in a more likely recombination with the Sγ1 than with the Sε [128]. Hence, the size, the sequence as well as the accessibility of the switch regions might have an important impact on how or whether IgE class switching occurs.

II.2.8 mIgE as a critical mediator of IgE-responses in vivo

The scarcity of IgE^+ B cells made the functional analysis of this cell population challenging. However, the development of genetic mouse models in the last decade enabled their identification and further functional analysis [122]. In this context, it was reported that the selective deletion or alteration of mIgE domains like the transmembrane- or cytoplasmic domain results in a widely deficient production of serum IgE *in vivo*. This further, emphasizes the importance of mIgE surface expression in primary IgE responses [100] [121]. Two other studies, using a murine *in vitro* B cell model, showed that the murine mIgE-BCR appears to regulate the terminal differentiation fate of IgE-switched B cells to antibody producing plasma cells in an antigen-independent or autonomous way [131] [132]. Among the various BCR signaling adapter molecules examined, CD19 stood out as essential, since the antigen-independent plasma cell differentiation was completely abrogated in CD19 deficient B cells *in vitro* [131]. Additionally, Haniuda et al. [133] observed an abundant co-purification of mIgE with CD19 in contrast to mIgM or mIgG1. This suggests a direct interaction between CD19 and the murine mIgE-BCR, through which CD19 is being recruited to activate the downstream signaling of the mIgE-BCR. This process finally facilitates plasma cell differentiation.

Notably, it remains unclear whether the human mIgE orthologue possesses a similar autonomous signaling activity. Currently, no data suggesting the opposite, exits.

In summary, these studies reveal that the mIgE-BCR is an essential determinant in the differentiation fate of IgE-switched B cells and the production of soluble IgE. With regard to its role in hypersensitivity reactions it appears reasonable to assume that the mIgE expression might be tightly regulated. The low-affinity IgE-specific receptor, also referred to as FcεRII or CD23, takes part in such regulatory processes. Further details regarding its role in the regulation of IgE will follow.

II.2.9 Principles of the IgE-specific Receptor CD23

FcεRII or CD23 is an IgE-specific receptor and was first discovered in B cells [103]. Membrane-bound CD23 is a type II trans-membrane glycoprotein. The CD23 structure consists of three identical, extracellular, C-type lectin-like, IgE-binding “head” domains that are connected to a glycosylated coiled-coil stalk, followed by a short trans-membrane domain and ending in a N-terminal cytoplasmic domain [102] [103] [132]. Human and murine CD23 exists in two isoforms CD23a and CD23b that are the result of alternative splicing events due to two transcription initiation sites in the CD23 gene and only differ in the first 6-7 N-terminal amino acids in the cytoplasmic domain [103] [134] [135]. In humans, CD23a is constitutively expressed on B cells [103] [136] [132], whereas in mice this isoform can also be found on

Follicular Dendritic Cells (FDCs) [137] [138]. In contrast to CD23a, the CD23b expression is usually upregulated by stimuli like IL-4 and IL-13 or the engagement of CD40 in B cells[137] [139] [140]. CD23b is expressed in FDCs or gut epithelial cells in mice and on a variety of hematopoietic cells like monocytes or eosinophils in humans [136].

It is reported that both isoforms seem to have different functions: CD23a is involved in cell survival and endocytosis of IgE-immune complexes (IC) and facilitates the presentation of allergen fragments to T-cells *in vivo* and *in vitro*. Functions of CD23b include IgE-mediated phagocytosis and regulation of cell proliferation [132] [141] [135].

Besides its expression on the cell surface fragments of CD23 are released into the circulation as soluble, IgE-binding proteins of different size and oligomeric state by proteolytic cleavage in the stalk of CD23. For this to occur, proteolytic activity is needed, originating from the disintegrin and metalloproteinase 10 (ADAM10) [142] [143] [144]. Its necessity for the cleavage of CD23 became apparent in human and murine B cell lines that were unable to express ADAM10. Accordingly, these cells exhibited an abrogated release of CD23 [144],[145],[146].

Compared to FcεRI, CD23 is often referred to as the “low-affinity” receptor, since its affinity for IgE is much lower [147] [148]. However, CD23 is a homotrimer and therefore can enhance the IgE-affinity to a level comparable to that of FcεRI [132] [149] [150]. The induced signaling processes, upon ligand-binding to these receptors, differ from each other: while binding of FcεRI results in mast cell degranulation, cross-linking of CD23 has a huge versatile impact on the IgE production in B cells [114] [116] [102].

II.2.10 Regulation of IgE synthesis by CD23

The interaction between CD23 and IgE occurs between the head domains of CD23 and the Cε3 domain of IgE-Fc, showing a 2:1 stoichiometry: i.e. two head domains of CD23 bind to the Cε3 domains in IgE with very little contribution of the Cε4 domain [151]. The IgE-CD23 interface is composed of several salt-bridges and hydrogen bonds. There is also a reciprocal prevention of a simultaneous binding of IgE to FcεRI and CD23. This is brought about by the position of the respective binding sites for FcεRI or CD23 opposite to each other at the Cε3 domain of IgE and due to allosteric mechanisms induced by the interaction with any of the IgE specific receptors. In this context, the interaction between CD23 and the Cε3 results in a conformational change, which makes the FcεRI binding site inaccessible and vice versa [152], [153].

In addition to IgE, CD23 interacts with other ligands like CD21 [154] [134]. CD21 is a complement receptor that binds antigen-bound complement protein C3d [79] [155]. It is expressed on B cells, FDCs and activated T cells. Its binding to CD23 in soluble or

membrane-bound form may occur in activated B cells resulting in extraordinary homotypic adhesions [132].

The most common function of CD23 is its role as a regulator of IgE production and –expression. Currently, there exist two models describing the regulatory mechanisms where CD23 is involved in [102] [140] (Fig. 2): these models feature the engagement of CD23 as a positive and negative regulator of the IgE synthesis depending on the given IgE concentrations. In this regard, provided that a high soluble IgE concentration exists, the cross-linking of CD23 and mIgE by IgE-allergen complexes leads to a negative regulation of the IgE-synthesis [140],[156]. Since this inhibitory effect could not be observed for soluble IgE, the cross-linking of CD23 is assumed to be, in fact, mandatory for the subsequent negative regulation of the IgE-synthesis [157].

The negative regulative role of CD23 on IgE production could also be observed in several studies with transgenic mice. CD23 deficient mice exhibited an enhanced production of antigen-specific IgE after immunization with antigen-adjuvants [142]. Of note is that the development of both B and T cells is independent of CD23 expression since their maturation was broadly normal in CD23 knock-out mice [158] [142]. In contrast, mice that over-expressed CD23 showed decreased levels of IgE titer and a significant reduction of the IgE-production upon treatment with antigen-adjuvants, comparing to wt mice [149] [150]. In addition, cross-linking of CD23 by IgE-ICs appeared to reduce proliferation and plasma cell differentiation of B cells in response to BCR cross-linking and treatment with IL-4 or Staphylocuccus aureus Cowan I *in vitro* [156] [159]. The inhibitory effect of CD23 on the IgE synthesis can also be achieved by the application of anti-CD23 antibodies on CD23 [148] [160]. In fact, it has been reported that the binding of CD23 by soluble IgE or anti CD23 has a stabilizing impact on the surface expression of CD23, preventing the cleavage by ADAM10 [140] [161]. Consequently, it is assumed that, low soluble IgE concentrations result in the release of soluble CD23 which in turn promotes the IgE-synthesis through cross-binding with mIgE and CD21 [157] [154] [162].

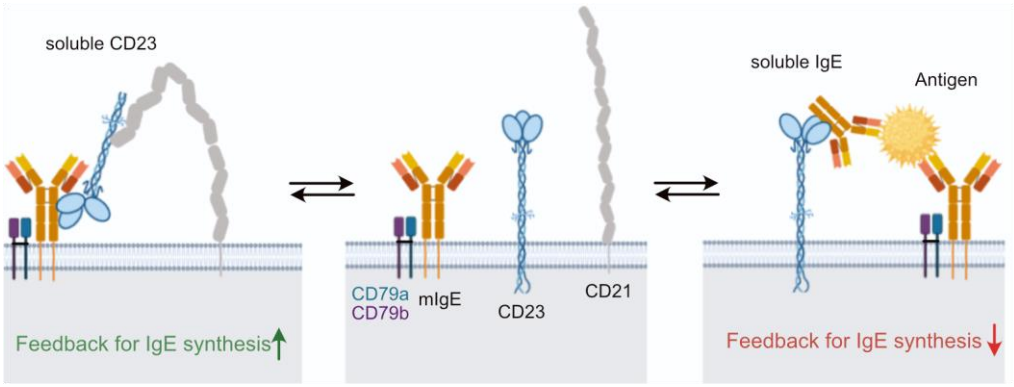

Figure 3: Models for the regulation of the cellular IgE synthesis
CD23 appears to have a bilateral role in the up- or downregulation of the IgE synthesis depending on the present IgE concentration. In this regard, a high concentration of soluble IgE results in cross-linking of mCD23 and mIgE by IgE-Allergen complexes leading to a negative regulation of the IgE-synthesis and proliferation [140],[156]. In contrast, low amounts of soluble IgE diminish the stability of CD23, leading to its cleavage by ADAM10. Finally, the resulting soluble CD23 supports the IgE-synthesis through cross-binding with mIgE and CD21. (modified from [102])

So far, the extent of soluble CD23's involvement in the positive or negative regulation of the IgE synthesis is not yet fully known. However, several studies report on the impact of soluble CD23 in regards to the up- or downregulation of the IgE production in stimulated B cells depending on their given oligomerization state and thus their IgE-affinity. Trimeric soluble CD23 shows a ten times higher IgE-affinity [103] and enhances the IgE-production via cross-linking to the complement receptor CD21. In contrast, monomeric soluble CD23 showing a comparatively lower IgE affinity as trimeric CD23, inhibits this interaction and thus diminishes the IgE-synthesis [148] [157] [145] [162].

In summary, in reference to several studies [157] [143] [142] [163], CD23 in its soluble and membrane bound form seems to have an significant impact on the IgE synthesis, which makes it a promising target for the development of therapeutics.

II.2.11 Aims of this study

Even though the role of IgE has been extensively studied in Immunobiology and allergic pathogenesis, details regarding the regulatory processes and other interaction partners controlling the IgE expression and its functionality are still mostly unknown. Several reports are suggesting that additional cell surface receptors have a regulative impact on the mIgE-BCR functionality.
In my PhD project, I investigated the receptor-receptor interactions of the murine and human mIgE-BCRs with the B cell surface molecules CD19 and CD23.

Published studies reported on an abundant interaction of CD19 with the murine mIgE-BCR [131] [133]. I intended to test these reported findings by establishing a murine cell model expressing the murine mIgE-BCR and CD19 and subsequently analyze the mIgE-CD19 interaction.

Most proposed models describing the regulative impact of CD23 on IgE expression presume a condition where at least one component is available in a soluble form (Fig. 3). The question arises if also a regulatory process between CD23 and IgE exists in case of them being co-expressed on the cell surface. Therefore, another focus of my thesis is on the investigation of the regulatory impact of CD23 on the expression and signaling of the human mIgE-BCRs. Using different human B cell models, expressing the human mIgE-BCRs as well as CD23, I intend to provide answers to the following questions:

1) How does mIgE interact with CD23?
2) Does this interaction have an impact on the expression of the human IgE-BCR isoforms?
3) Does CD23 have a regulatory impact on the functionality of the human IgE-BCRs?

III Materials and Methods

III.1 Materials

III.1.1 Chemicals, Commercially acquirable substances and Consumables

Table 1: List of Consumables and solutions

Consumables	Company
Agarose universal	Peqlab
Albumin Fraction V	Roth
β-Mercaptoethanol	PanReac Aplichem
Blue Prestained Protein Standard, Broad Range	New England Biolabs
Bromphenolblue	Roth
Capture Select – LC lambda (mouse) Affinity Matrix	Thermo Fischer Scientific
Cell culture equipment (pipettes, tubes, culture dishes)	Greiner Bio-one
Cytofix Fixation Buffer	BD
Doxycycline	Clonetech
Ethanol	Roth
GeneRuler™ 1 kb DNA ladder	Thermo Fischer Scientific
dATPs	NEB
dNTPs	NEB
FCS	PAA
FACS Clean FACS Flow	BD
FACS tubes	Sarstedt
Filtropur filters 0,2µm	Sarstedt
Glycerin (86%)	Roth
Hexadimethrine Bromide (Polybrene)	Sigma
Hydrogen Peroxide 30%	Roth
Hygromycine	InvivoGen

Immersion oil	Merck
Indo1-AM	Invitrogen
IPTG (Isopropyl-β-D-thiogalactopyranosid)	Sigma
Luminol sodium salt	Sigma
Methanol	Roth
Microscope paper	neoLab
Neubauer improved counting chamber	Brand
Nitrocellulose membrane Hybond ECL™	GE Healthcare
4-Hydroxy-3-iodo-5-**ni**tro**p**henylacetyl (NIP) -BSA-Biotin	
NP-40 (IGEPAL CA-630)	Sigma-Aldrich
p-Coumaric acid	Sigma
Phosflow Perm Wash Buffer I	BD
Pluronic F127 powder	Sigma
Prestained Protein Marker, Broad Range (6.5-175 kDa)	New England Biolabs
Protease Inhibitor Cocktail (P2714)	Sigma
Protein AG-Agarose	Santa Cruz Biotechnology
Puromycin	InvivoGen
Sodium Pyruvat 100mM	Gibco
Syringe (5ml, 10ml, 20ml)	BD
Rotiporese Gel 30 (Acrylamidmix)	Roth
RPMI 1640 (+Glutamax)	Gibco
Streptavidin-sepharose Beads	GE Healthcare
TransIT®-293 Transfection Reagent	Mirus
TRIS	Roth
Trypsin/EDTA (0.05 %)	Gibco
Tween 20	Roth
Whatman Filter (folded)	GE Healthcare
Whatman Gel Blotting Paper	GE Healthcare

X-gal (5-bromo-4-chloro-3-indolyl-beta-Dgalacto-pyranoside)	Roth

III.1.2 Buffers and Solutions

All chemicals and reagents used in this work were purchased from Carl Roth, Sigma, Merck or Invitrogen unless categorically specified. The Buffers as well as the solutions have been prepared with pure water.

Table 2: List of used buffers and composed solutions

Buffer/Solution	Composition
Acid Buffer	85 mM NaCL, 5mM KCl, 10mM EDTA, 50mM Na-Acetat; ph: 4,0
1X Blotting buffer	39 mM Glycine, 48 mM Tris, 0.0375% (w/v) SDS, 0.01% (w/v) NaN3, 20% (v/v) Methanol, add. ddH2O
Blocking solution	10% BSA, 0.001% NaN3, add. 1X TBST
1X Tris buffer saline with tween (TBST)	20 mM Tris pH 7.6, 137 mM NaCl, 0.1% tween-20, add. ddH2O
Enhanced chemiluminiscence (ECL) (Solution A)	200 ml 0.1 M Tris pH 8.6, 50 mg luminol
ECL solution B	50 ml DMSO, 55 mg para-hydroxycoumaric acid
FACS – Buffer	PBS, 2% FCS, 0,1 % NaN_3
1X Krebs ringer solution	140 mM NaCl, 4 mM KCl, 10 mM D-glucose, 10 mM HEPES pH 7.4, separate addition of 1 mM $CaCl_2$
2X Laemmli buffer	62.5 mM TrisHCL pH 6.8, 2% SDS, 20% glycerol, 5% β-Mercaptoethanol, 0.025% bromophenolblue, add. ddH2O
NP-40 (B cell) Lysis Buffer	137.5 mM NaCl, 50 mM Tris pH 7.8, 1 mM, Na3VO4, 0.5 mM EDTA pH 8.0, 10% glycerol, 1X protease inhibitor cocktail, 1% NP-40 detergent, add. ddH2O

10% Resolving gel SDS-PAGE	375 mM Tris pH 8.8, 0.1% SDS, 10% Acrylamide and bisacrylamide, 0.00065% APS, 0.001% TEMED, add. ddH2O
5% Stacking gel SDS-PAGE	125 mM Tris pH6.8, 0.1% SDS, 5% Acrylamide and bisacrylamide, 0.001% APS, 0.001% TEMED, add. ddH2O
1X SDS-PAGE running buffer	25 mM Tris, 192 mM glycine, 0.1% (w/v) SDS, add. ddH2O
1X Tris acetate EDTA (TAE)	40 mM Tris-acetate pH8.0, 10 mM NaOAc, 1 mM EDTA, add. ddH2O

III.1.3 Commercial Kits

Table 3: Commercially available Kits

Reaction systems	Application	Company
TA Cloning® Kit	Cloning	Invitrogen
QIAprep® Spin Miniprep	Plasmid-DNA purification	Qiagen
Wizard® Plus SV Minipreps DNA Purification System	Plasmid-DNA purification	Promega
Pure Yield™ Plasmid Midiprep System	Plasmid-DNA purification	Promega
Wizard® SV Gel and PCR Clean-Up System	PCR clean-up, gel extraction	Promega

III.1.4 Mammalian Celllines

J558L:

This cellline is a mouse plasmacytoma B cell line isolated from a BALB/C mouse myeloma. Their properties include an isotype class switch to IgA which is not expressed, even though they express endogenous Igβ and secrete a λ light chain [43] and was kindly provided by Michael Reth, Freiburg, Germany

J558L_mεmVNP_Wt:

This J558L cellline were retroviraly transfected with a vector containing the murine ε heavy chain of the IgE immunoglobulin. The transfection efficiency could be checked via an IRES eGFP site.

Platinum E (Plat-E):

The cellline Plat-E (platinum retroviral packaging cell line) is a retroviral packaging cell line based on the HEK293T cells. It contains the stably integrated Moloney murine leukemia virus (MMLV) genes *gag*, *pol* and *env* which expression is driven by the strong EF1α promoter. High retroviral titers in these cells are facilitated by an internal ribosome entry site (IRES) site between the *gag*, *pol* and *env* genes and selection markers like blasticidin and puromycin [164].

For production of virus - in context of a retroviral transfection – which can infect non-murine cells Plat-Es are transiently transfected with a plasmid encoding for the glycoprotein of the vesicular stomatitis virus (VSV-G) enabling efficient infection [164].

Ramos:

The Ramos cellline is a Human Burkitt lymphoma B cell line originally established from the ascetic fluid of a 3-year-old boy with American-type Burkitt lymphoma in 1972. The cells were described as EBV-negative and carry the (8;14) IgH;MYC translocation and TP53 mutations. They express sIgM along with the λ light chain [165] and was kindly provided by Michael Reth, Freiburg, Germany.

Ramos EB:

This is a Ramos subline, which is equipped with an ecotropic receptor (EB) and thus enables the retroviral transfection with MMLV.Thus, additional transient transfection of Plat-E cells with VSV-G constructs is not necessary any more.

Ramos H/L KO λ1-RFP:

This Ramos cellline is deficient for the Ig heavy chain (H) and the Ig λ light chain (L). It was reconstituted with a mouse lambda-1 light chain by using a λ1-IRES-RFP construct and sorted for RFP positive cells. It was kindly provided by Kanika Vanshylla [52].

III.1.5 Cell culture Media for mammalian celllines

R10 Medium: The above-mentioned mammalian celllines were cultured in RPMI 1640 (+GlutaMax) to which following ingredients were added:

- 10% heat inactivated fetal calf serum (FCS)
- 1% penicillin/streptomycin
- 50µm β-Mercaptoethanol
- 1mM sodium pyruvate
- 1mM L-glutamine

R0 Medium: This Medium corresponds to R10 Medium but does not contain FCS.

Freezing Medium: For freezing the cells for long-term periods, they are kept in freezing medium, which is prepared with 90% heat inactivated FCS and 10% DMSO.

Selection markers: Within the scope of selection, the following selection markers and their concentrations were used in this project:

Hygromycin	0,6 mg/ml
Puromycin	2 µg/ml

III.1.6 Bacterial strains

TOP10F': This E.coli bacterial strain – derived from Invitrogen - was used for standard cloning experiments and has the following genotype:
F´{lacIq Tn10 (TetR)} mcrA ∆(mrr-hsdRMS-mcrBC) Φ80lacZ∆M15 ∆lacX74 recA1 araD139 ∆(ara-leu)7697 galU galK rpsL endA1 nupG

III.1.7 Culture Medium and Agar plates for Bacteria

Luria Bertani (LB) Medium:
For the above mentioned E.coli strain TOP10F' LB-Medium was used which was prepared after following protocol: 10 g/L Tryptone, 5 g/L yeast extract, 5 g/L NaCl, pH 7.0.
The mixture was finally autoclaved at 121°C, 1.25 bar for 30 min.

Agar plates:

Agar plates were prepared with autoclaved (121 °C, 1.25 bar, 30 min) LB-medium containing 2 % (w/v) agar-agar. The required antibiotic was added to the cooled down Medium (approx.. 60 °C), before casting the dishes. The Agar plates were stored at 4 °C.

III.1.8 Selection markers

The Selection was performed using LB-medium with the following antibiotic end concentrations:

Ampicillin	100 µg/ml
Kanamycin	50 µg/ml

III.1.9 Antibodies and Conjugates

The Following tables show the complete list of antibodies, which have been used for this study.

Table 4: Antibodies used for FACS or AP

Antigen	Conjugate	Clone	Species	Company
Mouse λ light chain	Biotin	Polyclonal	Goat	Southern Biotech
IgM	FITC	polyclonal	Goat $F(ab)_2$	Southern Biotech
IgM	Alexa Fluor 647	polyclonal	Goat $F(ab)_2$	Southern Biotech
IgE	PE-Cy7	MHE-18	Mouse	BioLegend
IgE	FITC	Polyclonal	Goat	Vector Lab.
IgE	Biotin	HP6029	Mouse	Southern Biotech
CD19	APC	6D5	Rat	BioLegend
CD19	APC/Cy7	HIB19	Mouse	BioLegend
CD23	FITC	EBVCS-5	Mouse	BioLegend
CD23	Brilliant Violet 421	EBVCS-5	Mouse	BioLegend

CD23	APC-Cy7	EBVCS-5	Mouse	BioLegend
CD79a	AL647	ZL7-4	Mouse	BioRad
CD79b	PECy7	CB3-1	Mouse	BioLegend
Streptavidin Alexa Fluor 647				BioLegend

Table 5: Antibodies for BCR Stimulation

Antigen	Species	Company
α-human IgE	Goat	Abcam
F(ab')$_2$ Human IgM (Fc5μ fragment specific)	Goat	Jackson ImmunoResearch

Table 6: Primary antibodies for Western blotting

Antibodies were mixed in TBS-T with 1 % BSA and 0.01 % NaN_3 and used according to the manufacturer's instructions.

Primary antibody	Conjugate	Clone	Species	Company
α-human IgE	unconjugated	Polyclonal	Goat	Abcam
α-human IgM	unconjugated	polyclonal	Goat	Southern Biotech
α-human CD23	unconjugated	EBVCS-5	Mouse	BioLegend
α-human CD23	unconjugated	polyclonal	Rabbit	Abcam
α-human/mouse CD19	unconjugated	D4V4B	Rabbit	CST
α-human CD79b	unconjugated	EPR6861	Rabbit	Abcam
α-mouse CD19	unconjugated	ID3	Rat	BD Pharmingen
α-Aktin	unconjugated	I3E5	Rabbit	CST
α-mouse IgE	unconjugated	polyclonal	Goat	Novus
α-mouse IgE	Biotin	polyclonal	Rat	BD Pharmingen
α-mouse IgE	Biotin	RME-1	Goat	BioLegend

Table 7: Secondary antibodies for Western Blotting

Antibodies were mixed in TBS-T in dilution 1:10000.

Secondary antibody	Species	Company
α-mouse IgG_1-HRPO	goat	Southern Biotech
α-mouse IgG_{2a}-HRPO	goat	Southern Biotech
α-mouse IgG_{2b}-HRPO	goat	Southern Biotech
α-mouse IgG-HRPO	goat	Southern Biotech
α-rabbit IgG-HRPO	goat	Southern Biotech
α-goat IgG-HRPO	Donkey (polyclonal)	Southern Biotech
α-human-IgM-HRPO	Mouse	Thermo Fischer Scientific
α-human-IgM-HRPO	Goat	Invitrogen

III.1.10 Enzymes and reaction buffers

Table 8: List of enzymes and respective reaction buffers

Enzymes	Company
Calf intestine phosphatase (CIP)	New England Biolabs, Frankfurt am Main
Phusion DNA polymerase	New England Biolabs, Frankfurt am Main
5x Phusion HF Reaction Buffer	New England Biolabs, Frankfurt am Main
Phusion HF DNA-Polymerase	New England Biolabs, Frankfurt am Main
T4 DNA ligase	New England Biolabs, Frankfurt am Main
Taq-Polymerase	New England Biolabs, Frankfurt am Main
10x Taq-Puffer	New England Biolabs, Frankfurt am Main
T4 DNA-Ligase Puffer (mit 10mM ATP)	New England Biolabs, Frankfurt am Main
10X NEBuffers 2.1/3.1/Cutsmart	New England Biolabs, Frankfurt am Main
6x DNA-loading buffer	New England Biolabs, Frankfurt am Main

III.1.11 Ingredients for CRISPR/Cas9 Neon Transfection System

Table 9: List of enzymes and respective reaction buffers for the Neon Transfection System

Enzymes	Company
Alt-R® S.p. HiFi Cas9 Nuclease V3	Integrated DNA Technologies (IDT)
Electrolytic Buffer E	Invitrogen
Nuclease Free - IDTE pH 7,5 (1x TE solution)	Integrated DNA Technologies (IDT)
Nuclease free Duplex Buffer	Integrated DNA Technologies (IDT)
Nuclease free Duplex Water	Integrated DNA Technologies (IDT)
Resuspension Buffer R	Invitrogen
Alt-R® CRISPR-Cas9 tracrRNA	Integrated DNA Technologies (IDT)
Alt-R® Cas9 Electroporation Enhencer	Integrated DNA Technologies (IDT)
sgRNA sequence: For µ-switch region: CTGTGTCGGGCTGAGCCAAGCTGG For ε-switch region: CAGGTTGAGGTTAACTGAACTGGG	Integrated DNA Technologies (IDT)

III.1.12 Primer and Plasmids

Synthetic DNA oligonucleotides were purchased from Eurofins Genomics and used according to the manufacturer's instructions.

Table 10: List of Primer used for cloning

Name	Sequence 5'-> 3'
Eco_Bgl_Xho_fwd	TACGAATTCTAGATCTCTCGAGGTTGGTGG
hCD23RI_fwd	GAATTCAAGCAGGACCGCCATG
hCD23RI_rev	GAATTCATGCTCAAGAGTGGAGAGG
hIgE BCR D409A_E412A_fwd	CACCCGAGCCTGGATCGCGGGGGAGACC
hIgE BCR D409A_E412A_rev	GGTCTCCCCCGCGATCCAGGCTCGGGTG
mCD19_Xho_RV_fwd	CAGCTCGAGGATATCTCAAGGCCCACCATGCCATC
mCD19_Xho_RV_rev	CAGCTCGAGGATATCTGGGCCCATGAGGCCTTACG

Table 11: Standard primers used for sequencing

Name	Sequence 5'-> 3'
M13fwd	TGTAAAACGACGGCCAGT
M13rev	CAGGAAACAGCTATGACC
MSCVfwd	CCCTTGAACCTCCTCGTTCGACC
MSCVrev	CAGACGTGCTACTTCCATTTGTC
RetroXfwd	AGGGCGCCTATAAAAGAGTGC
RetroXrev	TGACGGCCCTCCTGTCTTAG

Table 12: List of Primers used for mutagenesis

Name	Sequence 5'-> 3'
hCD23 R188A_fwd	CAGTGGGTCCACGCCGCGTATGCCTGTGAC
hCD23 R188A_rev	CGTCACAGGCATACGCGGCGTGGACCCACTG
hCD23 R224A_fwd	CCTGGATTGGCCTTGCGAACTTGGACCTGAAG
hCD23 R224A_rev	TTCAGGTCCAAGTTCGCAAGGCCAATCCAGG
hCD23 H186A_Y189A_fwd	CAGTGGGTCGCCGCCGCGGCTGCCTGTGAC
hCD23 H186A_Y189A_rev	GTCACAGGCAGCCGCGGCGGCGACCCACTG

Table 13: List of Plasmids used for cloning

Name	Source
pCR2.1_Topo	Invitrogen
pMiRFP	L. König
pMSCVpuro	Clontech
pMSCVhygro	N. Engels
pMiGRII	Invitrogen
pMiGRII_mem_VNP	K. Vanshylla
pCR2.1_Topo_hγ2asHC wt	N. Engels
pRetroX_TetOne_Puro	N. Engels

Table 14: List of Retroviral Expression vectors used for expression in mammalian cells

Name	Insert	Source
pCMV_VSV-G	VSV-G	Manfred Juecker
pMiRFP_mα	Murine Igα	N.Engels
pMiGRII_hεml_VNP	ε heavy chain (HC) of human IgE-L BCR	Produced in this study
pMiGRII_hεms_VNP	ε heavy chain (HC) of human IgE-S	Produced in this study
pMiGRII_hμHC_VNP	μ heavy chain (HC) of human IgM BCR	Produced in this study
pMiGRII_mεm VNP_Wt	ε heavy chain (HC) of murine membrane bound IgE	K. Vanshylla
pMSCV_mCD19	Murine CD19	Produced in this study
pMSCV_hCD23m Wt_puro	Human membrane bound CD23 Wt	Produced in this study
pMSCV_hCD23m$_{R188A_R224A}$_puro	Human membrane bound CD23 $_{R188A\_R224A}$	Produced in this study
pMSCV_hCD23m$_{R188A_R224A_H186A_Y189A}$_puro	Human membrane bound CD23 $_{R188A\_R224A\_H186A\_Y189A}$	Produced in this study
pRetroX_TetOn_hCD23m Wt_Puro	Human membrane bound CD23 Wt	Produced in this study
pRetroX_TetOn_hCD23m $_{R188A_R224A}$_Puro	Human membrane bound CD23 $_{R188A\_R224A}$	Produced in this study
pRetroX_TetOn_hCD23m$_{R188A_R224A_H186A_Y189A}$_Puro	Human membrane bound CD23 $_{R188A\_R224A\_H186A\_Y189A}$	Produced in this study

III.1.13 Instruments and Software

Table 15: List of Instruments

Instruments	Company
Analytical balance MC1, TF 612	Sartorius
Bacteria incubator Heraeus Kelvitron®t	Heraeus
Bacteria incubator Unitron	Infors AG
Bio Photometer	Eppendorf
Cell culture incubator HeraCell 150	Heraeus
Cell culture safety cabinet Herasafe	Heraeus
Centrifuge 5415D	Eppendorf
Centrifuge Multifuge 3 S-R	Heraeus
Centrifuge RC 3B Plus	Sorvall
Centrifuge 5417R	Eppendorf
Chemi Lux Imager	Intas
Cytometer LSRII	BD
Electrophoresis Power Supply	Amersham Biosciences
FACS Calibur	BD
Freezer HERAfreeze	Heraeus
Freezer Platilab 340	Angelantoni
Galaxy Mini centrifuge	VWR
Gel Electrophoresis system	Peqlab
Gel Imager	Intas
Ice machine	Ziegra Eismaschinen
Inverted microscope Axiovert 35	Zeiss
Magnetic stirrer M21/1	Framo®-Gerätetechnik
Mastercycler epgradient	Eppendorf
MiniRocker MR-1	Peqlab
NanoDrop 2000 Spectrophotometer	Thermo Fischer Scientific
pH meter	InoLab

Platform shaker Duomax 1030/1040	Heidolph
Platform shaker 3005	GFL
Refrigerator Gastro Line, Comfort	Liebherr
Rotator SB3	Stuart
SE 600 Ruby standard dual cooled vertical system (Electrophoresis unit)	GE Healthcare
Shaking Incubator Infors	Unitron
TE77 semidry western blot transfer unit	GE Healthcare
Thermomixer comfort	Eppendorf
Ultra-low Temperature Freezer (-150 °C)	Panasonic
Ultrasonic device Sonoplus	Bandelin
UV illuminator	Intas
Vortex-Genie 2	Scientific Industries
Water bath	GFL
Water purification system arium® G11	Sartorius

Table 16: List of used Software

Software	Company
Affinity Designer	Serif (Europe) Ltd, USA
BD FACSDiva Software v 5.0.3.	Becton Dickinson, Heidelberg
Clone Manager	Sci-Ed Software
FACS Diva 6.1.2	Becton Dickinson, Heidelberg
Countess™ Automated Cell Counter	Invitrogen
FlowJo 7.6.5 (TriStar)	Flow cytometry data analysis
GATCViewer™ für Windows	GATC Biotech AG, Konstanz
Graph Pad Prism 5	GraphPad, USA
Leica Confocal Software	Imaging
Mendeley Desktop 1.16.1	Mendeley Ltd, USA

Microsoft Office *Excel 2010* *Power Point 2010* *Word 2010*	Microsoft, USA
NCBI database	NCBI
Serial Cloner 2.6.1	SerialBasics, F
Uniprot protein database	Uniprot Consortium

III.2 Methods

III.2.1 Cell Culture Methods

III.2.1.1 Culturing mammalian cells

As far as nothing else is mentioned all B cell lines were grown in 10 cm culture dishes using R10 Medium under 37°C and 5% CO2 in the HeraCell 150 incubator. The cells were passaged at a dilution of 1:10 every second to third day.

The adherent Plat-E cells were cultured under the same conditions as the non-adherent B cell lines. For passaging these cells the medium was removed, washing was performed with 1ml 1x PBS and incubated with 1 ml 0.05 % Trypsin-EDTA at 37°C for 3 min to detach the cells. Subsequently, the cells were re-suspended in 9ml additional R10 Medium and 1ml of the cell suspension was seeded onto a new dish.

III.2.1.2 Freezing and thawing of mammalian cells

For freezing, the cells were harvested at 400 g for 5 min at room temperature (RT), the supernatant was discarded and the cells were re-suspended in 1ml freezing medium (10 % DMSO in FCS). The suspension was subsequently transferred to cryo-tubes, kept on ice and stored at -140°C for long term- or -80°C for short term storage.

Cells were thawed in a 37°C water bath, collected in prepared 12 ml R10 Medium and harvested at 400 g for 5 min at RT. After discarding the supernatant the pellet was taken up in 10ml and seeded on a 10 cm dish.

III.2.1.3 Retroviral transduction of B cells

For production of viruses carrying the DNA of interest, the Plat-E cells were used as a packaging cell line. Once this adherent cell line were grown to about 60-70% on a 10 cm dish, the medium was carefully replaced with 5 ml fresh, pre-warmed R10, the transfection solution was added and the culture grown at 37°C O/N.

The transfection solution was prepared as follows: 500µl R0 was mixed well with 16µl TransIT and incubated at RT for 15min. Subsequently, 6-8µg DNA was added also mixed well and incubated at RT for 30 min.

The viral particles, which were produced by the packaging cell line, were used to infect the target B cell line that carried the murine ecotropic receptor which facilitates the recognition by the virus. Cells lacking the respective ecotropic receptor need the addition of the packaging vector pCMV-VSV-G to the transfection solution encoding the vesicular stomatitis virus-glycoprotein and therefore enabling the infection.

3,5ml fresh pre-warmed R10 was added the next day to the Plat-E culture and further incubated at 37°C O/N. Eventually, the supernatant was carefully collected and mixed with 4µg/ml Polybrene. Potentially detached Plat-E cells in the supernatant were pelleted by centrifugation. Simultaneously, about $2x10^6$ Ramos or J558L cells were harvested, pelleted and re-suspended in 4 ml of the viral soup per approach. The cells were infected at 37°C for one day in a 6 cm dish, harvested afterwards and recovered in fresh R10 medium for 2 days in a 10cm dish. Eventually, the cells were put under selection with either Puromycin or Hygromycin. After a few days of selection, the infection efficiency was analyzed via FACS using flow cytometry based staining if it is about molecules, which are either fluorescently tagged (i.e. with GFP or RFP) or expressed on the cell surface and therefore can be detected with a corresponding antibody.

III.2.1.4 Genome editing via CRISPR-Cas9 system using the Neon® Transfection System

This Transfection System was performed to achieve the expression of the human mIgE from the endogenous immunoglobulin heavy chain promotor in Ramos EB cells, which normally expresses mIgM. That should be accomplished by induced immunoglobulin class-switch recombination (CSR), applied by CRISPR/Cas9 genome editing system. During CSR portions of the heavy chain locus are removed by double stranded breaks from the chromosome that are usually introduced by a B cell-specific enzyme called the activation-induced deaminase (AID). The idea is to mimic the function of AID by using CRISPR/Cas9 and a set of specifically adapted sgRNAs for the switching regions of the µ heavy chain and the ε heavy chain. The sgRNAs were ordered at Integrated DNA Technologies (IDT). In this context, I used the Neon® Transfection system established by IDT, which was further optimized by M. Münchhalfen. The howl procedure was performed under S2- and RNAse free conditions.

At the beginning, the respective lyophilized sgRNAs were re-suspended in 10µl IDTE 7.5 buffer to a final concentration of 200µM, were kept at RT for 25min and then stored at -20°C.

Meanwhile, a duplex mix was prepared for each used sgRNA in a PCR tube: accordingly, 2.24 µl IDT duplex buffer, 0,88µl sgRNA and 0.88 µl tracrRNA were mixed together and incubated at 95°C in the PCR cycler with an eventual cool–down to RT.
Additionally, the Cas9 mix was prepared separately in a PCR tube: this was done by mixing 0.4µl buffer R and 0,6 µl of the Cas9 Nuclease. After that, 1µl of the Cas9 mix was mixed equally with 1µl of the previously prepared duplex mix in new PCR tubes. In this case, the two sgRNA were transfected into the target cellline at the same time. Hence, 1µl of the Cas9 mix was mixed with 2 x 0.5 µl of the two duplex mixes, each containing either the sgRNA for the switching regions of the Ig µ heavy chain or the Ig ε heavy chain. This Cas9/duplex mix was incubated for 20min at RT.
Meanwhile, the enhancer was diluted to an end-concentration of 10.8µM by applying 2µl of the 100µM stock solution to 16.5 µl nuclease-free water. Additionally R20 was prepared (i.e. RPMI-Medium with 20% FCS but without antibiotics), pre-warmed at 37°C and 500µl was distributed on a 24 well plate. Moreover, $1*10^6$ of the target cells were harvested and pelleted in a 15ml falcon.
Eventually, 4µl of the enhancer dilution was added to the Cas9/duplex mix in the PCR tubes. The cell pellet was diluted carefully in 16µl of Buffer R and finally added to the Cas9/duplex mix. At this step, it was important to avoid bubble formation. The cell mix was finally electroporated for 20ms, via 1400V through 2 pulses. Eventually, the cells were slowly transferred into the previously prepared, pre-warmed 500µl R20 in the 24 well plate. The media was exchanged by fresh R10 Medium about 7 days after transfection. Eventually, the cells have been sorted for negative IgM expression.
The respective cells have been subsequently tested for IgE-expression. Only those showing an even IgE expression were used to generate an oligoclonal IgE-switched cell population (for procedures refer to II.2.1.6).

III.2.1.5 Cell sorting

The cells were sorted at the Cell Sorting Facility of the University Medical Center Göttingen via FACS with the technical assistance of Sabrina Becker. For preparation 5-8ml cell suspension of a 70-80% confluent dish were harvested, stained with corresponding fluorescently labeled antibodies if applicable, washed with 1x PBS and eventually re-suspended in 500µl 1x PBS for cell sorting. If positive cells are GFP or RFP marked these were only harvested, washed and collected in 500µl 1x PBS. Sorted cells were generally collected in 5ml R10 medium, washed and re-suspended in fresh R10 medium. Depending on the amount of sorted cells these were first grown in multi-well plates and slowly expanded up to 10 cm dishes before using and storing.

III.2.1.6 Minimal Cell Dilution

A minimal cell dilution was performed to separate and seed individual cells with different expression properties. The original cell suspension was counted and diluted to a minimum concentration of 4 cells/ml. From this dilution two to three 96 well plates were seeded with 150µl R10 Medium per well, so that it is more likely that one clone is seeded per well. The plates have been incubated for ca. 7-14 days before screening the plates for small individual colonies. Wells displaying more than one colony were sorted out. Eventually, only those cells which showed a similar expression level of the protein of interest were collected to an oligoclonal cell population.

III.2.2 Protein biochemistry

III.2.2.1 Preparation of Clear Cellular lysates

For eventual protein analysis via Western Blot Clear Cellular Lysates (CCL) were prepared from human or murine B cell lines. The cells were grown in 35ml R10 total volume in a 15cm dish to about 80% confluence, harvested at 400 g at RT for 5min and washed once in 1x PBS. The cell pellet was re-suspended in 1x PBS and counted via Countess™ Automated Cell Counter. Accordingly, about $2{,}5x10^7$ cells were collected per approach in 1ml 1x PBS and harvested at 400 g for 5min at 4°C in the tabletop centrifuge. The cells were than lysated in 1ml 1% NP40 Lysis Buffer for 5-10min on ice. Subsequently, the samples were centrifuged at 16000g at 4°C for 10min. The resulting CCLs were transferred into new 1,5 Eppendorf tube whereby the cellular debris was discarded. Per lysate sample 50µl aliquots were taken and mixed with 25µl 2x Laemmli Buffer, boiled at 95°C for 5min and stored at -20°C for long term storage. The rest of the lysates were used for affinity purification of the proteins of interest (see. II.2.2.2). Prior analysis via SDS-PAGE the respective CCLs were boiled again for 5 min and a lysate volume corresponding to $1x10^6$ cells was applied on SDS-PAGE and further analyzed via Western Blot.

III.2.2.2 Affinity purification via biotinylated peptides or antibodies

In this study, I used either biotinylated peptides or purified antibodies for analyzing proteins of interest via affinity purification (AP).

In case of purification of murine or human mIgE-BCR or CD19 from the cell surface, $2{,}5x10^7$ cells were harvested and counted, collected in 1ml 1xPBS and incubated with biotinylated peptides for 5min on ice after carefully vortexing. To remove unbound (biotinylated) peptides the cells were subsequently washed twice with 1xPBS via centrifugation in the tabletop centrifuge. The cell pellet was then re-suspended in 1ml 1% NP40 Buffer and lysated for 5min on ice before centrifugation of the cell debris at 16000g at 4°C for 10min. The

supernatant was discarded, 50µl of the resulting CCLs were aliquoted and prepared as mentioned in 2.8 for later analysis via Western blot. The rest of the lysates was incubated with 40 µl of corresponding beads for purification for 2h at 4°C with mild agitation. The beads were than washed three times with 1% NP40 Buffer at 1800 rpm, 4°C for 3min, before addition of 50µl of 2x Laemmli buffer and boiling at 95°C for 5min. Eventually the samples were applied on SDS-PAGE and analyzed by Western Blot.

For purification of the intracellular protein pool the remaining lysates following the surface AP were incubated with the biotinylated antibodies and corresponding beads for 2h at 4°C with mild agitation.

In case of purification of the total stock of proteins of interest, the cells were first lysated as previously described in II.2.2.1 and the resulting CCLs were incubated with the biotinylated peptides together with the corresponding beads for 2h at 4°C with mild agitation. The beads were than washed three times with 1% NP40 Buffer at 1800 rpm, 4°C for 3min, before addition of 50µl of 2x Laemmli buffer and boiling at 95°C for 5min. Eventually the samples were analyzed via SDS-PAGE and Western Blot.

The biotinylated proteins or antibodies and their corresponding purifying beads, which were used in this study, are additionally depicted in Table 17.

Table 17: Combinations of biotinylated peptides and corresponding purifying beads

Biotinylated Peptides	**Applied amount per 2,5x10^7 cells:**	**Purifying Beads**	**Application**
NIP-BSA-Biotin	10µg	Streptavidin-Sepharose Beads	Purification of surface or total murine mIgE-BCR
Anti-mouse IgE Biotin	5 µg	Streptavidin-Sepharose Beads	Purification of surface or total murine mIgE-BCR
Anti- human IgE Biotin	5 µg	Streptavidin-Sepharose Beads	Purification of surface or total human mIgE-BCR
Anti-mouse λ light chain Biotin	5 µg	Streptavidin-Sepharose Beads	Purification of surface or total murine or human mIgE-BCR
Anti-CD19 purified (Clone: D4V4B)	0,04 µg/µl	Protein A/G-Agarose Beads	Purification of total murine CD19

III.2.2.3 BCR purification via anti - λ light chain beads

Ramos or J558L cells were grown to about 80% confluence in 35ml R10 and if necessary prepared with 1µM Doxycycline 24h beforehand, if the respective BCR's expression is regulated by a Doxycycline inducible promotor. The cells were harvested, $2{,}5x10^7$ were counted and lysated as previously described in II.2.2.1. After centrifugation of the lysated cells at 16000g for 10 min at 4°C the debris was removed and the resulting CCLs were transferred to new 1,5 ml Eppendorf tubes. 50µl of the lysates were aliquoted and prepared as mentioned in 2.9 for later analysis via Western blot. The rest was prepared with 40µl of Capture Select – LC lambda (mouse) beads (Thermo Scientific) for purification of the total BCR amount and incubated for 2h at 4°C at the rotor. The beads where than washed three times with 1% NP40 Buffer at 1800 rpm, 4°C for 3min before addition of 50µl 2x Laemmli Buffer and eventually boiling for 5min at 95°C. The beads as well as the CCLs were than either long-term stored at -20 °C or analyzed by applying on SDS-PAGE and subsequent immunoblotting.

III.2.3 Flow Cytometry

III.2.3.1 Analysis of protein surface expression by surface staining via flow cytometry

Measurement of the surface expression of specific proteins was performed using appropriate fluorescently labeled antibodies against the proteins of interest. About $1x10^6$ cells were harvested at 400 g, RT for 5 min, the supernatant discarded and the pellet re-suspended in 100 µl 1x PBS. 1-1,5µl of the corresponding antibodies were added to the solution, vortexed and incubated for 20min on ice in the dark. The cells were washed with 1ml 1x PBS and then collected 500µl 1x PBS for subsequent measurement at the BD LSRII. Unstained cells or cells negative for the protein of interest served as negative controls. Data was acquired via FACS Diva software and subsequently analyzed with FlowJo.

III.2.3.2 Analysis of ectopically expressed proteins tagged with a fluorophore

For analysis of proteins, which are fluorophore-tagged about $1x10^6$ cells were harvested, washed once with 1x PBS and re-suspended in 500µl PBS before subsequent measurement at the LSRII.

III.2.3.3 Intracellular staining analysis via flow cytometry

About $1x10^6$ cells were harvested and re-suspended in 100µl pre-warmed R10 and 100µl Cytofix Fixation Buffer. After vortexing the cells were than fixated by incubation at 37°C for 10min before harvesting at 400 g for 5min at RT. Next, the cells were re-suspended in 400µl

of 1x Phosflow Perm Wash Buffer (1:10 in dH_20) and incubated for 25 min at RT, before washing in additional 600µl 1x Perm Wash Buffer (400 g, 5 min, RT). After discarding the supernatant, the cells were stained in 200µl 1x PermWash Buffer with the respective antibodies in the dilution according to manufacturer's instructions for 25 min at RT in the dark. Eventually, the cells were washed twice in 1ml 1x PermWash Buffer before re-suspending in 500µl PermWash Buffer and measuring at the BD LSRII.

III.2.3.4 Kinetics-analysis of surface and total expression level of human membrane-bound CD23

The kinetics analysis of the expression level of CD23 in my Ramos B cell model is dependent from a Doxycycline inducible promotor that regulates its expression. Thus, 1µM Doxycycline has been individually added to the CD23 encoding celllines on three different time points (24 h, 10 h or 4 h) before they have been eventually analyzed via FACS.

One day before measurement, each cellline has been seeded on 4 wells of a 6 well plate – three for each individual time point for Doxycycline addition and one for an untreated sample. The cells were applied in a volume of 5ml per well and a confluence of about 50%. 1µM Doxycycline has been added to the cells 24 h, 10h or 4h before harvesting and preparation for the eventual FACS analysis. Doublets of the respective samples have been prepared during harvesting. One-half of the samples served for the analysis of the surface pool of the respective proteins that have been prepared as described in II.2.3.1. The other half was prepared according to the instructions in II.2.3.3 for intracellular staining.

III.2.3.5 Ca^{2+} Measurement with B cell lines expressing the mIgE-BCR

The influx of Ca^{2+} into the cytosol was performed using Indo1-AM, a fluorophore, which shifts it emission maximum from 475nm to 400nm (e.g. from blue to violet) when bound to Ca^{2+}. Thus, the increase of cytosolic Ca^{2+} can be observed based on the violet-blue ratio.

First, the cells were grown to a density of about 90%. Up to $4*10^6$ cells were harvested and re-suspended in 500µl R10 and transferred to a brown 1,5ml tube. Than a staining master mix was prepared: for each sample 200µl R10, 2µ 5% Pluronic F127 and 0,7µl Indo1-AM were mixed and vortexed. Subsequently, 200 µl of this master mix was added to each cell sample. The cell solutions were than vortexed and incubated at 30°C under mild agitation for 30 minutes (e.g. in the Eppendorf ThermoMix at 700 rpm). After that, the cells were washed two times with Krebs Ringer (KR) solution containing 1mM $CaCl_2$ for 1,5 min at 300 g at RT. Finally, the cells were re-suspended in 900µl KR + $CaCl_2$ and left for resting at 30°C for at least 15 min to ensure a stable baseline signal. The tubes were inverted every 5 minutes to avoid deposition of the cells. Eventually, 300µl of each sample was transferred to a flow

cytometry tube and measured via LSRII flow cytometer (BD). The signal baseline was recorded by measuring the violet-blue ratio of Indo1-AM for 30sec. In the next step, to induce Ca^{2+} signaling of the BCR 20µg/ml anti-human IgE or 20µg/ml anti-human IgM F(ab)'2 fragments were quickly added to the sample. After briefly vortexing the sample, the Indo1-AM fluorescence was further recorded for 5 min. The data for the Ca^{2+} kinetics induced upon BCR stimulation was further analyzed using FlowJo software.

III.2.3.6 Acid Treatment of Cells to detach passively bound proteins on the cell surface

In case of the IgE-switched Ramos B cell line an additional treatment of the cells with an acid buffer was performed before staining in order to detach possibly bound soluble IgE from the cell surface and thus avoid false positive signals in the surface staining. The whole procedure was performed on ice and as quick as possible.

The cells were harvested in 15ml falcons and re-suspended in 1ml Acid-Buffer by pipetting. The samples were than incubated on ice for exactly 1.5 min before addition of ice cold 500µl FCS. A second incubation for exactly 1.5 min was performed. Than the sample volume was filled up to 5ml with cold PBS and washed twice with 5ml FACS Buffer at 4°C. The samples were eventually filled up to 10-15ml with FACS buffer and centrifuged at 400g, 5min at 4°C.

III.2.4 SDS-PAGE

The general approach for size based separation of proteins gained from previously prepared CCLs and AP samples (see chapter II.2.2) was the SDS-Polyacrylamide Gel Electrophoresis (SDS-PAGE). As previously described by Weber and Osborne [166] the separation according to the individual molecular weight of the proteins of interest could be performed after denaturation and boiling at 95°C for 5min with reducing Laemmli buffer. The preparation of the SDS-gel included a 5% polyacrylamide stacking gel and a 9% polyacrylamide resolving gel. The samples were applied on the stacking gel along with a pre-stained protein ladder and a sample containing only Laemmli buffer as a purity control. The gels were prepared with the tools from the SE600 Ruby system by GE Healthcare and eventually run in 1x SDS running buffer at 7mA, 170V per gel.

III.2.5 Immunoblotting

The detection of the proteins of interest, which were previously separated via SDS-PAGE, was done by western blotting and subsequent detection via ECL solution. In this context, the proteins had to be first transferred onto a nitrocellulose membrane by semi-dry blotting as previously described [167] and performed in this study as covered below:

A blotting chamber was prepared with a layer of Whatman paper, the nitrocellulose membrane, the gel and a second layer of Whatman paper. All 4 sheets were presoaked in blotting buffer beforehand. After placing the second layer of Whatman paper on the gel the surplus buffer was carefully removed together with potential air bubbles by putting some pressure with a rolling glass pipette. This step is important for efficient blotting, The blotting reaction was performed at 16V, 240mA for 80min. Subsequently, the blot was blocked in 10% BSA/TBST solution for 2h at room temperature on the shaker and eventually incubated exerting mild agitation O/N with a suitable primary antibody, which was specific for the protein of interest in a dilution according to manufacturer's instructions. Afterwards, the membrane was shortly rinsed in 1x TBS-T before addition of a Horse radish peroxidase (HRP) labeled secondary antibody which was incubated for 1h at 4°C on the shaker. This antibody was specially recognizing the Fc-region of the previously used primary antibody and enables the visualization of the protein of interest in combination with the ECL detection system. Eventually the membrane was washed in 1x TBS-T for at least 2h on the shaker at RT before protein detection. The latter step was performed by mixing 4ml ECL solution A, 1,2µl H_2O_2 and 400 µl ECL solution B which was then poured onto the membrane. In the following HRP-reaction, the included luminol is oxidized by HRP resulting in excitation of light, which was detected via the Chemi Lux Imager (Intas).

III.2.6 Molecular biology and Cloning techniques

III.2.6.1 Mini-preparations of plasmid DNA

For extraction of small scale plasmid DNA i.e. mini-preparation, 4ml LB-medium containing the appropriate antibiotic were inoculated with an E.coli colony for 17h at 37°C and 220 rpm agitation. The bacterial plasmid DNA was isolated via Qiagen QIAprep^R Spin Miniprep kit according to manufacturer's instructions. The DNA was eluted in 35µl Elution Buffer (attached in Miniprep Kit).

III.2.6.2 Analyzing DNA quality and sequence

The measurement of nucleic acid concentrations was generally performed using a NanoDrop 2000. Sequencing analysis was carried out by SEQLAB Sequence Laboratories GmbH Göttingen. The sample preparation included 1200ng of purified DNA and 3µl of sequencing primer (10pmol/µl) in a total volume of 15 µl, adjusted by ddH_2O. The sequencing data was evaluated by the Basic Local Alignment Search Tool (BLAST) from the NCBI database as well as the cloning programs Clone Manager and Serial Cloner.

III.2.6.3 Enzymatic digestion of DNA

For generation of compatible sticky or blunt ends in PCR products, plasmids or vectors these were cleaved by specific endonucleases in respective NEBuffers. 1µg of DNA was incubated with 0,5-1µl restriction enzyme together with the appropriate NEBuffer and ddH_2O according to the manufacturer's instructions for 1 hour at 37°C. In context of cleaved and therefore linearized vectors 0,5 µl calf intestine phosphatase (CIP) was added for 1 additional incubation hour to remove phosphates from the 5'- and 3'- ends and thus prevent vector re-ligation. Eventually, the samples were prepared with 6X DNA loading dye before running on an agarose gel and evaluating via Gel Imager.

III.2.6.4 Agarose gel electrophoresis and purification of DNA fragments

Agarose gel electrophoresis was performed using 1% agarose gels with 0,5 µg/ml ethidium bromide in 1x TAE buffer. The samples were mixed with 6x DNA-loading dye before loading on the gel. Depending on the size of the DNA fragments and the gel itself the electrophoresis was performed at 100-140V for 30-45 min and the DNA fragments were subsequently analyzed using the Gel Imager under ultraviolet light. To determine the size of the DNA fragments a 1kb DNA-ladder was used as a scale. The appropriate bands were separately cut out from the agarose gel and extracted using the Promega Wizard® SV Gel and PCR Clean-Up System. The purified DNA was eluted in 30µl ddH_2O.

III.2.6.5 Ligation of DNA Fragments

The ligation of insert and vector was performed by mixing 1µl T4 DNA ligase, Insert and Vector in a 2:1 or 3:1 ratio, 1,5µl 10x T4 ligase buffer an ddH_2O for adjusting the reaction volume to 15µl. The reaction was performed overnight (O/N) at 14°C.

The next day 1µl of the ligation mix was transformed into competent E.coli TOP10F' and plated onto LB-Amp agar plates (100µg/ml ampicillin).

III.2.6.6 Transformation of plasmid DNA into competent bacterial cells

The transformation of plasmid DNA into competent E.coli TOP10F' was performed using a 50 µl aliquot of competent E.coli TOP10F' cells, which was incubated with 1-1,5 µl of the ligation reaction on ice for 30 min and subsequently heat shocked at 42°C for 42sec. The cells were then immediately put on ice for 5 min. Eventually, the cells were plated onto a LB-agar plate, containing the required antibiotics, which was then incubated O/N at 37°C.

In context of the TA-cloning strategy the transformation of TOP10F' cells with the vector pCR2.1 were performed via blue-white screening. Thus, before plating the transformed cells on the agar plates the plates have been prepared with 50 µl X-gal (5-bromo-4-chloro-3-

indolyl-beta-D-galacto-pyranoside) (50 mg/ml in DMF) and 50 µl IPTG (Isopropyl-β-D-thiogalacto-pyranoside) (0.1 M).

III.2.6.7 Polymerase Chain Reaction (PCR)

Specific cDNA fragments of genomic or plasmid templates were amplified via standard PCR reaction, which was carried out via Phusion High Fidelity Polymerase. A list of all primers used in this work can be found in chapter II.1.12.

The PCR master mix with a total volume of 25µl was prepared as described in Table 18.

Table 18: Standard PCR master mix

Ingredient	Amount
DNA template	~ 200ng
dNTPs (10µM)	1 µl
Primer fwd (10µM)	1 µl
Primer rev (10µM)	1 µl
5x Phusion HF Reaction Buffer	2,5 µl
Phusion HF DNA-Polymerase	1 µl
ddH_2O	18,5µl – Volume of template

Total volume: 25 µl

The annealing temperature was chosen according to the recommendations in the SnapGene software. The basic basic PCR program is depicted in Table 19. The resulting PCR products were applied on an agarose gel and further purified as described before.

Table 19: Standard PCR reaction

Step	Temperature	Time	Cycle
Initial denaturation	94°C	2 min	1
Denaturation	94°C	30 sec	20 - 25 cycles
Annealing	variable	1 min	
Extension	68°C	2 min /kb	
Final Extension	68°C	10 min	1
	4°C	hold	

III.2.6.8 Site directed mutagenesis

The introduction of specific mutation in the DNA sequence of a template plasmid required the design of primers containing the mutations of interest. Table 20 depicts the exact composition of the PCR master mix per approach.

Table 20: PCR master mix for side directed mutagenesis

Ingredients	Amount
Template DNA	~ 200ng
10X Pfu Buffer	5 µl
10 mM dNTPs	1 µl
10 µM Primer Fwd	1 µl
10 µM Primer Rev	1 µl
Pfu Polymerase	1 µl
ddH2O	41 µl – template volume

Total volume: 50 µl

Each approach was divided in half i.e. 2x 25 µl aliquots per approach. One aliquot was loaded on an agarose gel to test the PCR efficiency whereby the other one was prepared with 1µl DpnI at 37°C for 1h. DpnI is an endonuclease, which digests methylated DNA. Since DNA methylation occurs in bacteria and eukaryotes but not during in vitro PCR, the DpnI enables the digestion of the remaining template DNA but not the amplified (mutated) PCR products. The PCR products were directly transformed into competent E.coli for further amplification and quality analysis of the mutagenesis via sequencing.

III.2.6.9 TA cloning - strategy

To clone PCR products into the pCR2.1 vector, the TA cloning kit from Invitrogen was used. Accordingly, 20µl of the purified PCR product mixed with 2µl 10x Taq polymerase buffer, 1µl dATPs and 1µl Taq polymerase were incubated at 70°C for 25 min in order to add 3' deoxyadenosine overhangs to the PCR products. The subsequent ligation with pCR2.1 was performed as described in II.2.6.5. For the eventual blue-white screening the respective agar plates containing the appropriate antibiotics had to be prepared with 50 µl X-gal and 50µl IPTG before plating 1-1,5µl of the ligation product on them.

IV Results

IV.1 Biochemical interaction analyses between the murine mIgE-BCR and CD19

IV.1.1 Properties of a murine B cell model used to analyze the interaction between the murine mIgE-BCR and CD19

In their studies about the role of the murine mIgE-BCR in the terminal differentiation of IgE-switched B cells to plasma cells, Haniuda et al. observed a direct interaction between the murine mIgE-BCR and CD19 that was not seen with other BCR isotypes [133]. To test these findings, I established a murine cell line model that I could genetically modify to meet my experimental needs. For this purpose, I used the murine myeloma B cell line J558L, which expresses a λ1 immunoglobulin light chain and Igβ, but lacks expression of an endogenous immunoglobulin heavy chain and Igα [43]. I stably transfected these cells with a 4-hydroxy-3-iodo-5-nitrophenylacetyl (NIP) – specific murine membrane-bound immunoglobulin (mIg) heavy chain of the ε isotype together with EGFP by retroviral transduction. EGFP expression was used as a marker to facilitate sorting of positive transfectants (Fig. 4A). NIP is widely used as a model antigen to study antigen-specific B cell responses and can be used in this case for mIgE-specific affinity approaches to facilitate the analysis of the mIgE interaction with CD19. Since it was reported that the murine mIgE-BCR depends on binding to Igα for the effective export from the endoplasmic reticulum (ER) [44], I generated J558L cell lines, which were additionally transduced with an Igα-IRES-RFP construct (Fig.4A). The transfected ε mIg heavy chain and the transfected Igα subunit pair with the endogenous Igβ subunit and λ light chain to form a functional BCR on the cell surface (Fig. 4C).
The construct encoding murine CD19 was introduced into the cell lines lacking or expressing the Igα-subunit and the murine ε mIg heavy chain, resulting in the cell lines depicted in the cartoons in Figure 4B.

Cell surface expression analysis of the mIgE-BCR in the different cell lines confirmed that mIgE needs expression of both Igα and Igβ to be transported to the cell surface (Fig. 4C).
In contrast to mIgE, CD19 was stably expressed on the cell surface in the absence of Igα (Fig. 4C). In summary, these results indicate that neither Igβ alone nor CD19 support surface expression of murine mIgE and thus show that CD19 does not serve as an alternative for Igα. However, the surface expression of CD19 appeared to be independent from the expression of the mIgE-BCR.

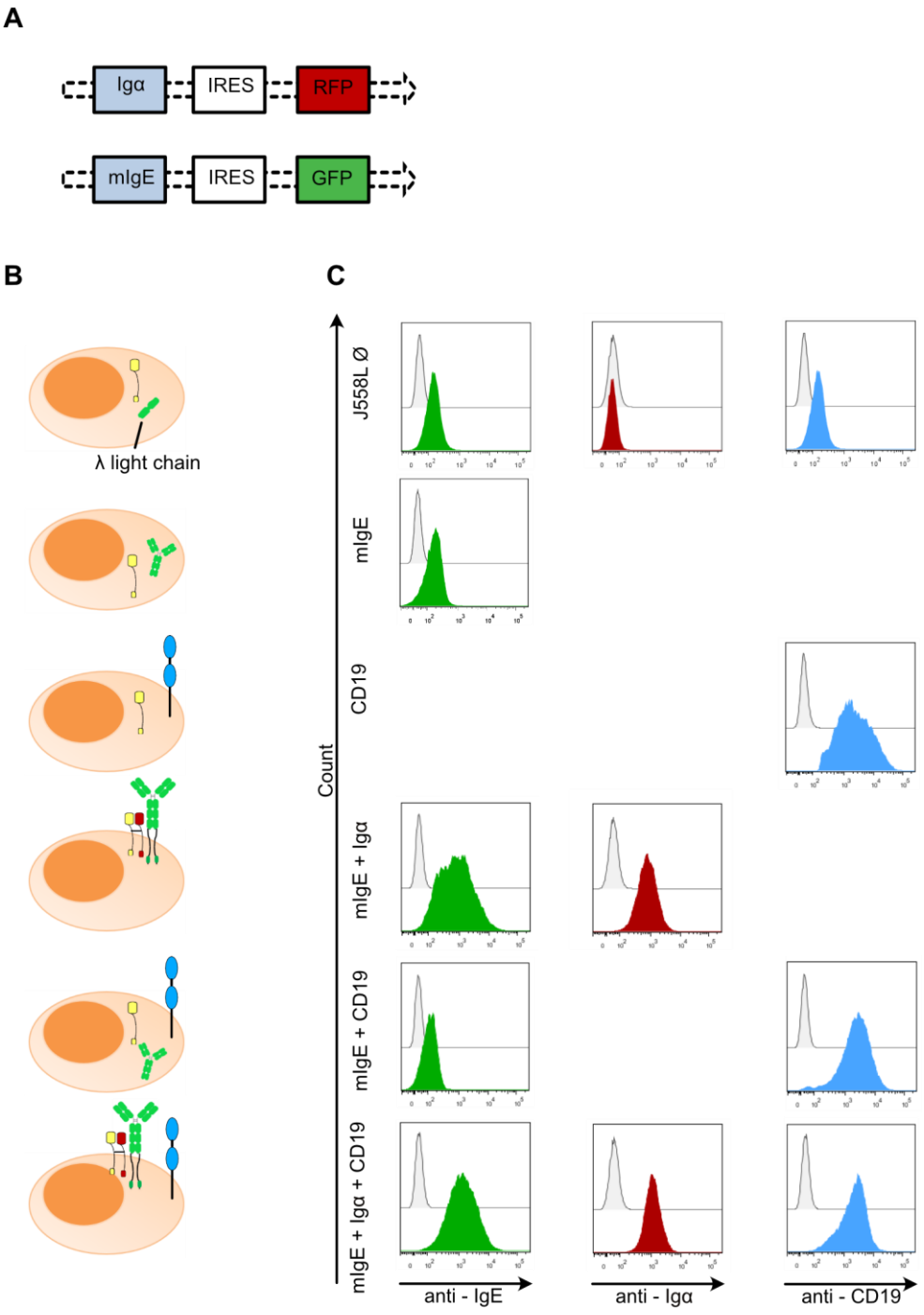

Figure 4: Generation of a murine B cell model system to analyze the interaction between mIgE and CD19.
A) Schematic illustration of the retroviral expression vectors used for transfection of J558L cells with either mIgE-IRES-GFP or Igα -IRES-RFP or both. B) Schematic illustration of the different J558L B cell lines that were generated to analyze the mIgE - CD19 interaction. The J558L cells were reconstituted with the NIP-specific murine εm heavy chain by using an IRES-GFP construct resulting in cells expressing mIgE-BCRs with NIP-specificity. These cells were sorted for GFP-positive ones. The cells were further reconstituted with Igα by using an Igα-IRES-RFP construct and subsequently sorted for RFP-positve cells. Additionally, a construct encoding murine CD19 was introduced into the cell lines lacking or expressing the Igα and the murine ε mIg heavy chain. C) Flow cytometric analysis of the mIgE-BCR, Igα and CD19 in the different J558L cell lines. The grey tinted peaks represent unstained cells whereas the fully colored ones correspond to cells stained with the indicated antibodies.

IV.1.2 CD19 showed no direct interaction with the murine mIgE-BCR

A previous report showed the successful co-purification of the murine mIgE-BCR and CD19 from lysates of B cells [133]. I used the exact same protocol to purify NIP-specific mIgE, which is based on labeling of the surface pool of the mIgE-BCR with biotin-conjugated NIP-BSA, followed by subsequent purification of biotin-NIP-BSA-bound mIgE using a streptavidin (SA) matrix.

Besides the affinity purification (AP) of the cell surface fraction of mIgE-BCRs I also performed APs of the total mIgE pool (Fig. 5A, B). The AP of the mIgE surface pool worked only for those cells also expressing the Igα subunit (i.e. J558L_mIgE_ Igα and J558L_migE_ Igα_CD19) consistent with the previous observation that Igα is needed for an efficient transport of the murine mIgE to the cell-surface (Fig. 4C) and [44], [168]. Surprisingly, the AP of the total cellular mIgE pool was also dependent on expression of Igα, which may indicate a stabilizing role of Igα also on the intracellular (i.e. ER/Golgi-resident) mIgE pool. As shown in Figure 5A and 5B, the lysates of the CD19 expressing cell lines showed an extraordinary high CD19 expression, which also appeared uneven among these three cell lines: while the CD19 and IgE_C19-expressing cells showed a similar CD19 expression, that of the mIgE_Igα_CD19 triple-positive cells showed a lower CD19 expression. Co-purified CD19 could be observed in the cell line expressing mIgE_Igα and to a lower extent also in the triple-positive cell line (Fig. 5A, B). Surprisingly, CD19 could also be purified with NIP-BSA + SA-matrix in the J558L cells expressing only CD19 but no mIgE-BCR. This questions the reliability of the observed CD19 purification in the cell lines expressing mIgE since it demonstrates an unspecific interaction between CD19 and ether NIP-BSA-biotin or the SA-matrix.

Thus, to determine the cause of this unspecific purification, I performed APs with or without addition of NIP-BSA-Biotin (Fig. 5C). CD19 unspecifically bound to NIP-BSA-Biotin but not by the Streptavidin Sepharose matrix.

To overcome these unspecific interactions, I established an alternative affinity purification approch, which turned out to be more specific. Since the murine mIgE-BCR contains a λ light chain, I used an anti-mouse λ light chain matrix for purification of the mIgE-BCR complex (Fig. 6). These beads are covalently conjugated to an anti-mouse λ light chain nanobody. The purification of the mIgE-BCR worked in all J558L cell lines. As side note, the mIgE purification showed a variation in its signal strength: the band for mIgE appeared stronger when Igα is additionally expressed in the cell. This hints once more to a potential role of Igα in maintaining the stability of intracellular mIgE, which might be of interest for future investigations.

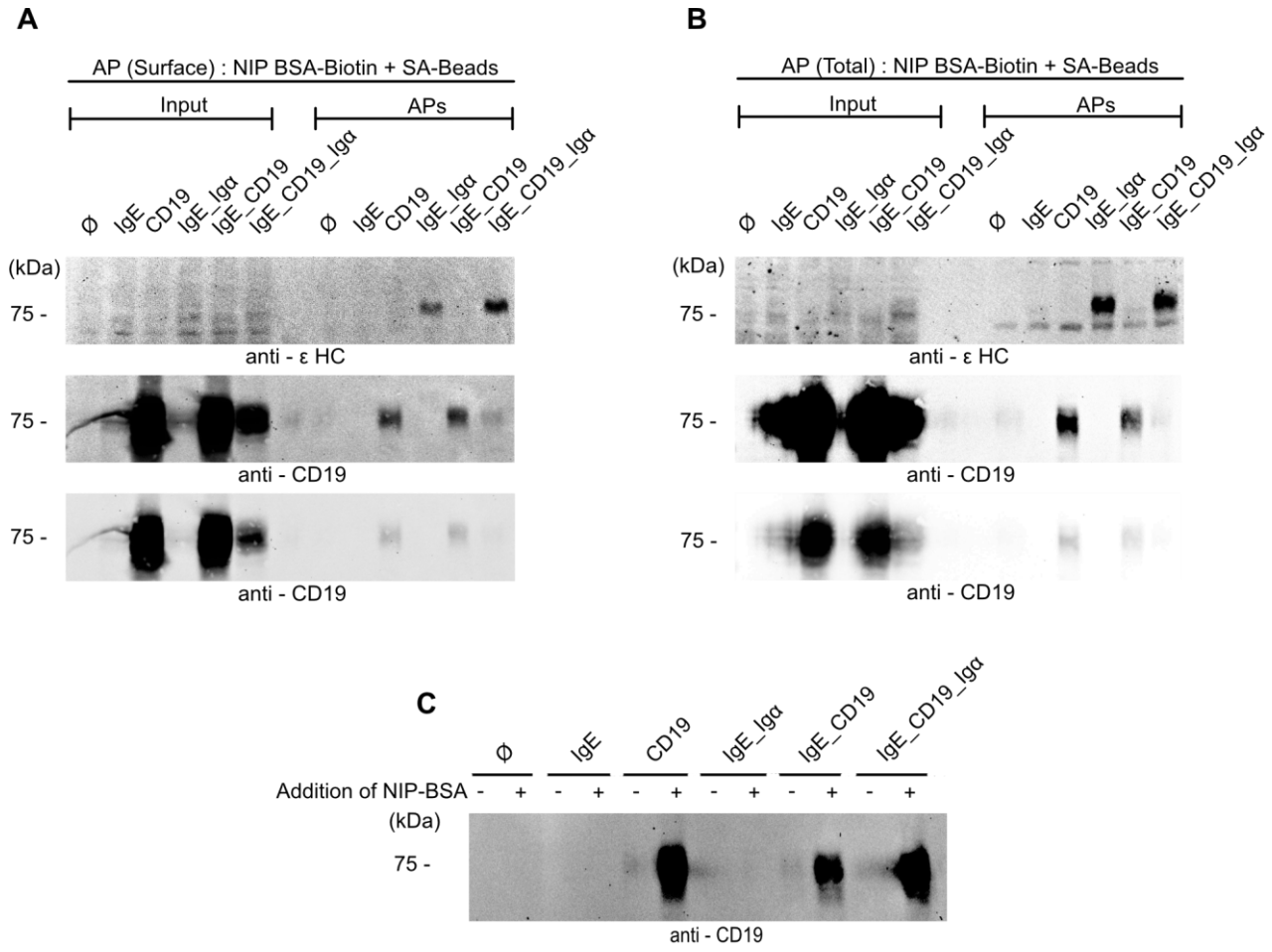

Figure 5: Affinity Purification (AP) of the murine mIgE-BCR via NIP-BSA-Biotin and SA-Beads
A) AP of surface or B) total mIgE pool. For purification of the surface mIgE fraction living cells were incubated with 10µg NIP-BSA-Biotin before preparing the lysates. For AP of the total mIgE pool, cells were lysated before addition of 10µg NIP-BSA-biotin. In both cases NIP-bound mIgE was purified from cellular lysates by addition of SA-beads. Cleared cellular lysates (CCL) were applied as input controls. Proteins were separated by SDS-PAGE and analyzed by western blot using antibodies specific for the ε HC and CD19. Blots incubated with anti-CD19 are depicted after longer (middle panel) and shorter exposure (lower panel) C) Specificity test of NIP-BSA-Biotin and SA-Beads. Total mIgE pool was purified separately ether with both NIP-BSA-Biotin and SA-Beads or only with SA-Beads. Proteins were analyzed as in A) and B). The molecular weight of marker proteins is indicated on the left in kDa.

The erratic CD19 expression, which is shown in Figure 5A and 5B, was adjusted by cell sorting for low CD19 expression in mIgE_CD19 and mIgE_CD19_Igα cells (Fig. 6). Thus, the cellular lysates from these cells showed a strong and consistent CD19 expression.
However, I could not detect any co-purification of CD19 with mIgE. Hence, with these data I could not confirm the findings about a direct interaction between the murine mIgE-BCR and CD19 as reported by Haniuda et al [133].

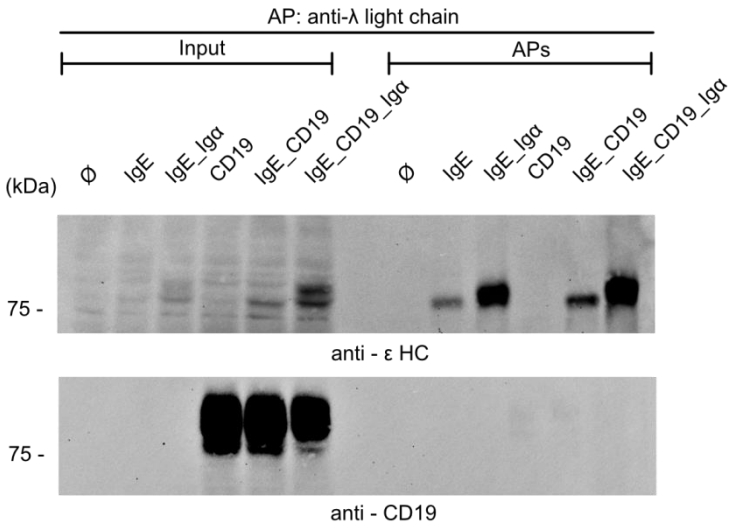

Figure 6: AP of the murine mIgE-BCR via anti λ light chain beads
For purification of the total mIgE pool, the cells were lysated and incubated with anti λ light chain beads. Cleared cellular lysates were used as input controls. Interaction between mIgE and CD19 was detected using SDS-Page and immunoblotting using antibodies against these proteins. Data are representative of three independent experiments. The molecular weight of marker proteins is indicated on the left in kDa

IV.2 Both human mIgE-BCR isoforms interact with CD23

As already introduced in the previous chapter there exist several models, which attribute a regulatory role in the synthesis of IgE to the low affinity receptor for IgE, CD23. The binding of soluble IgE to CD23 results in negative feed-back of the IgE synthesis, whereas cross-linking of mIgE-BCR with CD21 via soluble CD23 enhances the production of IgE. This raises the question whether a similar feed-back mechanism also exists when the mIgE-BCR isoforms (e.g. either the mIgE-S or mIgE-L isoform) and CD23 are co-expressed on the cell surface. This question was addressed by creation of a human B cell model which co-expresses CD23 and the mIgE-BCR. Since the CD23-induced regulation of the IgE synthesis is based on an interaction with IgE, the first step was to analyze, whether mIgE-BCR and co-expressed CD23 also interact with each other.

IV.2.1 Properties of a human B cell model for the expression of CD23

For the planned receptor-receptor interaction analysis I used the human Burkitt lymphoma cell line Ramos. Ramos cells express an endogenous mIgM-BCR. I used a knockout clone of this cell line lacking the IgH and IgL chains, which was reconstituted with a mouse λ1 light chain_IRES_RFP construct (hereafter referred to as Ramos H/L -/- λ1_RFP) (generated by K. Vanshylla [52]) (Fig. 7A). These cells still express endogenous Igα and Igβ, which remain in intracellularly because of the absence of a mIg. This genetic background makes this

knockout cell line appropriate to introduce other mIgs for the analysis of their expression and functionality [52].
I transduced these cells with the human εms heavy chain (mIgE-S) or εml heavy chain (mIgE-L) via retroviral transfection. The resulting cells expressed either one of the two human mIgE-BCR isoforms (schematically depicted as Ramos H/L -/- λ1 + huεmHC in Fig.7A). For comparison, I additionally generated cells which were transduced with the human µm heavy chain (mIgM) resulting in the expression of the human mIgM-BCR (Fig. 7B, last panel). A uniform expression of the various BCRs was ensured by sorting for the respective mIgs (Fig. 7B). It is known that the EMPD as part of the mIgE-L isoform acts as an ER retention domain and restricts its expression on the cell surface [116]. That explains the lower anti-IgE staining in comparison to the mIgE-S version (Fig. 7B).

To enable the interaction analysis between the mIgE-BCR and CD23, I next transduced the mIgE and mIgM expressing cell lines with a CD23 construct, in which the CD23 expression is regulated by a Doxycycline-inducible promotor (schematically depicted as Tet-On promotor in Fig. 7A). To test the functionality of the inducible CD23 expression system, the cell lines expressing the various BCRs and also carrying the coding sequence for CD23 were incubated with 1µM Doxycycline for 24h or were left untreated (Fig. 7B+C). I could exclude any CD23 expression in absence of Doxycycline addition (Fig. 7B, right panel). Cells lacking the expression of a mIg but encoding the sequence of CD23 were used as a control (Fig. 7B-D). Both, the CD23 and mIgE expression was tracked via FACS (Fig. 7B,D-G). 24h after addition of Doxycycline a major proportion of the cells were CD23 positive (Fig. 7C-G) and showed a uniform expression on the cell surface (Fig. 7C upper panel). Also with regard to the total CD23 pool, I could detect an even CD23 expression level among the cells (Fig. 7C lower panel).
In summary, these data show that the Doxycycline inducible system is efficiently working.

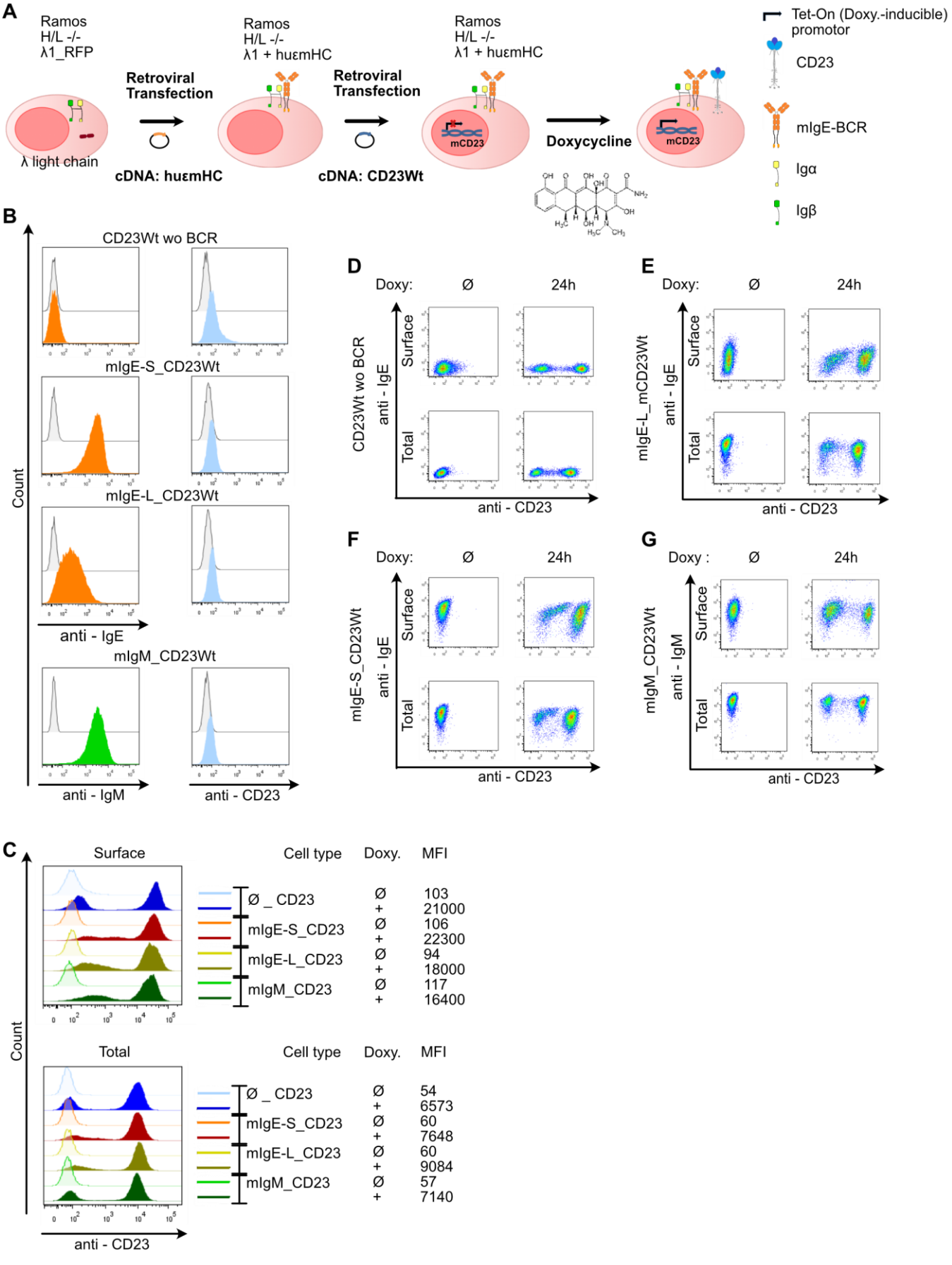
A
Ramos H/L -/- λ1_RFP
λ light chain
Retroviral Transfection
cDNA: huεmHC
Ramos H/L -/- λ1 + huεmHC
Retroviral Transfection
cDNA: CD23Wt
Ramos H/L -/- λ1 + huεmHC
mCD23
Doxycycline
mCD23
Tet-On (Doxy.-inducible) promotor
CD23
mIgE-BCR
Igα
Igβ
B
CD23Wt wo BCR
mIgE-S_CD23Wt
mIgE-L_CD23Wt
mIgM_CD23Wt
Count
anti - IgE
anti - IgM
anti - CD23
C
Surface
Total
Count
anti - CD23
Cell type
Doxy.
MFI
Ø _ CD23
mIgE-S_CD23
mIgE-L_CD23
mIgM_CD23
Ø 103
+ 21000
Ø 106
+ 22300
Ø 94
+ 18000
Ø 117
+ 16400
Ø 54
+ 6573
Ø 60
+ 7648
Ø 60
+ 9084
Ø 57
+ 7140
D
Doxy: Ø 24h
CD23Wt wo BCR
Surface
Total
anti - IgE
anti - CD23
E
Doxy: Ø 24h
mIgE-L_mCD23Wt
Surface
Total
anti - IgE
anti - CD23
F
Doxy: Ø 24h
mIgE-S_CD23Wt
Surface
Total
anti - IgE
anti - CD23
G
Doxy : Ø 24h
mIgM_CD23Wt
Surface
Total
anti - IgM
anti - CD23

Figure 7: Properties of a Doxycycline inducible expression system for the expression of CD23
A) Experimental Setup: Ramos H/L -/- λ1_RFP cells were reconstituted with either human εms or εml heavy chains or the human µm heavy chain resulting in cells expressing either mIgEshort or mIgElong isoform or mIgM-BCR. These cells were further transduced with a CD23 construct, in which the CD23 expression is regulated by a Doxycycline inducible promotor. B) Flow cytometric analysis of surface mIgE, mIgM and CD23 in the generated Ramos cell lines in absence of Doxycycline. C) Surface and total CD23 expression in mIg empty, mIgE or mIgM expressing cells, either left untreated (tinted peaks) or treated with 1µM Doxycycline (Doxy) (fully colored peaks) for 24h. The mean florescence intensity (MFI) is given on the right side of each panel. Data are representative of three independent experiments D-G) CD23 expression was induced by incubation with 1µM Doxycycline for 24h (right panel). It's surface and total expression was eventually analyzed together with the respective BCRs via flow cytometry along with untreated cells (left panel). For analyzing the total protein pool the respective cells were harvested followed by fixation and permeabilization before staining against CD23 and the respective BCRs.

IV.2.2 CD23 directly associates with both human mIgE-BCR isoforms

In order to determine, whether there exists a direct association between the human mIgE-BCR isoforms and CD23, I prepared lysates from mIgE_CD23 expressing cells which had been treated with Doxycycline for 24 hours or were left untreated, and used them to affinity purify the different BCRs using a matrix conjugated to anti-mouse λ light chain antibodies (Fig.8, right panels). I confirmed the successful and specific purification of the different mIg isoforms (Fig. 8 right panel). In addition, I verified the induction of the CD23 expression (input controls, Fig. 8 left panel). I observed an abundant co-purification of CD23 in the cell lines expressing mIgE but not in cells expressing mIgM. This indicated a direct isotype-specific interaction between the mIgE-BCR isoforms and CD23.

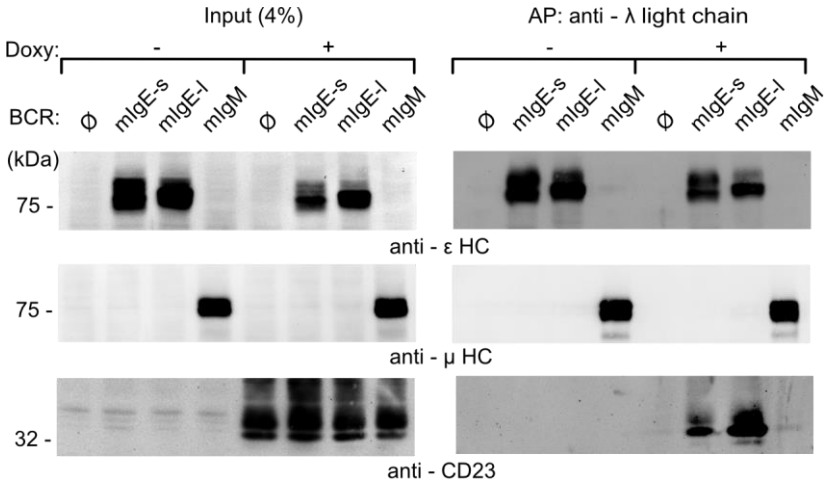

Figure 8: CD23 directly binds to the human mIgE-BCR isoforms
Anti – mouse λ light chain beads were used to purify the total pool of mIgE molecules. Cleared cellular lysates were used as input controls and volume corresponding to one million cells was applied for interaction analysis. Purified proteins were separated by SDS-PAGE and analyzed by immunoblotting with antibodies to the ε HC (upper panel), µ HC (middle panel) and CD23 (lower panel). Ramos cells lacking a BCR were used as negative control. Data are representative of three independent experiments.

Next, I performed a biochemical analysis of the observed mIgE-CD23 interaction in order to identify a direct association between these receptor types. Dhaliwal et al and Borthakur et al [152], [153], [169] gave detailed descriptions of the IgE-CD23 interface, which is mainly based on salt bridges and hydrogen bonds of specific amino acids in the head domains of CD23 and the Cε3 domain of IgE. Based on this knowledge, I generated double-mutants and quadruple-mutants of CD23 carrying alanine substitutions in two or four different amino acid positions in the IgE-binding site of the CD23 head domain. The resulting double-mutant of CD23 was characterized by alanine residues at position 188 (R188A) and 224 (R224A) and will be referred to as CD23_2xA. The quadruple-mutant additionally carried alanine substitutions at positions 186 (H186A) and 189 (Y189A) and will be referred to as CD23_4xA. The amino acid sequence of the human CD23 with its substituted amino acids and its alignment with other species is depicted in Figure 9A. These CD23 mutants were retrovirally transfected into the respective mIgE-BCR expressing cell lines.

Upon Doxycycline addition CD23_4xA showed surface and total expression similar to that of CD23. The double-mutant was less efficiently expressed on the cell surface as well as intracellularly (Fig. 9B & C). To test the effect of the amino acid substitutions on the mIgE-CD23 association, I purified the mIgE-molecules using anti-mouse λ light chain beads as before. The co-purification of CD23 in the double-mutants with both the mIgE-S- and mIgE-L-BCR was strongly reduced compared to wild-type CD23 and was barely perceptible in the CD23_4xA expressing cell lines (Fig. 9D). The IgE-specific nature of this interaction was demonstrated by the purification of the mIgM-BCR, which did not show any association to CD23 (Fig. 9E). These results show that the observed mIgE-CD23 association occurs through the head domains of CD23. Additionally, mutagenesis of at least two of the mentioned amino acids in the IgE-binding site of CD23 strongly reduces this interaction emphasizing their essential role in the IgE-binding.

Since the direct mIgE-CD23 interaction was observed by using the total mIgE pool, one cannot clearly state whether this complex is only occurring on the cell surface or already intracellularly. In order to determine where the mIgE-CD23 interaction is happening, I affinity-purified the mIgE-BCR isoforms from different cellular compartments of the respective Ramos cell lines and determined the amount of co-purified CD23 (Fig. 10). Specifically, I purified mIgE from the cell surface and subsequently used the remaining lysates for purification of the intracellular pool (IC). Furthermore, cellular lysates were used to purify the total mIgE pool. For BCR purification, I used biotinylated anti mouse λ light chain antibodies and subsequently used SA-Beads for protein purification. Obviously, the co-purification of CD23 was much more efficient from the intracellular compartments in both mIgE-S and

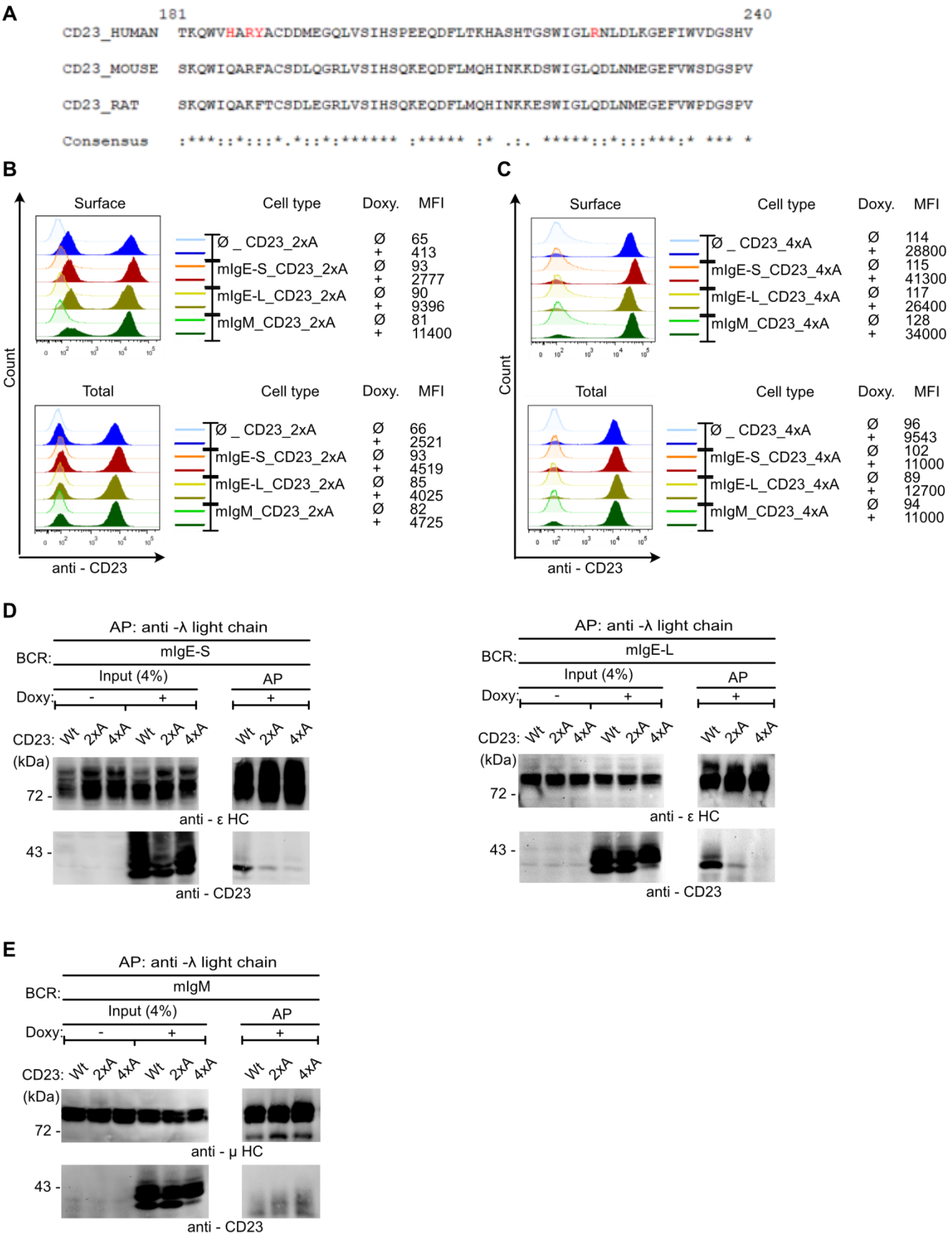
A
181
240
CD23_HUMAN TKQWVHARYACDDMEGQLVSIHSPEEQDFLTKHASHTGSWIGLRNLDLKGEFIWVDGSHV
CD23_MOUSE SKQWIQARFACSDLQGRLVSIHSQKEQDFLMQHINKKDSWIGLQDLNMEGEFVWSDGSPV
CD23_RAT SKQWIQAKFTCSDLEGRLVSIHSQKEQDFLMQHINKKESWIGLQDLNMEGEFVWPDGSPV
Consensus :***::*:::*.*::*:****** :***** :* .:. *****::*:::***:* *** *
B
Surface
Cell type
Doxy.
MFI
Ø _ CD23_2xA
mIgE-S_CD23_2xA
mIgE-L_CD23_2xA
mIgM_CD23_2xA
Ø 65
+ 413
Ø 93
+ 2777
Ø 90
+ 9396
Ø 81
+ 11400
Total
Cell type
Doxy.
MFI
Ø _ CD23_2xA
mIgE-S_CD23_2xA
mIgE-L_CD23_2xA
mIgM_CD23_2xA
Ø 66
+ 2521
Ø 93
+ 4519
Ø 85
+ 4025
Ø 82
+ 4725
Count
anti - CD23
C
Surface
Cell type
Doxy.
MFI
Ø _ CD23_4xA
mIgE-S_CD23_4xA
mIgE-L_CD23_4xA
mIgM_CD23_4xA
Ø 114
+ 28800
Ø 115
+ 41300
Ø 117
+ 26400
Ø 128
+ 34000
Total
Cell type
Doxy.
MFI
Ø _ CD23_4xA
mIgE-S_CD23_4xA
mIgE-L_CD23_4xA
mIgM_CD23_4xA
Ø 96
+ 9543
Ø 102
+ 11000
Ø 89
+ 12700
Ø 94
+ 11000
Count
anti - CD23
D
AP: anti -λ light chain
BCR: mIgE-S
Input (4%)
AP
Doxy: - + +
CD23: Wt 2xA 4xA Wt 2xA 4xA Wt 2xA 4xA
(kDa)
72 -
anti - ε HC
43 -
anti - CD23
AP: anti -λ light chain
BCR: mIgE-L
Input (4%)
AP
Doxy: - + +
CD23: Wt 2xA 4xA Wt 2xA 4xA Wt 2xA 4xA
(kDa)
72 -
anti - ε HC
43 -
anti - CD23
E
AP: anti -λ light chain
BCR: mIgM
Input (4%)
AP
Doxy: - + +
CD23: Wt 2xA 4xA Wt 2xA 4xA Wt 2xA 4xA
(kDa)
72 -
anti - μ HC
43 -
anti - CD23

Figure 9: The direct interaction between CD23 and mIgE-BCR is disrupted by mutagenesis
A) Amino acid sequence alignment of the human, mouse and rat CD23 head domain segment from position 181 to 240. The amino acids selected for side-directed mutagenesis are marked in red. B)+C) Surface and total expression of CD23 double-mutants (2xA) or quadruple-mutants (4xA) was analyzed by flow cytometry, untreated (tinted peaks) or treated with 1µM Doxycycline (Doxy.) for 24h (fully colored peaks). The mean florescence intensity (MFI) is listed on the right side of each panel. D) Anti – mouse λ light chain beads were used to purify the total pool of mIgE molecules from cells that had been treated with 1µM Doxy for 24h to induce the CD23 expression or left untreated. A volume corresponding to one million cells was applied as input controls. Purified proteins were separated by SDS-Page and analyzed by Western Blot with antibodies to the ε HC (upper panel) and CD23 (lower panel). E) AP of mIgM molecules was performed and analyzed as in D). Data is representative of three independent experiments.

mIgE-L expressing cell lines in comparison to the cell surface (Fig. 10A+B, lane 4-6). Hence, I concluded that the mIgE isoforms and CD23 had already bound to each other in the ER and that CD23 as part of this complex is less efficiently transported to the cell surface. Furthermore, the surface pool of mIgE-S ran at a higher molecular weight than its intracellular pool (Fig. 10A). This observation had already been made by Vanshylla et al [52] indicating that this, most likely, might be due to the more complex glycosylation of the surface expressed mIgE-S molecules. In contrast, mIgE-L showed a very faint glycosylation due to its retention in the ER. In fact, the lower glycosylation level of mIgE-S in the IC appeared to have no impact on its association with CD23. The same could be observed for the mIgE-L isoform that is retained in the ER (Fig. 10B, lane 4-6). As already observed in Figure 9, the introduction of two alanine substitutions in the IgE binding site of CD23 resulted in a clear reduction of co-purified CD23 in the intracellular compartments and was completely abrogated in case of the 4xA mutants (Fig. 10A+B, lane 7-12). As control, I performed the same experiment with mIgM-BCRs, which did not show any interaction with CD23 (Fig. 10C). In summary, these data show that the direct association between the mIgE-BCRs and CD23 occurs mainly in the ER.

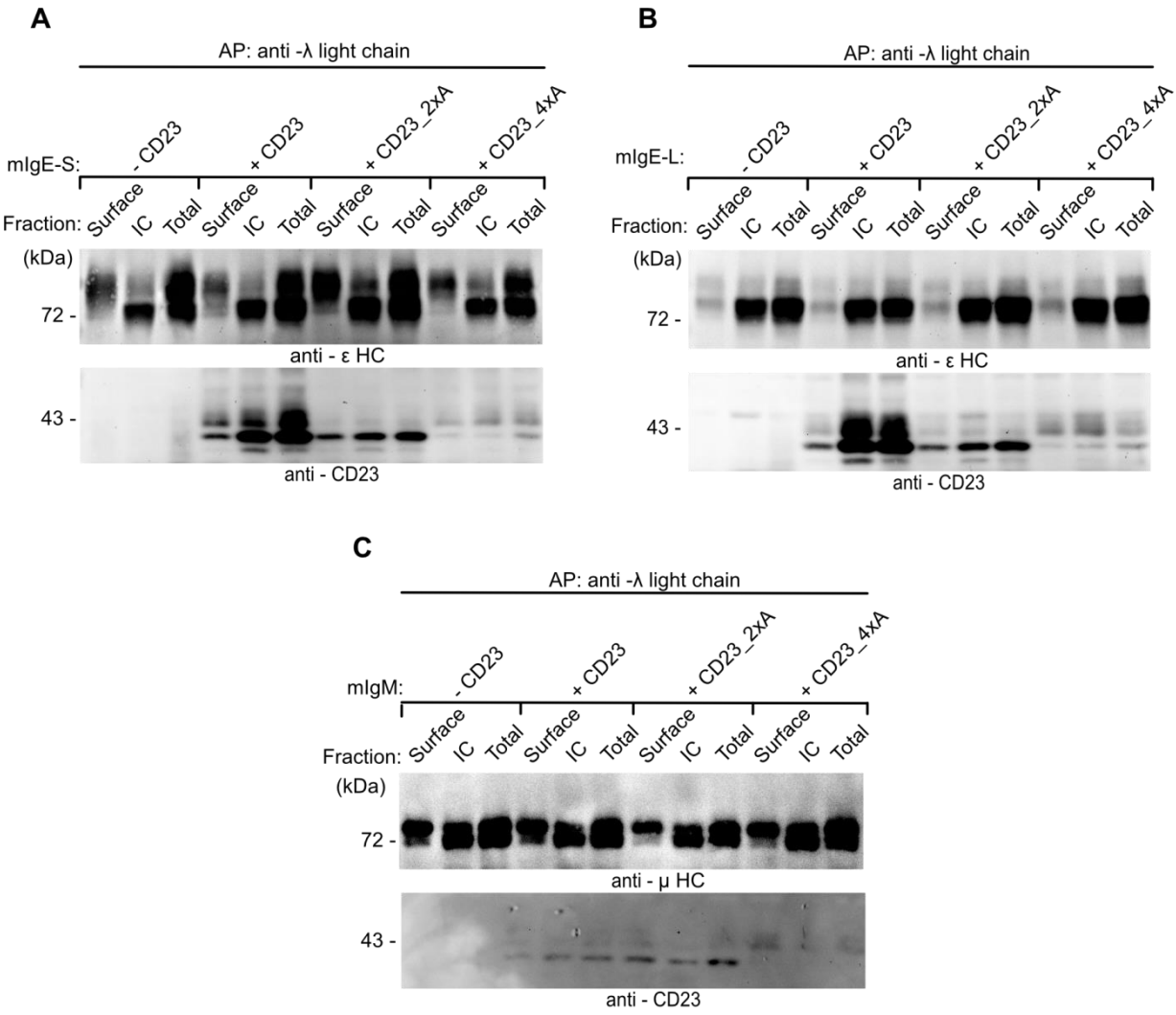

Figure 10: The mIgE-CD23 interaction mainly occurs intracellularly
A)+B) The two mIgE-BCR isoforms were affinity purified (AP) via biotinylated anti-mouse λ light chain antibodies and streptavidin sepharose from cells that had been labeled with the antibodies before lysis to purify the mIgE surface pool. The remaining lysates were used to purify the intracellular pool (IC) of mIgE molecules. Purified proteins were subsequently separated by SDS-PAGE and analyzed via Western Blot with antibodies to the ε HC (upper panel) or CD23 (lower panel). Ramos cells only expressing mIgE served as AP negative controls. The CD23 expression was induced by addition of 1μM Doxycycline to the cells 24h before performing the experiment. C) mIgM molecules were purified from the cell surface, IC or total cell lysates as mentioned in A)+B). Data is representative of three independent experiments.

IV.2.3 Induction of CD23 expression results in diminished mIgE-BCR induced Ca^{2+} -mobilization and reduced mIgE-S surface expression

Having shown that CD23 specifically binds to mIgE when co-expressed in the cell, the question arose, whether the mIgE-CD23 association might have an impact on the functionality of the mIgE-BCR. This was determined by analyzing the mIgE-BCR induced Ca^{2+}-mobilization in absence or presence of CD23 (Fig.11).

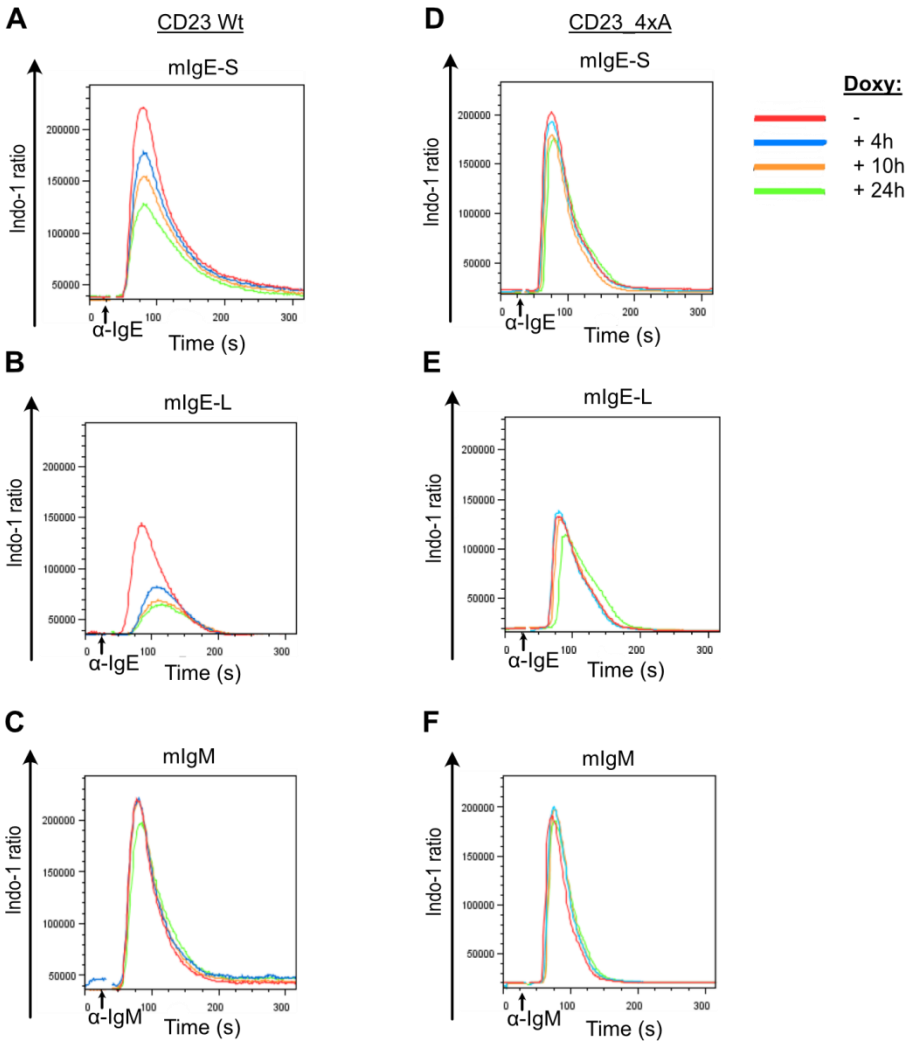

Figure 11: Induction of CD23 expression results in diminished mIgE-BCR induced Ca2+ -mobilization
Comparison of the Ca^{2+} mobilization of Ramos cell lines expressing CD23 (A-C) or CD23_4xA (D-F). The induction of CD23 expression was performed at various time points before measurement: 1µM Doxycycline was added 4h, 10h or 24h to the cells before starting the experiment. Untreated cells served as controls. Ca^{2+} mobilization was analyzed using Indo-1-AM. The baseline for Ca^{2+} levels were monitored for 30sec, following the addition of 20µg/ml stimulating anti-human IgE or anti-human IgM F(ab)'$_2$ fragments (indicated by arrows). Data are representative of three independent experiments

In order to track the impact of the increasing CD23 expression on the mIgE-BCR induced Ca^{2+} flux over the course of 24h, I added Doxycycline to the cells on different time points (e.g. 4h, 10h and 24h) before measurement. I could observe a clear reduction in the Ca^{2+} response of the mIgE-BCRs already 4h after induction of CD23 expression (Fig. 11A & B, blue lines). 24h after induction of CD23, the mIgE expressing cells showed a strongly diminished Ca^{2+} mobilization (Fig. 11A & B, green lines). In contrast, the mIgM-BCR-induced Ca^{2+} response remained unaffected by the expression of CD23 (Fig. 11C & F). By contrast, expression of CD23_4xA did not affect Ca^{2+} mobilization in any of the analyzed cells (Fig. 11D & E). Thus, this experiment revealed that the formation of mIgE-mCD23 complexes reduces the Ca^{2+} flux of activated mIgE-BCRs.

Since the association between CD23 and the different mIgE isoforms affected the BCR-induced Ca^{2+} response, I tested whether this effect correlated with a reduced mIgE-BCR surface expression. To this end, I analyzed the surface and total expression of both mIgE isoforms at various time points after induction of CD23 (Fig. 12). The surface expressed mIgE-S was significantly reduced 10h after induction of wild-type CD23 and was more than halved after 24h (Fig. 12A). Analysis of the total pool of mIgE-S revealed a trend towards reduced expression after induction of CD23, which however did not reach statistical significance. Notably, surface expression of the mIgE-L isoform was hardly affected by induction of CD23, whereas the total pool of mIgE-L was somewhat reduced, which – as for mIgE-S – did not reach statistical significance (Fig. 12A & B). The missing effects on the surface pool of mIgE-L may be due to its inefficient surface expression, which is caused by retention of this mIgE isoform in the ER [116]. Interestingly, the presence of the CD23_4xA mutant resulted in a mild but not statistically significant reduction of mIgE-S on the cell surface, whereas the surface pool of mIgE-L molecules remained unchanged as before (Fig. 12C). In summary, I discovered with these data that CD23, when co-expressed already in small amounts with the mIgE-S BCR, significantly reduces its surface expression.

Taken together, I showed that there exists an association between co-expressed CD23 and mIgE-BCRs, which mainly occurs in the ER. This receptor-receptor interaction not only leads to an inefficient transport of CD23 to the cell surface but also negatively regulates the surface expression of the mIgE-BCRs. This discovery appears to be directly associated with diminished Ca^{2+} mobilization. However, I could not at this stage exclude the contribution of additional intermediates in this regulatory process.

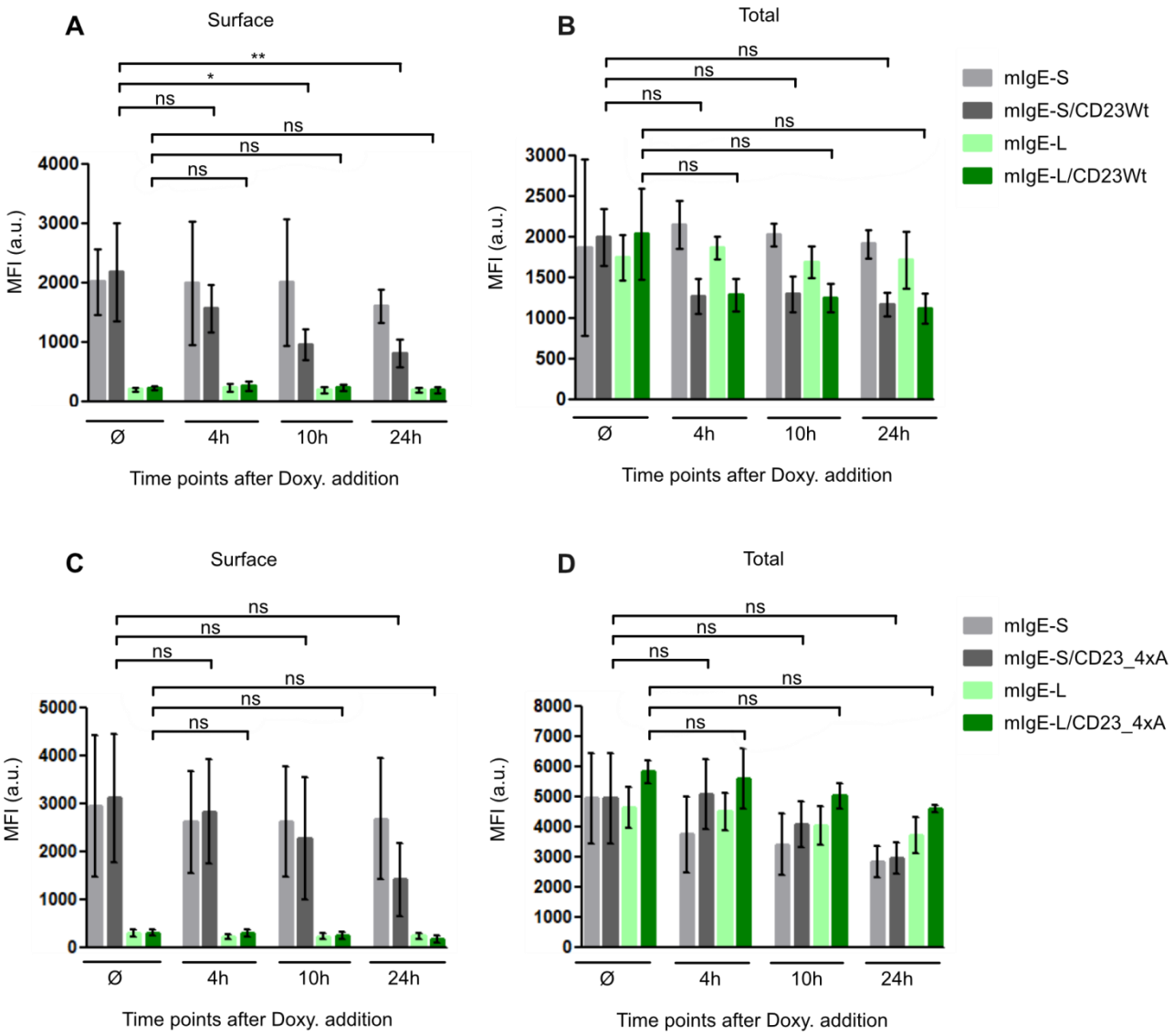

Figure 12: CD23 significantly reduces mIgE-S surface expression
Kinetics analysis of surface and total mIgE-expression after induction of CD23 (A+B) or CD23_4xA (C+D).The CD23 expression was induced by addition of 1µM Doxycycline to the cells, 4h, 10h or 24h before starting the experiment. Untreated cells served as controls. For analysis of the total mIgE-pool, the cells were fixed, permeabilized and stained with ant-human IgE PE-Cy7. The Mean fluorescence intensity (MFI) was determined by flow cytometry and the error bars indicate standard deviation of three independent experiments. Significances were calculated using two-way ANOVA followed by Tukey's multiple comparison test. **: $p<0.01$, *:$p<0.05$, ns: not significant, a.u.: arbitrary unit

IV.3 Analysis of the interaction between endogenously expressed human IgE and CD23

Since my results indicated that binding of CD23 to the human mIgE-BCR isoforms had an impact on both the surface expression as well as its signaling activity, the next important step was to compare this situation in B cells expressing the human mIgE-BCR isoforms using their endogenous promotor. That is important since so far I have been using expression vectors with promotors designed to overexpress cDNAs of the mIgE-BCRs. Thus, I induced the expression of the mIgE isoforms from the endogenous immunoglobulin heavy chain (IgH) locus in Ramos cells that normally express mIgM. This would enable a physiological mIgE expression on the plasma membrane.

IV.3.1 Properties of a novel B cell model expressing endogenous IgE

The generation of Ramos cells expressing mIgE in physiological amounts was accomplished by induced class-switch recombination (CSR), applied by the CRISPR/Cas9 genome editing system. During CSR, a part of the Ig heavy chain (HC) locus is removed from the chromosome, which is enabled by the induction of DNA double strand breaks, which are introduced by the B cell-specific enzyme AID. The idea was to mimic the function of AID by using CRISPR/Cas9 and a set of specifically adapted sgRNAs that bind to the μ switch region and the ε switch region, respectively. This enabled expression of the Ig ε HC under control of all endogenous, regulatory elements and therefore most likely results in natural amounts of mIgE expression on the plasma membrane. The detailed procedure is described in the Materials and Methods section in chapter II.2.1.4 and the experimental setup is additionally depicted in Figure 13A. In brief, the cell line Ramos was transfected with a mixture containing Cas9 and the respective sgRNAs via electroporation. Subsequently, the cells were sorted for lack of mIgM expression (Fig. 13A+B). The sorted mIgM-negative cell population had lost IgM expression in comparison to the pre-sorted culture (Fig. 13C). In order to eliminate stray mIgM-positive cells from the expanded cell population, the sorted cells were singularized by single cell dilution. Various sub-clones from this dilution were picked and screened for their surface and total IgE expression. I could barely detect mIgE or mIgM surface expression among the clones (Fig.13D, clones #35, #83 and #32, bright colored peaks). Consequently, I decided to base the identification of IgE+ clones on the staining results for the total IgE expression (Fig. 13D, clones #35, #83 and #32, dark colored peaks). The Clones #35, #83 and #32 display examples for an (m)IgE+ clone, an (m)IgM+ clone and a mixed population of (m)IgE+ and (m)IgM+ clones, respectively. From 30 screened sub-clones, 17 were (m)IgE positive and were merged to an oligoclonal population that displayed a very low mIgE surface expression (Fig. 13E).

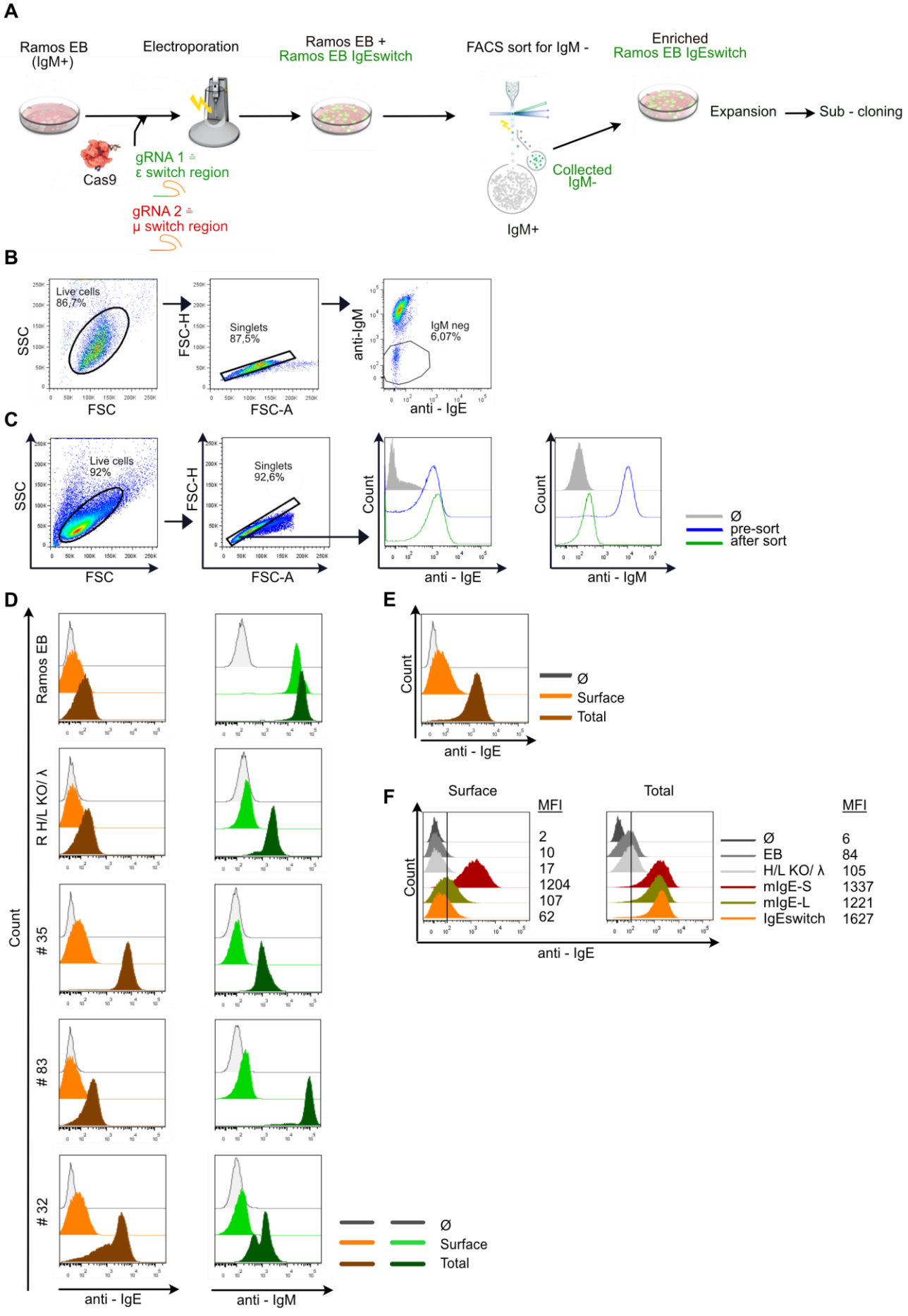
A
Ramos EB (IgM+)
Electroporation
Ramos EB + Ramos EB IgEswitch
FACS sort for IgM -
Enriched Ramos EB IgEswitch
Expansion
Sub - cloning
Cas9
gRNA 1 ≙ ε switch region
gRNA 2 ≙ μ switch region
Collected IgM-
IgM+
B
Live cells 86,7%
SSC
FSC
Singlets 87,5%
FSC-H
FSC-A
IgM neg 6,07%
anti-IgM
anti - IgE
C
Live cells 92%
Singlets 92,6%
Count
anti - IgE
anti - IgM
Ø
pre-sort
after sort
D
Ramos EB
R H/L KO/ λ
35
83
32
Count
anti - IgE
anti - IgM
Ø
Surface
Total
E
Count
anti - IgE
Ø
Surface
Total
F
Surface
Total
MFI
2
10
17
1204
107
62
MFI
6
84
105
1337
1221
1627
Ø
EB
H/L KO/ λ
mIgE-S
mIgE-L
IgEswitch
Count
anti - IgE

Figure 13: Properties of a novel B cell model expressing endogenous IgE
A) Experimental Setup: Induced class-switch recombination (CSR) was performed in Ramos EB cells by application of CRISPR/Cas9 genome editing system (for procedure s. Materials and Methods section, chapter III.2.1.4). B) Obtained mix-culture of IgM+ and IgE-switched cells was sorted for IgM- portion. C) Flow cytometric analysis of sorted and expanded IgM- cells and was singularized via single cell-dilution. D). Sub-clones were screened for IgE surface and total expression via flow cytometry. Clones #35, #83 and #32 display examples for an IgE+ clone, IgM+ clone and a mixed clone-population, respectively. 17 clones were screened IgE+ and gathered together as an oligoclonal population. Ramos EB cells were used as IgM positive controls and Ramos H/L KO/λ cells served as Ig negative control. Tinted peaks represent unstained samples, bright colored peaks depict surface Ig expression and dark colored peaks represent total Ig staining, respectively. E) Flow cytometric analysis of surface and total IgE expression in oligoclonal IgEswitch population F) compared to cell lines expressing mIgE-BCR isoforms. The MFI is listed on the right side of each panel. Gating on positive populations is indicated by vertical lines.

By comparing the mIgE surface pool of the IgE-switched cells with that of mIgE-S or mIgE-L expressing Ramos cells, I discovered that the amount of mIgE on the cell surface of IgE-switched cells is even lower than that of the mIgE-L expressing cells (Fig. 13F, left panel). Staining of IgE in permeabilized cells, however, revealed that the total amount of IgE in the three different cell types was comparable (Fig. 13F, right panel). In summary, these data show that the CRISPR/Cas9-induced switch to the ε locus resulted in the successful (m)IgE expression, which might possibly reflect the natural expression on the cell surface.

In order to identify the mIgE isoform expressed by the IgE-switched cell population, I purified the total IgE pool from these cells using biotinylated antibodies against the human ε heavy chain. To have a reference for the identification of the purified IgE-switched isoform, I performed the same approach with the mIgE-S and mIgE-L expressing cells, respectively. In this context, I observed that the IgE pool from the IgE-switched cells run at a lower molecular weight than the mIgE-S and mIgE-L isoforms (Fig. 14, lane 3-5).
This result implied that the novel cell model is expressing soluble IgE. To test this hypothesis, I additionally performed the IgE purification approach with the respective cellular medium of these cells giving a band in the medium samples for the IgE-switched cell, but not for mIgE-S and mIgE-L expressing cells (Fig. 14, lane 7-11) thus showing that the IgE-switched cells indeed produced soluble IgE. As a side note, the purified soluble IgE from the cellular lysates ran at a lower molecular weight in comparison to the secreted one in the medium. This is most likely due to the higher glycosylation of the soluble IgE after having left the intracellular compartment. In summary, these data show that the induced CSR resulted unexpectedly in cells preferentially expressing soluble IgE. In fact, similar observations about the preferential production of soluble IgE and a low membrane/ soluble IgE ratio were also made in murine B220+ IgE B cells upon previous stimulation [170], [123], [171]

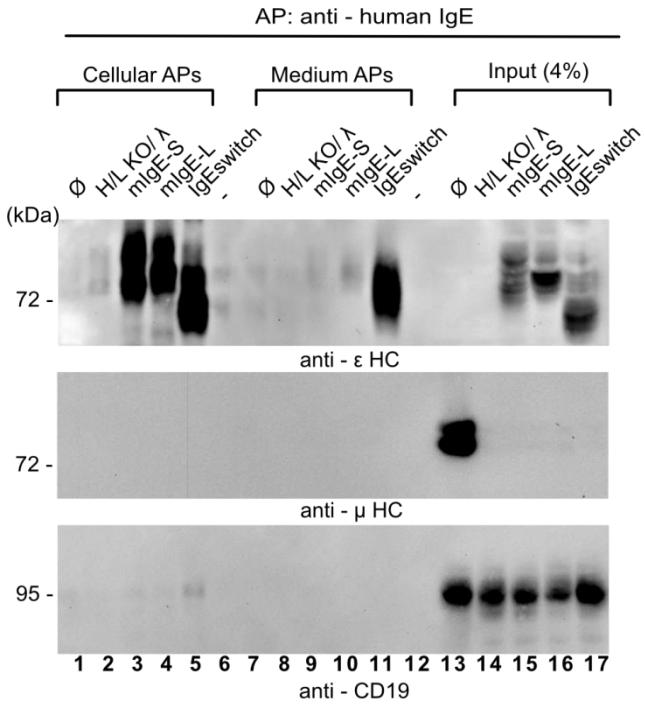

Figure 14: The IgE-switched B cells preferentially express soluble IgE
Biotinylated anti human IgE antibodies and streptavidin sepharose beads were used to purify the total pool of mIgE-S, mIgE-L and IgE-switched cells (lanes 1-5). To purify soluble IgE in the cellular medium, 2ml of the medium of the respective cell lines was prepared with anti human IgE and straptavidin sepharose beads (lanes 7-11). Cleared cellular lysates of $25x10^6$ cells were used as input controls and volume corresponding to one million cells was applied for analysis (lanes 13-17). Purified proteins were seperated by SDS-Page and analyzed by immunoblotting with antibodies to the ε HC (upper panel), μ HC (middle panel) and CD19 (lower panel). Ramos EB and Ramos H/L KO/ λ cells served as negative controls. Data is representative of three independently performed experiments.

In order to analyze the impact of permanently expressed CD23 on both the IgE-switched BCR and the mIgE isoforms, I introduced CD23 into the IgE-switched cells via retroviral transduction. In this context, I used a CD23-encoding construct, which enabled constitutive CD23 expression in the cells. Comparing the generated IgE-switched cells with those additionally expressing CD23, I observed a significant increase in the IgE surface signal of the CD23 transduced cells (Fig. 15A & C). Regarding the specificity of CD23 for soluble IgE, the question arose whether this signal might be the result of passively bound soluble IgE, which was produced by these cells in significant amounts (Fig. 14).

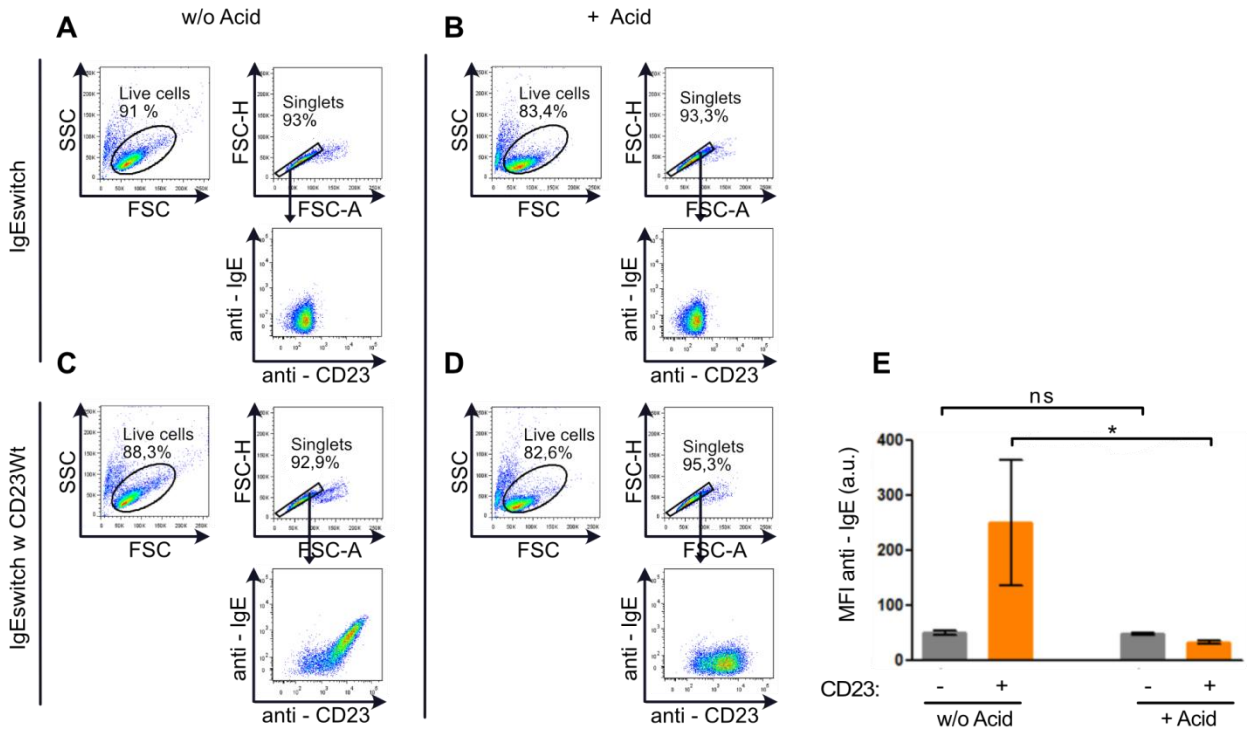

Figure 15: IgE-switched cells co-expressing CD23 give higher IgE signals than CD23 negative ones
Flow cytometric analysis of IgE-switched cells A)+B) and IgE-switched cells co-expressing CD23 C)+D).The cells have been left untreated A)+C) or treated with Acidic buffer B)+D) to get rid of passively bound secreted IgE, which results in reducing the IgE signal. E) Mean fluorescence intensities (MFI) of anti-IgE surface staining of IgE-switched cells in absence or presence of co-expressed CD23, either with or without Acidic treatment. Error bars indicate standard deviation of three independently performed experiments. Significances were calculated using unpaired student t-test. *: p<0,05, ns: not significant; a.u.: arbitrary unit; Data are representative for three independent experiments

To address this question, I briefly treated the cells with acidic buffer to get rid of any passively bound soluble IgE on the cell surface. Indeed, the acid treatment of CD23-expressing IgE-switched cells completely abrogated the IgE signal (Fig. 15B,D & E). This showed that the signal for IgE was caused by soluble IgE, which was passively bound to co-expressed CD23. In order to prevent these IgE signals, the following flow cytometric analyses of the IgE-switched cells were performed after acidic treatment.

IV.3.2 Co-expression of CD23 reduces mIgE-BCR surface expression and signaling

In the next step, I wanted to analyze whether the reducing impact of CD23 on the IgE surface expression can also be observed in Ramos cells expressing mIgE from the endogenous Ig locus, i.e. the IgE-switched cells. For this purpose, I used retroviral constructs encoding either CD23 or the CD23_4xA mutant, which enabled their constitutive expression in mIgE-expressing cells. Additionally, for comparison, I also transfected mIgM-expressing cells with

the same CD23 variants. After sorting out CD23-negative cells from all transfectants, CD23 expression was comparable among the cell lines (Fig. 16A-C and E-G, blue peaks in histograms). Further observations lead me to the assessment that CD23 expression in cells expressing the mIgE-BCR isoforms or the switched mIgE is 4 to 6 times higher in those expressing the CD23_4xA mutant in comparison to CD23 (Fig. 16, compare histograms A-C with E-G). This is consistent with the previous hypothesis that the IgE-CD23 complex is retained in the ER (Fig. 10), which hampers an efficient transport of CD23 to the cell surface. By contrast, CD23 expression remained unaffected in mIgM expressing cells (Fig. 16D & H).

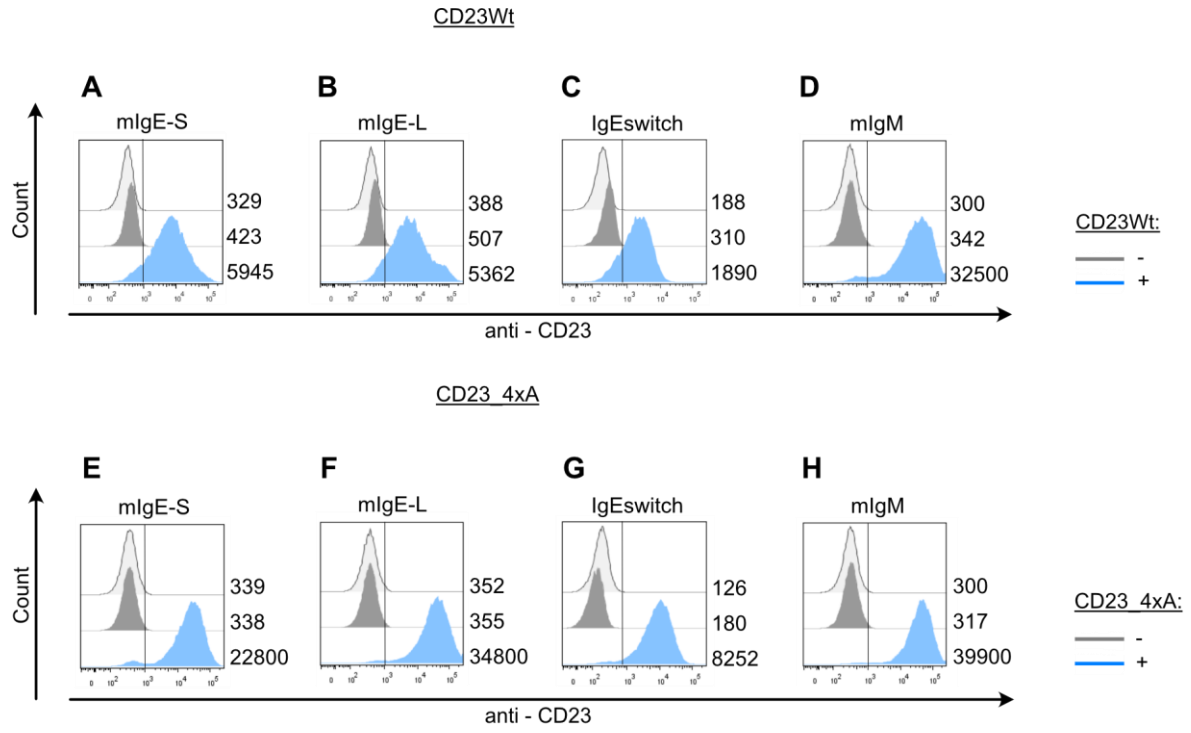

Figure 16: Intracellular IgE-CD23 association inhibits an efficient surface expression of CD23
A)-D) Surface expression of CD23 and E)-H) CD23_4xA mutant in mIgE-BCR or mIgM-BCR expressing Ramos cells. The tinted peaks in the histograms represent unstained samples, the grey colored peaks depict the respective BCR expressing cells without CD23 and blue colored peaks correspond to CD23 expression after sorting. Gating on positive populations is indicated by vertical lines.

I subsequently tracked the mIgE surface and total expression in absence or presence of the CD23 variants. The results are depicted in Figure 17. The BCR expression without CD23 is depicted in grey peaks whereas the colored peaks represent the respective BCR expression in the presence of CD23. Whereas the mIgE-L expression was not significantly affected by CD23 (Fig. 17B), I detected a significant reduction for the mIgE-S surface pool in the presence of CD23. Moreover, its total expression was more than halved (Fig. 17A). This inhibitory effect was abrogated when the IgE-CD23 interface was inactivated in the CD23_4xA mutant (Fig. 17E). Despite its low surface expression, also the BCR on IgE-switched cells revealed a clear reduction upon CD23 expression on the cell surface whereas

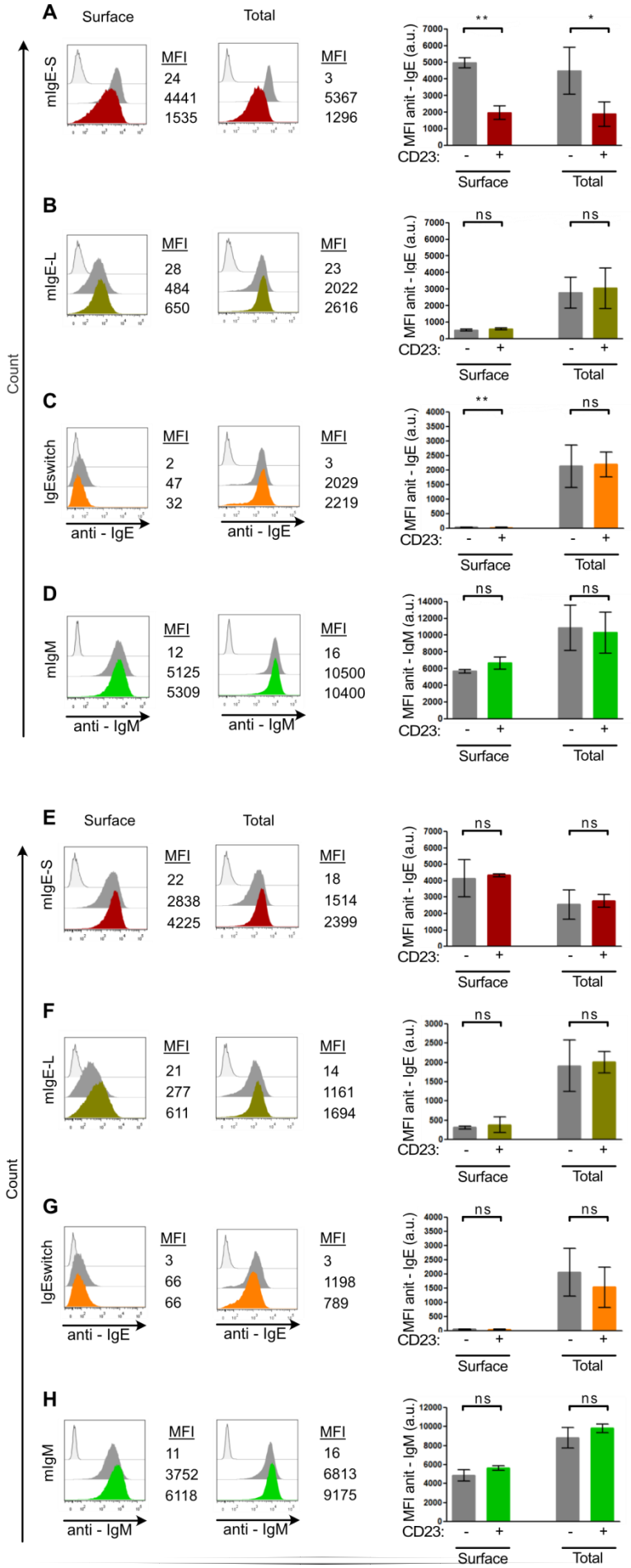
A
Surface
Total
mIgE-S
MFI
24
4441
1535
MFI
3
5367
1296
MFI anit - IgE (a.u.)
**
*
CD23:
Surface
Total
B
mIgE-L
MFI
28
484
650
MFI
23
2022
2616
ns
C
IgEswitch
anti - IgE
MFI
2
47
32
MFI
3
2029
2219
**
D
mIgM
anti - IgM
MFI
12
5125
5309
MFI
16
10500
10400
MFI anit - IgM (a.u.)
Count
E
mIgE-S
MFI
22
2838
4225
MFI
18
1514
2399
F
mIgE-L
MFI
21
277
611
MFI
14
1161
1694
G
IgEswitch
MFI
3
66
66
MFI
3
1198
789
H
mIgM
MFI
11
3752
6118
MFI
16
6813
9175

Figure 17: Permanently co-expressed CD23 significantly reduces the mIgE surface expression
Surface and Total mIgE expression was determined in Ramos cells expressing either mIgE-BCR or mIgM-BCR in absence (grey colored peaks and bars) or presence of CD23 A)-D) or CD23_4xA expression (colored peaks) E-H). The data are representative of three independent experiments. The tinted peaks correspond to unstained samples. For analyzing the total protein pool the respective cells were fixated and permeabilized before staining against IgE or IgM. The Mean florescence intensity (MFI) is listed on the right side of each panel. The statistics of the flow cytometric analysis are depicted in Bar graphs. The MFI was determined by flow cytometry and the error bars indicate the standard deviation of three independent experiments. Significances were calculated using unpaired student t-test. **: $p<0.01$, *:$p<0,05$, ns: not significant; a.u.: arbitrary unit

its total expression pool remained constant (Fig. 17C). Since, the IgEs-switched cells predominantly express soluble IgE (Fig. 13E & F, Fig. 14) one can conclude that their surface-expressed mIgE pool only represents a low proportion of their total IgE amount. This might be an explanation for their consistent IgE total pool in presence of CD23. In addition, the CD23_4xA mutant did not show a statistical significant impact on the total IgE-switched pool (Fig. 17G, orange bars). In contrast to the mIgE expressing cells, I could not detect significant changes in the expression of mIgM when co-expressed with CD23 (Fig. 17D & H). In summary, this data show that the direct interaction between CD23 and mIgE significantly diminishes the surface expression of mIgE-S. Similar findings could be observed for the IgE-switched cells.

It is well established that most mIgs need to associate with Igα and Igβ in order to get efficiently transported to the cell surface [43], [44], [170]. Hence, it was reasonable to assume that binding to CD23 impairs the assembly of mIgE-S with Igα/β, thus preventing the expression of a functional BCR on the cell surface. To test this hypothesis, I tracked the surface expression of both Igα and Igβ in the absence or presence of CD23 or CD23_4xA in mIgE-BCR expressing cells. Indeed, upon co-expression of CD23, the mIgE-S expressing cells showed a significant decrease in Igα and Igβ on the cell surface (Fig. 18A+B, blue and pink peaks and bars). However, this effect was lost in the presence of CD23_4xA (Fig. 18C+D, blue and pink peaks and bars). By contrast, both the mIgE-L expressing and IgE-switched cells obtained a constant Igα and Igβ expression independent of the co-expressed CD23 variants. In addition, CD23 also did not show any impact on the surface pool of both subunits in mIgM expressing cells. Thus, these data show that CD23 disrupts the association between mIgE-S and its subunits Igα and Igβ.

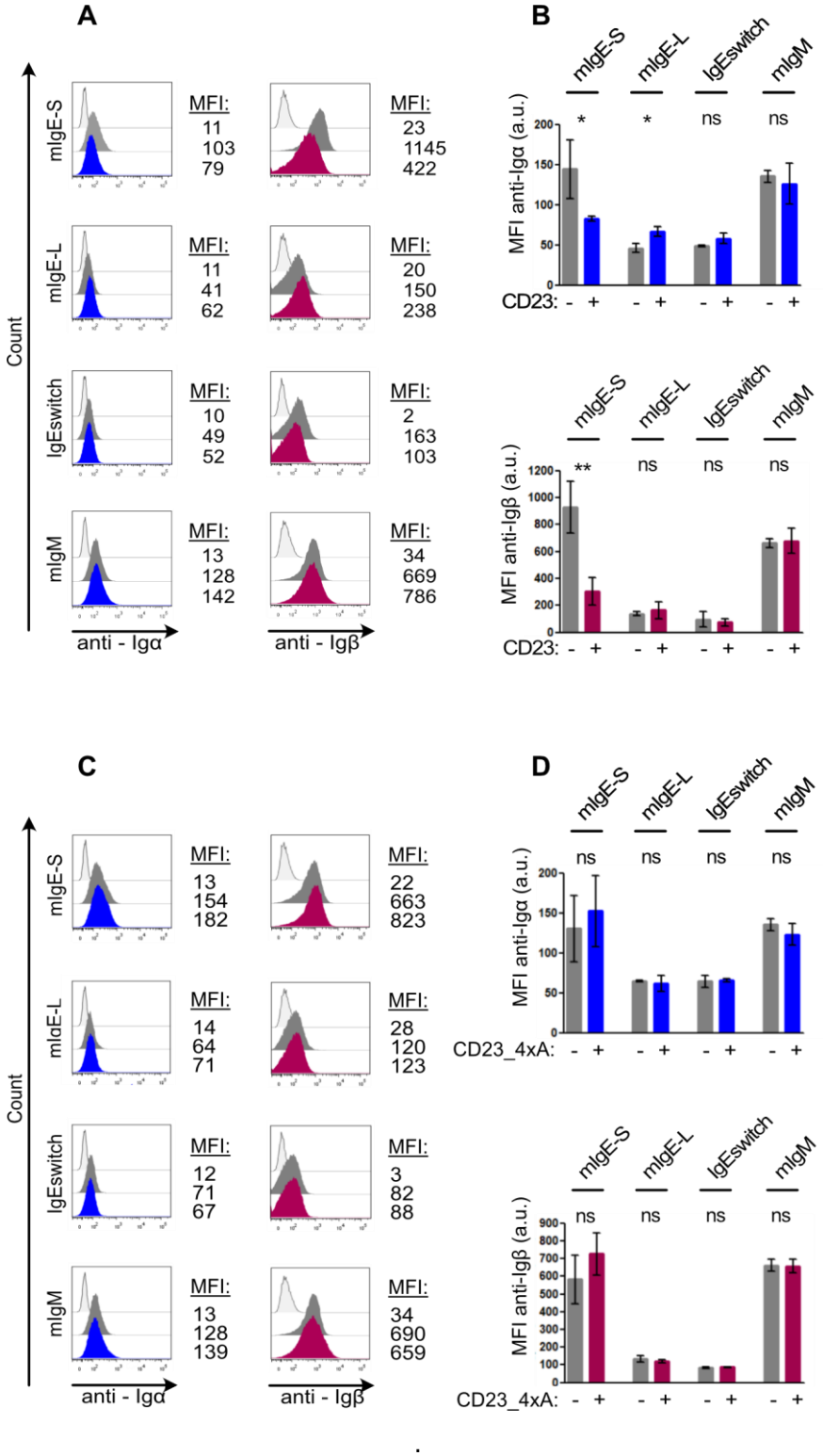

Figure 18: CD23 disrupts the association of Igα and Igβ subunits to the mIgE-S BCR
The surface expression of Igα (blue) and Igβ (pink) was analyzed in cells expressing either mIgE-BCR or mIgM-BCR in absence (grey colored bars and peaks) or presence (bright colored bars and peaks) of permanent CD23 (A+B) or CD23_4xA expression (C+D) by flow cytometry. Data in A + C is pooled from three independent experiments and error bars represent standard deviation. The histograms in B+D are representative of three independent experiments. The Mean florescence intensity (MFI) is given on the right side of each panel. Significances were calculated using unpaired student t-test. **: p<0.01, *:p<0,05, ns: not significant;

Having observed that the reducing impact of CD23 also applies for the IgE expression in IgE-switched B cells I was interested in its impact on the functional capabilities of the mIgE-BCRs. I found that Ca^{2+} mobilization of mIgE-S or mIgE-L BCR-expressing cells in the presence of wild-type CD23 was strongly reduced as compared to CD23-negative cells (Fig. 19A-C). This result is similar to the findings gained with the CD23 inducible system (Fig. 11A+B). Interestingly, despite the extremely low amount of surface BCR in IgE-switched cells, I could observe a subtle but detectable Ca^{2+} signal in these cells, which is clearly showing that their BCR is functional. It's induced Ca^{2+} signaling however disappeared with co-expression of CD23 (Fig. 19C). Since co-expression of the CD23_4xA mutant did not have an impact on the Ca^{2+} mobilization, it is reasonable to assume that the observed inhibitory effect of CD23 is based on its association to the mIgE-BCR (Fig. 19E-G). It is important to mention that mIgM-BCR induced Ca^{2+} signaling remained unaffected by CD23. This shows that the reducing impact of CD23 on the Ca^{2+} flux is IgE-specific (Fig. 19D+H).
In summary, the findings in Figure 19 show that the reducing impact on the mIgE surface expression of CD23 not only applies to the functionality of both mIgE-BCR isoforms, but also for the IgE-switched cell model and is also dependent on an intact IgE-CD23 interface. With regard to the diminished Ca^{2+} mobilization, it was fair to assume that this was also the result from a possibly reduced surface expression of the mIgE-BCRs.

In conclusion, I could show that CD23 also has a negative impact on the BCR signaling capability of endogenously expressed IgE. It is up to future investigations to find out, whether these findings are due to a direct association between the IgE-switched BCR and CD23. The results from the analysis of the Ca^{2+} mobilization would fit to this hypothesis. The reduced Ca^{2+} flux, which was observed for the IgE-switched BCR and the more abundantly expressed mIgE-S isoform, is probably due to a less efficient surface expression that might be based on a competitive binding of CD23 with the Igα and Igβ subunits.

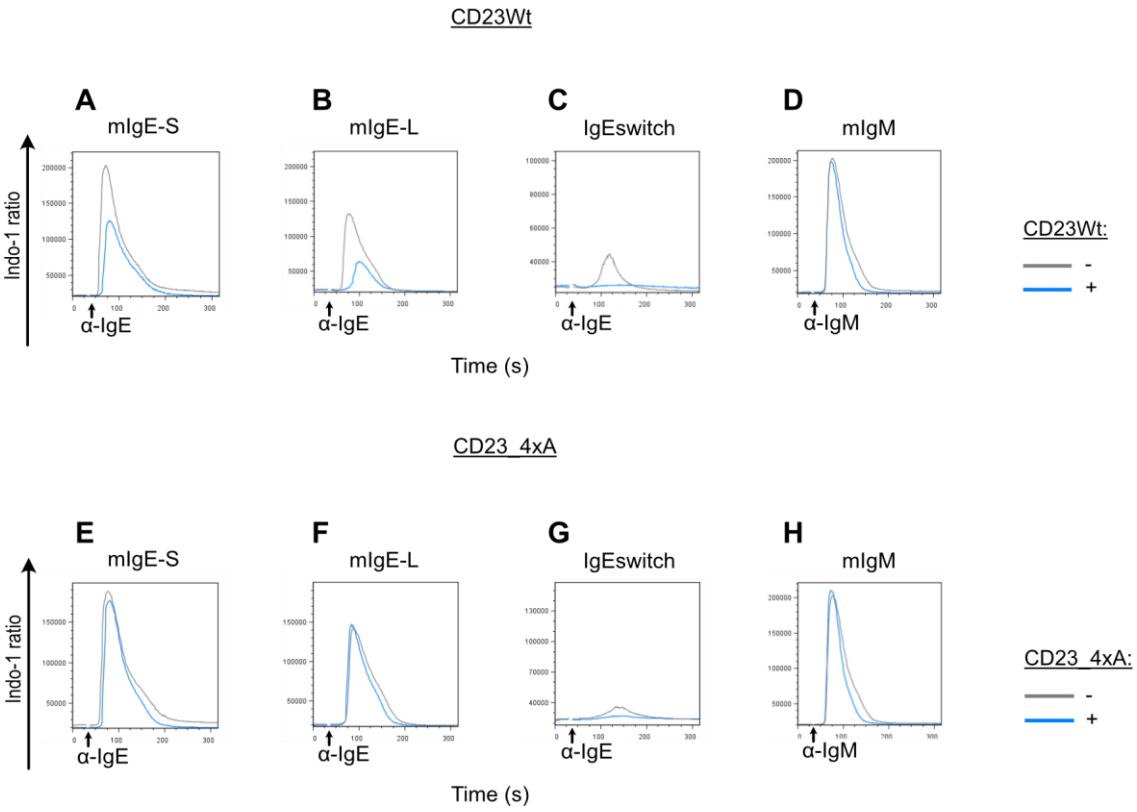

Figure 19: Constitutively co-expressed CD23 reduces mIgE-BCR induced Ca^{2+} mobilization
Comparison of the Ca^{2+} mobilization kinetics of mIgE- or mIgM-BCR expressing cells in absence or presence of either CD23 A)-D) or the CD23_4xA mutant E)-H) Ca^{2+} mobilization was analyzed using Indo-1-AM. The baseline for Ca^{2+} levels were monitored for 30sec, following the addition of 20µg/ml stimulating anti-human IgE or anti-human IgM F(ab)'2 fragments (indicated by arrows). Data are representative of three independent experiments

V Discussion

Due to the development of genetic mouse models that allow a deeper analysis of the functionality of mIgE-expressing B cells, our understanding regarding the biology of this scarce cell population has significantly improved [124], [125], [171]. IgE antibodies are principal mediators of most type I allergic reactions. Considering the fact that one third of the population of developed countries are effected by IgE-mediated allergic diseases, finding new and improving already existing strategies to inhibit IgE production or to block IgE-FcεRI complex formations is of great importance. In order to accomplish this goal, it is necessary to take a closer look at the processes, which regulate IgE expression and its functionality, as well as other protein interaction partners, which might have an impact on the mIgE-BCR functionality. In the course of my work I used murine and human B cell lines to investigate the receptor-receptor interactions of the murine and human mIgE-BCRs with the B cell co-receptor CD19 and the low affinity receptor for soluble IgE, CD23.

V.1 Testing the association of the murine mIgE-BCR with CD19 – an incomplete story

This chapter is dedicated to my work on testing a putative the direct interaction between the murine mIgE-BCR and the co-receptor CD19. Similar work has already been done and put on record in a previous publication of Haniuda et al., in which the authors reported about the role of the murine mIgE-BCR in the terminal differentiation fate of IgE-switched B cells to plasma cells. They observed in this context a direct interaction between the mIgE and CD19 in contrast to the mIgM- or mIgG1-BCR [133]. This observation was based on the successful co-purification of the murine mIgE-BCR and CD19 from whole cell lysates of B cells. I have studied their affinity purification approach and tested this interaction in the established murine cell line model J558L, which I have stably transfected with the murine CD19 and the same NIP-specific murine mIgE-BCR as indicated in the respective paper. Despite performing the mIgE-BCR purification approach as indicated in their materials and methods section and using the same substances with their appropriate concentrations, I could not observe a specific interaction between CD19 and NIP-BSA. Even multiple iterations of this experiment lead to the same result. Using an anti-mouse λ light chain matrix enabled a more specific purification of the murine mIgE-BCR. However, I still could not detect any association of CD19 with mIgE.

In their study, Haniuda et al [133] used a self-developed cell culture system in which splenic B cells derived from B1-8f Cγ1-Cre mice eventually express only a particular BCR of choice. It is conceivable that my cellular model system may not express unknown intermediates required as linkers for the interaction between CD19 and murine mIgE. For instance, CD19 is

also part of a multi-protein complex consisting of the complement receptor CD21 and CD81, where CD19 functions as a signaling-transducing element [75],[79],[87]. In this regard, it would be reasonable to assume that CD21 or CD81 might function as mediators of the interaction with the mIgE-BCR.

Even though the interaction analysis between the murine mIgE-BCR and the co-receptor CD19 did not lead to conclusive results, my analysis of the interaction between the human mIgE-BCR isoforms and CD23, however, was more successful.

V.2 New insights into the regulation of the human mIgE-BCR

CD23 is part of a complex regulatory mechanism controlling IgE synthesis in B cells. Based on the data presended in this chapter of my study, I propose that CD23 directly associates with the human mIgE-BCR isoforms and, subsequently negatively regulates the surface expression and functionality of the human mIgE. Furthermore, CD23 might hamper the regular assembly of the Igα/Igβ subunits to the mIgE, which probably leads to the ER retention of mIgE resulting in a reduced surface expression and a subsequently diminished BCR induced Ca^{2+} mobilization.

V.2.1 CD23 can directly associate with the human mIgE-BCR isoforms

Not long ago it was possible to identify the properties of the CD23-binding site in IgE via side directed mutagenesis and nuclear magnetic resonance (NMR) technique [153]. In my work I revealed for the first time that CD23 and the human mIgE-BCR isoforms directly associate with each other if co-expressed in the B cell. Side-directed mutagenesis of the amino acids Histidine 186, Arginine 188, Tyrosine 189 and Arginine 224 in the IgE binding site of CD23 additionally indicated that this protein-protein interaction is based on the prevalent association between the CD23 lectin head domains and the Cε3 domain. Interestingly, I observed that this IgE-specific receptor association mainly occurs in the ER. Even though CD23 is part of the C-type lectin superfamily its association to IgE occurs in a carbohydrate independent manner (e.g. no lectin- like activity of the CD23 head domains is necessary) [92],[169],[172]. This correlates with my observation that mIgE-S, independent from its glycosylation, associates with CD23, which happens while passing the ER and the Golgi apparatus. This hypothesis is supported by mIgE-L, which could also associate with CD23 but did not show differences in its glycosylation due to its ER retention [116].

In contrast to the intracellular situation, the amount of surface-expressed mIgE and CD23 was quite low hinting towards two possible explanations: first, the surface detected mIgE-S remained mostly unbound from CD23 and second, the mIgE-CD23 association resulted in an ER-retention of CD23 preventing its efficient surface expression.

The idea of an ER-retention of CD23 due to its association with mIgE corresponds to the FACS data presented in Figure 16 that shows that the mIgE expressing cells have a lower surface expression for CD23 in comparison to the CD23_4xA variant. It is currently unknown whether the IgE association might have a conformational effect on CD23. Therefore, future investigations of the structure of the CD23-mIgE association are required in order to make a clear statement in this regard.

V.2.2 The inhibitory impact of the mIgE-CD23 association on the mIgE surface expression and its functionality

My further investigations regarding the consequences of the mIgE-CD23 association revealed a significant reduction of the surface expression of the mIgE-S isoform. This is in accordance with the reported inhibitory effect of IgE-crosslinked CD23 on the IgE expression in transgenic mouse models [149], [159], [160]. However, to my knowledge the inhibitory impact of CD23 has not yet been individually analyzed for each of the human mIgE-BCR isoforms. Based on my data, I came to the conclusion that the inhibitory effect of CD23 might be based on its association with mIgE occurring in the ER. This association was disrupted in cells co-expressing the CD23_4xA variant resulting in an unaffected IgE expression. One possible explanation for the less efficient surface expression of mIgE-S upon binding to CD23 is an incorrect assembly of mIgE-S with the subunits Igα and Igβ due to their displacement by CD23. Indeed, the surface expression of Igα and Igβ was significantly reduced in mIgE-S expressing cells upon expression of CD23. Similar to other mIg isotypes, the mIgE-BCR complex consists of mIgE together with the Igα/Igβ heterodimer [49],[44],[43],[111]. The mIg-Igα/Igβ complex must be assembled correctly in the ER to guarantee its efficient transport to the plasma membrane. Hence, a competitive binding and blocking of the Igα/Igβ subunits by CD23 in the ER would result in a defective mIgE-BCR complex formation and thus in its inefficient transport to the cell surface.
Additionally, recent research showed that mIgE-S can be expressed on the B cell surface in the absence of the Igα/Igβ heterodimer, a property that depends on the cytoplasmic tail of mIgE [52]. In this context, analyzing how the absence of Igα/Igβ effects the mIgE-CD23 association might be a good starting point for future investigations.

Another possible explanation for the reduced surface expression of mIgE-S might be conformational changes arising from its association to CD23. In fact, the structural interaction between IgE and CD23 has been well documented and revealed that IgE-FC can exist in open and closed conformations with only the closed state being capable of binding CD23 [153],[173],[174]. A detailed study of the crystal structure showed a high flexibility in the Cε3

helix. It includes the binding sites of both CD23 and the high-affinity IgE-specific FcεRI, however at opposite ends [173], [174]. Furthermore, it has been reported that despite the opposing binding position of the IgE-specific receptors on the IgE-Fc domain, they are allosterically coupled thus, resulting in a conformational change of IgE, which disables a simultaneous binding of FcεRI and vice versa. Hence, a coincidental binding of both IgE specific receptors at IgE is impossible due to reciprocal allosteric inhibition [153], [174], [175],[147]. Considering the huge conformational changes that are induced by the IgE-CD23 interaction, one could assume that these structural alterations might also compromise mIgE-S's subsequent expression on the cell surface.

However, the CD23-induced negative effects on the mIgE surface expression could barely be observed for the mIgE-L isoform. This may be due to its inefficient surface expression, which is caused by its retention in the ER through the EMPD [111],[116]. Even though I could not detect an effect on the surface expression of mIgE-L, CD23 may also have an impact on this isoform. Similar findings could be observed for the IgE-switched cells whose surface expression was even lower than that of mIgE-L. Whereas the mIgE surface pool on IgE-switched cells showed a significant reduction upon CD23 expression, their total mIgE pool remained unaffected. A possible explanation may be that the majority of the total IgE pool in these cells is expressed intracellularly.

A typical approach for monitoring B cell signaling is the analysis of BCR induced Ca^{2+} mobilization. Upon BCR stimulation, I observed that the mIgE-CD23 association resulted in a significant reduction of the Ca^{2+} flux for both human mIgE isoforms as well as the IgE-switched cells. In case of mIgE-S this might be due to its significantly reduced expression.

In this context, the impaired assembly of mIgE-S with the Igα/Igβ heterodimer due to the mIgE-CD23 association resulted in a reduced surface expression and thus a lower amount of mIgE-S BCRs that could be activated and monitored. The same may apply for the mIgE-L isoform and the IgE-switched BCR despite their low surface expression.

Another explanation for the reduced BCR induced Ca^{2+} mobilization could be that CD23 directly affects components of the mIgE-BCR signaling cascade. The mechanisms underlying the inhibitory impact of CD23 on the mIgE-BCR activation are still largely unknown. There already exist reports about the negative impact of murine CD23 on the phosphorylation of Bruton's tyrosine kinase (BTK). BTK is an essential part of the Ca^{2+} initiation complex [176]. Since the phosphorylation of BTK requires a number of prior steps like the activation of kinase Syk, CD23 may actually have an impact on earlier stages and components of the BCR singling cascade [176]–[178]. Additionally, Btk activation can be enhanced by the co-receptor complex CD19/CD21/CD81 [179]. This suggests that CD23 may be able to directly interfere with the Btk activation through its interaction with CD21

[134], [154] and thus restrict the assembly of a functional Ca^{2+} initiation complex. It is up to future investigations to find out whether and how the association between CD23 and mIgE affects the IgE signaling cascade.

In order to find possible explanations regarding the impact of CD23 on the mIgE-BCR functionality, taking a look at the phosphorylation of CD23 may prove useful. Phosphorylation in lymphocytes is tightly associated with the regulation of protein expression, functionality and various cell signaling pathways [180]. CD23a is one of two existing isoforms of CD23 and is constitutively expressed on B cells. It contains a tyrosine residue at position 6 and a serine residue at position 7 both of which are predictive sites for phosphorylation. In regards to the suppressive impact of CD23 on the IgE production in transgenic mice [142], [149], [150], it is reasonable to assume that phosophorylation of constitutively expressed CD23a, induced via its crosslinking with IgE might contribute to the regulation of the mIgE expression. It would be interesting for future investigations to analyze, whether CD23 is phosphorylated in association with mIgE and, if applicable, how this condition effects the expression of mIgE.

V.3 What we can learn from the IgE-switched B cell model

Over the course of my work, I managed to generate a human B cell model expressing IgE from its endogenous promotor using the CRISPR/Cas9 editing system. To my knowledge, this is the first one of its kind and may reflect mIgE expression in physiological amounts. Interestingly, this model revealed an unexpected preferential production of soluble IgE and a significantly lower mIgE-surface expression in comparison to my mIgE-L expressing cells. These properties can also be observed in another Burkitt-Lymphoma B cell line called DG75 (data not shown) and are comparable to properties of a plasma cell, despite plasma cells normally lose the expression of mIg and switch to the production of soluble Ig. In addition, plenty of reports about mIgE expression in mouse and human plasma cells already exist [123], [124], [171], [181]. In fact, the low membrane IgE/soluble IgE ratio as implied in my B cell model, has already been observed previously in human and murine plasma cells *in vivo* [123],[182],[181], [171]. According to these reports, the discrepancy between both IgE forms may be the result of the inefficient polyadenylation of mIgE. Usually, the consensus AATAAA sequence represents the internal polyadenylation signal for soluble IgE in both human and mouse IgE genes. In contrast, there are three divergent polyadenylation sequences (AGTAA, AAGAAA, and ATTAAA) for mIgE located in the 3'UTR downstream of the M exons (see Fig. 2). These unusual polyadenylation signals hamper the necessary polyadenylation for mIgE and thus result in the preferential production of soluble IgE instead of mIgE [170],[182].

This might serve as a proper explanation for the permanent difficulties in the past to successfully identify mIgE expressing B cells.
Currently, most studies agree on a transient presence of mIgE expressing GC B cells and a long living pool of mIgE positive plasma cells [52],[123],[182],[181]. Studies of mIgE-positive B cells in mice reported that the majority of these cells were plasma cells [125], [183]. Considering the preferable production of soluble IgE in my IgE-switched B cell model, it is reasonable to assume that mIgE positive B cells might already express plasma cell-like properties. An important aspect of B cell memory is the long-term production of soluble Ig by plasma cells, which result from a rapid expansion and differentiation of quiescent B cells upon antigen re-encounter [184]. In view of the preferential expression of soluble IgE by human and murine IgE positive B cells [123], [182] it appears questionable whether there exist such a quiescent state for IgE positive B cells. The existence of an IgE memory is still subject of in-depth discussions. The predominant consensus in this field is that IgE memory originate from mIgG1- positive B cells, which undergo sequential class-switching and differentiation to IgE producing plasma cells upon antigen encounter [123], [171]. This could be demonstrated by γ1 remnants in the switch regions of the ε locus. However, concrete details regarding molecular mechanisms behind the IgE memory is still largely unknown since most reports in this field are based on mIgG1 expressing B cells [52].

In conclusion, by applying this innovative IgE-switched B cell model I could show that induced isotype class switching to IgE might result in a preferential expression of soluble IgE and a low mIgE/soluble IgE ratio. Throughout numerous reports, it has been stated that the mIgE surface expression is a critical determinant for the differentiation fate of IgE-switched cells and the subsequent production of IgE antibodies [124], [125], [183]. Therefore, it appears reasonable to assume that the low expression of mIgE-BCR on the cell surface might represent another natural regulatory mechanism, which might have evolved to restrict the production of soluble IgE especially in regards to its powerful and harmful anaphylactic properties.

V.4 Conclusions

The results of my PhD thesis reveal a mechanism by which CD23 interacts with the human mIgE-BCR isoforms and regulates their surface expression and functionality. So far, several models have been proposed explaining how CD23 regulates IgE synthesis. Whereas soluble CD23 enhances IgE expression, membrane CD23 suppresses IgE synthesis. It appears that a balance between the two CD23 forms may exist, which may regulate the level of IgE expression. However, in order to understand the mechanisms of IgE regulation and to develop therapeutics for IgE conditioned diseases, it is necessary to study the structure of CD23 and its interaction with IgE. Based on my results, CD23 is capable of directly associating to co-expressed human mIgE-BCRs in the ER, which leads to a less efficient surface expression of mIgE-S alongside a significant inhibition of the BCR-induced Ca^{2+} mobilization.

As far as I know, this is the first analysis of the regulatory impact of CD23 on the human mIgE-BCR isoforms. Currently, immunotherapies of patients with severe allergies are based on neutralizing soluble IgE, which inhibits the IgE-FcεRI interaction. However, this therapy does not target IgE already bound to mast cells, which is the reason why the treatment has to continue throughout [140]. Therefore, strategies to block the IgE synthesis are of extreme interest. The data presented herein may provide the basis for future investigations focusing on the inhibition of IgE synthesis.

VI Bibliography

[1] D. D. Chaplin, “1. Overview of the human immune response,” *Journal of Allergy and Clinical Immunology*, vol. 117, no. 2 SUPPL. 2. 2006.

[2] R. Medzhitov and C. A. Janeway, “How does the immune system distinguish self from nonself?,” *Semin. Immunol.*, 2000.

[3] D. D. Chaplin, “Overview of the immune response,” *J. Allergy Clin. Immunol.*, 2010.

[4] C. A. Janeway Jr. and R. Medzhitov, “Innate immune recognition,” *Annu Rev Immunol*, 2002.

[5] OpenStax, *OpenStax, Anatomy & Physiology*. OpenStax CNX., 2016.

[6] P. S. Hiemstra, “The role of epithelial β-defensins and cathelicidins in host defense of the lung,” in *Experimental Lung Research*, 2007.

[7] U. Holmskov, S. Thiel, and J. C. Jensenius, “ C OLLECTINS AND F ICOLINS : Humoral Lectins of the Innate Immune Defense ,” *Annu. Rev. Immunol.*, 2003.

[8] A. P. Sjöberg, L. A. Trouw, and A. M. Blom, “Complement activation and inhibition: a delicate balance,” *Trends in Immunology*. 2009.

[9] B. Beutler, K. Hoebe, X. Du, and R. J. Ulevitch, “How we detect microbes and respond to them: the Toll-like receptors and their transducers,” *J. Leukoc. Biol.*, 2003.

[10] M. Schnare, G. M. Barton, A. C. Holt, K. Takeda, S. Akira, and R. Medzhitov, “Toll-like receptors control activation of adaptive immune responses,” *Nat. Immunol.*, 2001.

[11] O. Takeuchi *et al.*, “Differential roles of TLR2 and TLR4 in recognition of gram-negative and gram-positive bacterial cell wall components,” *Immunity*, 1999.

[12] A. Iwasaki and R. Medzhitov, “Control of adaptive immunity by the innate immune system,” *Nature Immunology*. 2015.

[13] C. A. Janeway, “Approaching the asymptote? Evolution and revolution in immunology,” in *Cold Spring Harbor Symposia on Quantitative Biology*, 1989.

[14] R. Medzhitov and C. A. Janeway, “Innate immune induction of the adaptive immune response,” in *Cold Spring Harbor Symposia on Quantitative Biology*, 1999.

[15] J. C. Zúñiga-Pflücker, “T-cell development made simple,” *Nature Reviews Immunology*. 2004.

[16] Y. Takahama, “Journey through the thymus: Stromal guides for T-cell development and selection,” *Nature Reviews Immunology*. 2006.

[17] F. A. Bonilla and H. C. Oettgen, “Adaptive immunity,” *J. Allergy Clin. Immunol.*, 2010.

[18] R. Shinnakasu and T. Kurosaki, “Regulation of memory B and plasma cell differentiation,” *Current Opinion in Immunology*, vol. 45. pp. 126–131, 2017.

[19] R. Alam and M. Gorska, “3. Lymphocytes,” *Journal of Allergy and Clinical*

Immunology. 2003.

[20] M. D. Cooper, “The early history of B cells,” *Nat. Rev. Immunol.*, 2015.

[21] J. V. Stein and C. Nombela-Arrieta, “Chemokine control of lymphocyte trafficking: A general overview,” *Immunology*. 2005.

[22] R. Ahmed and J. Sprent, “Immunological memory,” *Immunologist*. 1999.

[23] T. Inoue, I. Moran, R. Shinnakasu, T. G. Phan, and T. Kurosaki, “Generation of memory B cells and their reactivation,” *Immunological Reviews*. 2018.

[24] R. A. GOOD and S. J. ZAK, “Disturbances in gamma globulin synthesis as experiments of nature.,” *Pediatrics*, 1956.

[25] A. Fagraeus, “Plasma cellular reaction and its relation to the formation of antibodies in vitro [1],” *Nature*. 1947.

[26] A. H. COONS, E. H. LEDUC, and J. M. CONNOLLY, “Studies on antibody production. I. A method for the histochemical demonstration of specific antibody and its application to a study of the hyperimmune rabbit.,” *J. Exp. Med.*, 1955.

[27] T. W. Lebien and T. F. Tedder, “B lymphocytes: How they develop and function,” *Blood*, 2008.

[28] M. D. Cooper and M. N. Alder, “The evolution of adaptive immune systems,” *Cell*. 2006.

[29] E. von Behring and S. Kitasato, “Ueber das Zustandekommen der Diphtherie-Immunität und der Tetanus-Immunität bei Thieren.,” *Mol. Immunol.*, 1991.

[30] J. F. Miller and G. F. Mitchell, “Cell to cell interaction in the immune response. I. Hemolysin-forming cells in neonatally thymectomized mice reconstituted with thymus or thoracic duct lymphocytes.,” *J. Exp. Med.*, 1968.

[31] X. Chi, Y. Li, and X. Qiu, “V(D)J recombination, somatic hypermutation and class switch recombination of immunoglobulins: mechanism and regulation,” *Immunology*. 2020.

[32] Z. Xu, H. Zan, E. J. Pone, T. Mai, and P. Casali, “Immunoglobulin class-switch DNA recombination: Induction, targeting and beyond,” *Nature Reviews Immunology*. 2012.

[33] H. W. Schroeder and L. Cavacini, “Structure and function of immunoglobulins,” *J. Allergy Clin. Immunol.*, 2010.

[34] A. F. Williams and A. N. Barclay, “The immunoglobulin superfamily - Domains for cell surface recognition,” *Annual Review of Immunology*. 1988.

[35] S. Tonegawa, “Somatic generation of antibody diversity,” *Nature*, 1983.

[36] J. Stavnezer, J. E. J. Guikema, and C. E. Schrader, “Mechanism and Regulation of Class Switch Recombination,” *Annu. Rev. Immunol.*, 2008.

[37] K. Yu and M. R. Lieber, “Current insights into the mechanism of mammalian immunoglobulin class switch recombination,” *Critical Reviews in Biochemistry and*

Molecular Biology. 2019.

[38] D. D. Dudley, J. Chaudhuri, C. H. Bassing, and F. W. Alt, “Mechanism and control of V(D)J recombination versus class switch recombination: Similarities and differences,” *Adv. Immunol.*, 2005.

[39] H. Zan and P. Casali, “Regulation of Aicda expression and AID activity,” *Autoimmunity*. 2013.

[40] P. Soulas-Sprauel *et al.*, “V(D)J and immunoglobulin class switch recombinations: A paradigm to study the regulation of DNA end-joining,” *Oncogene*. 2007.

[41] M. Muramatsu, K. Kinoshita, S. Fagarasan, S. Yamada, Y. Shinkai, and T. Honjo, “Class switch recombination and hypermutation require activation-induced cytidine deaminase (AID), a potential RNA editing enzyme,” *Cell*, 2000.

[42] M. Reth and J. Wienands, “INITIATION AND PROCESSING OF SIGNALS FROM THE B CELL ANTIGEN RECEPTOR,” *Annu. Rev. Immunol.*, vol. 15, no. 1, pp. 453–479, 1997.

[43] J. Hombach, T. Tsubata, L. Leclercq, H. Stappert, and M. Reth, “Molecular components of the B-cell antigen receptor complex of the IgM class,” *Nature*, 1990.

[44] A. R. Venkitaraman, G. T. Williams, P. Dariavach, and M. S. Neuberger, “The B-cell antigen receptor of the five immunoglobulin classes,” *Nature*, 1991.

[45] P. Ehrlich, “On immunity with specific reference to cell life,” *Proc R Soc London*, 1900.

[46] P. Ehrlich, “Partial cell functions : Nobel lecture, December 11, 1908.,” in *Physiology or Medicine: including presentation speeches and laureates’ biographies ; 1901-1921 (1967)*, 1908.

[47] M. D. Cooper, D. A. Raymond, R. D. Peterson, M. A. South, and R. A. Good, “The functions of the thymus system and the bursa system in the chicken.,” *J. Exp. Med.*, 1966.

[48] F. M. Burnet, *The clonal selection theory of acquired immunity.* 2011.

[49] W. W. A. Schamel and M. Reth, “Stability of the B cell antigen receptor complex,” *Mol. Immunol.*, 2000.

[50] W. W. A. Schamel and M. Reth, “Monomeric and oligomeric complexes of the B cell antigen receptor,” *Immunity*, vol. 13, no. 1, pp. 5–14, 2000.

[51] K. S. Campbell, E. J. Hager, and J. C. Cambier, “Alpha-chains of IgM and IgD antigen receptor complexes are differentially N-glycosylated MB-1-related molecules.,” *J. Immunol.*, 1991.

[52] K. Vanshylla, “The membrane IgE tail imparts unique signaling properties to the B cell antigen receptor,” 2016.

[53] C. Volkmann, N. Brings, M. Becker, E. Hobeika, J. Yang, and M. Reth, “Molecular requirements of the B- cell antigen receptor for sensing monovalent antigens,” *EMBO*

J., 2016.

[54] P. Tolar, H. W. Sohn, W. Liu, and S. K. Pierce, “The molecular assembly and organization of signaling active B-cell receptor oligomers,” *Immunological Reviews*. 2009.

[55] J. Yang and M. Reth, “Oligomeric organization of the B-cell antigen receptor on resting cells,” *Nature*, 2010.

[56] J. Yang and M. Reth, “The dissociation activation model of B cell antigen receptor triggering,” *FEBS Letters*. 2010.

[57] K. Kläsener, P. C. Maity, E. Hobeika, J. Yang, and M. Reth, “B cell activation involves nanoscale receptor reorganizations and inside-out signaling by Syk,” *Elife*, 2014.

[58] P. C. Maity, A. Blount, H. Jumaa, O. Ronneberger, B. F. Lillemeier, and M. Reth, “B cell antigen receptors of the IgM and IgD classes are clustered in different protein islands that are altered during B cell activation.,” *Sci. Signal.*, vol. 8, no. 394, p. ra93, 2015.

[59] R. J. Benschop and J. C. Cambier, “B cell development: Signal transduction by antigen receptors and their surrogates,” *Curr. Opin. Immunol.*, 1999.

[60] J. Wienands, O. Larbolette, and M. Reth, “Evidence for a preformed transducer complex organized by the B cell antigen receptor,” *Proc. Natl. Acad. Sci. U. S. A.*, 1996.

[61] M. Reth, “Antigen receptor tail clue [5],” *Nature*. 1989.

[62] H. Flaswinkel and M. Reth, “Dual role of the tyrosine activation motif of the Ig-alpha protein during signal transduction via the B cell antigen receptor.,” *EMBO J.*, 1994.

[63] J. A. Taddie, T. R. Hurley, B. S. Hardwick, and B. M. Sefton, “Activation of B- and T-cells by the cytoplasmic domains of the B-cell antigen receptor proteins Ig-α and Ig-β,” *J. Biol. Chem.*, 1994.

[64] M. R. Clark, S. A. Johnson, and J. C. Cambier, “Analysis of Ig-alpha-tyrosine kinase interaction reveals two levels of binding specificity and tyrosine phosphorylated Ig-alpha stimulation of Fyn activity.,” *EMBO J.*, 1994.

[65] D. L. Burg, M. T. Furlong, M. L. Harrison, and R. L. Geahlen, “Interactions of Lyn with the antigen receptor during B cell activation,” *J. Biol. Chem.*, 1994.

[66] R. Schmitz, G. Baumann, and H. Gram, “Catalytic specificity of phosphotyrosine kinases Blk, Lyn, c-Src and Syk as assessed by phage display,” *J. Mol. Biol.*, 1996.

[67] M. R. Gold, L. Matsuuchi, R. B. Kelly, and A. L. DeFranco, “Tyrosine phosphorylation of components of the B-cell antigen receptors following receptor crosslinking,” *Proc. Natl. Acad. Sci. U. S. A.*, 1991.

[68] L. I. Pao, S. J. Famiglietti, and J. C. Cambier, “Asymmetrical phosphorylation and function of immunoreceptor tyrosine-based activation motif tyrosines in B cell antigen

receptor signal transduction.," *J. Immunol.*, 1998.

[69] N. Engels, B. Wollscheid, and J. Wienands, "Association of SLP-65/BLNK with the B cell antigen receptor through a non-ITAM tyrosine of Ig-α," *Eur. J. Immunol.*, 2001.

[70] M. Takata and T. Kurosaki, "A role for Bruton's tyrosine kinase in B cell antigen receptor-mediated activation of phospholipase C-γ2," *J. Exp. Med.*, 1996.

[71] S. Bhattacharyya *et al.*, "NFATc1 affects mouse splenic B cell function by controlling the calcineurin-NFAT signaling network," *J. Exp. Med.*, 2011.

[72] Y. Baba and T. Kurosaki, "Role of calcium signaling in B cell activation and biology," *Curr. Top. Microbiol. Immunol.*, 2015.

[73] T. T. Su *et al.*, "PKC-β controls IκB kinase lipid raft recruitment and activation in response to BCR signaling," *Nat. Immunol.*, 2002.

[74] R. Sen, "Control of B Lymphocyte Apoptosis by the Transcription Factor NF-κB," *Immunity*. 2006.

[75] Y. Wen *et al.*, "The regulators of BCR signaling during B cell activation," *Blood Sci.*, 2019.

[76] R. Elgueta, M. J. Benson, V. C. De Vries, A. Wasiuk, Y. Guo, and R. J. Noelle, "Molecular mechanism and function of CD40/CD40L engagement in the immune system," *Immunol. Rev.*, vol. 229, no. 1, pp. 152–172, 2009.

[77] J. C. Cambier, C. M. Pleiman, and M. R. Clark, "Signal transduction by the B cell antigen receptor and its coreceptors," *Annual Review of Immunology*. 1994.

[78] D. Depoil *et al.*, "CD19 is essential for B cell activation by promoting B cell receptor-antigen microcluster formation in response to membrane-bound ligand," *Nat. Immunol.*, 2008.

[79] D. T. Fearon and M. C. Carroll, "Regulation of B lymphocyte responses to foreign and self-antigens by the CD19/CD21 complex," *Annual Review of Immunology*. 2000.

[80] H. Ying, Z. Li, L. Yang, and J. Zhang, "Syk mediates BCR- and CD40-signaling integration during B cell activation," *Immunobiology*, 2011.

[81] G. A. Bishop and B. S. Hostager, "The CD40-CD154 interaction in B cell-T cell liaisons," *Cytokine and Growth Factor Reviews*. 2003.

[82] M. Fujimoto, J. C. Poe, P. J. Jansen, S. Sato, and T. F. Tedder, "CD19 amplifies B lymphocyte signal transduction by regulating Src- family protein tyrosine kinase activation," *J. Immunol.*, 1999.

[83] M. Hasegawa, M. Fujimoto, J. C. Poe, D. A. Steeber, and T. F. Tedder, "CD19 Can Regulate B Lymphocyte Signal Transduction Independent of Complement Activation," *J. Immunol.*, vol. 167, no. 6, pp. 3190–3200, Sep. 2001.

[84] R. H. Carter and D. T. Fearon, "CD19: Lowering the threshold for antigen receptor stimulation of B lymphocytes," *Science (80-.).*, vol. 256, no. 5053, pp. 105–107, Apr.

1992.

[85] A. Cherukuri, P. C. Cheng, H. W. Sohn, and S. K. Pierce, “The CD19/CD21 complex functions to prolong B cell antigen receptor signaling from lipid rafts,” *Immunity*, vol. 14, no. 2, pp. 169–179, Feb. 2001.

[86] R. C. Rickert, “Regulation of B lymphocyte activation by complement C3 and the B cell coreceptor complex,” *Current Opinion in Immunology*, vol. 17, no. 3. Curr Opin Immunol, pp. 237–243, Jun-2005.

[87] “Atlas of immunology,” *Choice Rev. Online*, 2011.

[88] R. C. Rickert, K. Rajewsky, and J. Roes, “Impairment of T-cell-dependent B-cell responses and B-1 cell development in CD19-deficient mice,” vol. 3, no. July, pp. 352–355, 1995.

[89] L. Mesin, J. Ersching, and G. D. Victora, “Germinal Center B Cell Dynamics,” *Immunity*. 2016.

[90] C. D. C. Allen, T. Okada, and J. G. Cyster, “Germinal-Center Organization and Cellular Dynamics,” *Immunity*. 2007.

[91] N. S. De Silva and U. Klein, “Dynamics of B cells in germinal centres,” *Nat. Rev. Immunol.*, vol. 15, no. 3, 2015.

[92] H. J. Gould and B. J. Sutton, “IgE in allergy and asthma today,” *Nature Reviews Immunology*. 2008.

[93] H. W. Schroeder and L. Cavacini, “Structure and function of immunoglobulins,” *J. Allergy Clin. Immunol.*, vol. 125, no. 2 SUPPL. 2, Feb. 2010.

[94] B. Corthésy, “Roundtrip Ticket for Secretory IgA: Role in Mucosal Homeostasis?,” *J. Immunol.*, 2007.

[95] A. W. Frankland, “Carl Prausnitz: a personal memoir.,” *J. Allergy Clin. Immunol.*, vol. 114, no. 3, pp. 700–705, Sep. 2004.

[96] S. T. Holgate, “New strategies with anti-IgE in allergic diseases,” *World Allergy Organization Journal*, vol. 7, no. 1. 2014.

[97] K. Ishizaka, T. Ishizaka, and M. M. Hornbrook, “Physicochemical Properties of Reaginic Antibody,” *J. Immunol.*, vol. 97, no. 6, 1966.

[98] S. G. O. Johansson, “The discovery of IgE,” *J. Allergy Clin. Immunol.*, vol. 137, no. 6, 2016.

[99] M. Dullaers, R. De Bruyne, F. Ramadani, H. J. Gould, P. Gevaert, and B. N. Lambrecht, “The who, where, and when of IgE in allergic airway disease,” *Journal of Allergy and Clinical Immunology*. 2012.

[100] L. C. Wu and A. A. Zarrin, “The production and regulation of IgE by the immune system,” *Nat. Rev. Immunol.*, 2014.

[101] C. L. King, R. W. Poindexter, J. Ragunathan, T. A. Fleisher, E. A. Ottesen, and T. B.

Nutman, “Frequency analysis of IgE-secreting B lymphocytes in persons with normal or elevated serum IgE levels.,” *J. Immunol.*, 1991.

[102] H. J. Gould and B. J. Sutton, “IgE in allergy and asthma today,” *Nature Reviews Immunology*, vol. 8, no. 3. pp. 205–217, 2008.

[103] H. J. Gould *et al.*, “The biology of IGE and the basis of allergic disease.,” *Annu. Rev. Immunol.*, vol. 21, pp. 579–628, 2003.

[104] J. Hu, J. Chen, L. Ye, Z. Cai, J. Sun, and K. Ji, “Anti-IgE therapy for IgE-mediated allergic diseases: from neutralizing IgE antibodies to eliminating IgE+B cells,” *Clin. Transl. Allergy*, vol. 8, no. 1, 2018.

[105] D. Maurer and G. Stingl, “Immunoglobulin E-binding structures on antigen-presenting cells present in skin and blood,” *Journal of Investigative Dermatology*. 1995.

[106] A. Navinés-Ferrer, E. Serrano-Candelas, G. J. Molina-Molina, and M. Martín, “IgE-Related Chronic Diseases and Anti-IgE-Based Treatments,” *Journal of Immunology Research*. 2016.

[107] P. Gasser and A. Eggel, “Targeting IgE in allergic disease,” *Current Opinion in Immunology*, vol. 54. 2018.

[108] W. Busse *et al.*, “Omalizumab, anti-IgE recombinant humanized monoclonal antibody, for the treatment of severe allergic asthma,” *J. Allergy Clin. Immunol.*, 2001.

[109] T. Kawakami and U. Blank, “From IgE to Omalizumab,” *J. Immunol.*, vol. 197, no. 11, 2016.

[110] S. Holgate, R. Buhl, J. Bousquet, N. Smith, Z. Panahloo, and P. Jimenez, “The use of omalizumab in the treatment of severe allergic asthma: A clinical experience update,” *Respir. Med.*, 2009.

[111] F. D. Batista, S. Anand, G. Presani, D. G. Efremov, and O. R. Burrone, “The two membrane isoforms of human IgE assemble into functionally distinct B cell antigen receptors,” *J. Exp. Med.*, vol. 184, no. 6, pp. 2197–2205, 1996.

[112] K. Zhang, A. Saxon, and E. E. Max, “Two unusual forms of human immunoglobulin E encoded by alternative RNA splicing of epsilon heavy chain membrane exons.,” *J. Exp. Med.*, vol. 176, no. 1, pp. 233–43, 1992.

[113] C. Peng *et al.*, “A new isoform of human membrane-bound IgE1,” *J.Immunol.*, vol. 148, no. 1, pp. 129–136, 1992.

[114] F. D. Batista, D. G. Efremov, T. Tkach, and O. R. Burrone, “Characterization of the human immunoglobulin epsilon mRNAs and their polyadenylation sites.,” *Nucleic Acids Res.*, vol. 23, no. 23, pp. 4805–4811, 1995.

[115] G. Achatz, M. Lamers, and R. Crameri, “Membrane Bound IgE: The Key Receptor to Restrict High IgE Levels,” *Open Immunol. J.*, 2008.

[116] K. Vanshylla, F. Opazo, K. Gronke, J. Wienands, and N. Engels, “The extracellular

membrane-proximal domain of membrane-bound IgE restricts B cell activation by limiting B cell antigen receptor surface expression," *European Journal of Immunology*, 2017.

[117] R. S. Geha, H. H. Jabara, and S. R. Brodeur, "The regulation of immunoglobulin E class-switch recombination," *Nature Reviews Immunology*. 2003.

[118] J. F. Gauchat *et al.*, "Induction of human IgE synthesis in B cells by mast cells and basophils," *Nature*, 1993.

[119] R. Pawankar, M. Okuda, H. Yssel, K. Okumura, and C. Ra, "Nasal mast cells in perennial allergic rhinitics exhibit increased expression of the FcεRI, CD40L, IL-4, and IL-13, and can induce IgE synthesis in B cells," *J. Clin. Invest.*, 1997.

[120] I. S. Grewal and R. A. Flavell, "The Role of CD40 Ligand in Costimulation and T-Cell Activation," *Immunol. Rev.*, vol. 153, no. 153, pp. 85–106, 1996.

[121] G. Achatz, L. Nitschke, and M. C. Lamers, "Effect of transmembrane and cytoplasmic domains of IgE on the IgE response," *Science (80-.).*, vol. 276, no. 5311, pp. 409–411, 1997.

[122] B. Laffleur, O. Debeaupuis, Z. Dalloul, and M. Cogné, "B cell intrinsic mechanisms constraining IgE memory," *Frontiers in Immunology*, vol. 8, no. NOV. 2017.

[123] J.-S. He *et al.*, "The distinctive germinal center phase of IgE $^{+}$ B lymphocytes limits their contribution to the classical memory response," *J. Exp. Med.*, vol. 210, no. 12, pp. 2755–2771, 2013.

[124] A. Erazo *et al.*, "Unique Maturation Program of the IgE Response In Vivo," *Immunity*, vol. 26, no. 2, pp. 191–203, 2007.

[125] O. Talay *et al.*, "IgE+ memory B cells and plasma cells generated through a germinal-center pathway," *Nat. Immunol.*, vol. 13, no. 4, pp. 396–404, 2012.

[126] J. M. Davies, T. A. Platts-Mills, and R. C. Aalberse, "The enigma of IgE+ B-cell memory in human subjects," *J. Allergy Clin. Immunol.*, 2013.

[127] A. A. Zarrin, M. Tian, J. Wang, T. Borjeson, and F. W. Alt, "Influence of switch region length on immunoglobulin class switch recombination," *Proc. Natl. Acad. Sci. U. S. A.*, vol. 102, no. 7, pp. 2466–2470, Feb. 2005.

[128] J. A. Hackney *et al.*, "Chapter 5 DNA Targets of AID. Evolutionary Link Between Antibody Somatic Hypermutation and Class Switch Recombination," *Advances in Immunology*. 2009.

[129] T. Honjo, K. Kinoshita, and M. Muramatsu, "Molecular Mechanism of Class Switch Recombinantion: Linkage with Somatic Hypermutation," *Annu. Rev. Immunol.*, 2002.

[130] S. Misaghi *et al.*, "Polyclonal hyper-IgE mouse model reveals mechanistic insights into antibody class switch recombination," *Proc. Natl. Acad. Sci. U. S. A.*, vol. 110, no. 39, pp. 15770–15775, Sep. 2013.

[131] Z. Yang *et al.*, “Regulation of B cell fate by chronic activity of the IgE B cell receptor,” *Elife*, vol. 5, 2016.

[132] M. Acharya *et al.*, “CD23/Fc??RII: Molecular multi-tasking,” *Clinical and Experimental Immunology*, vol. 162, no. 1. pp. 12–23, 2010.

[133] K. Haniuda, S. Fukao, T. Kodama, H. Hasegawa, and D. Kitamura, “Autonomous membrane IgE signaling prevents IgE-memory formation,” *Nat. Immunol.*, vol. 17, no. 9, pp. 1109–1117, 2016.

[134] J. P. Aubry *et al.*, “CD23 interacts with a new functional extracytoplasmic domain involving N-linked oligosaccharides on CD21.,” *J. Immunol.*, vol. 152, no. 12, pp. 5806–13, 1994.

[135] A. Yokota *et al.*, “Two species of human Fcε receptor II (FcεRII CD23): Tissue-specific and IL-4-specific regulation of gene expression,” *Cell*, vol. 55, no. 4, pp. 611–618, Nov. 1988.

[136] D. H. Conrad, J. W. Ford, J. L. Sturgill, and D. R. Gibb, “CD23: An overlooked regulator of allergic disease,” *Current Allergy and Asthma Reports*. 2007.

[137] A. Getahun, F. Hjelm, and B. Heyman, “ IgE Enhances Antibody and T Cell Responses In Vivo via CD23 + B Cells ,” *J. Immunol.*, 2005.

[138] K. Maeda *et al.*, “Murine follicular dendritic cells and low affinity Fc receptors for IgE (Fc epsilon RII).,” *J. Immunol.*, vol. 148, no. 8, 1992.

[139] M. A. Ewart, B. W. Ozanne, and W. Cushley, “The CD23a and CD23b proximal promoters display different sensitivities to exogenous stimuli in B lymphocytes,” *Genes Immun.*, 2002.

[140] D. H. Conrad, J. W. Ford, J. L. Sturgill, and D. R. Gibb, “CD23: An overlooked regulator of allergic disease,” *Current Allergy and Asthma Reports*, vol. 7, no. 5. pp. 331–337, 2007.

[141] M. Sarfati, S. Fournier, C. Y. Wu, and G. Delespesse, “Expression, regulation and function of human FcεRII (CD23) antigen,” *Immunol. Res.*, vol. 11, no. 3–4, pp. 260–272, Dec. 1992.

[142] P. Yu, M. Kosco-Vilbois, M. Richards, G. Köhler, and M. C. Lamers, “Negative feedback regulation of IgE synthesis by murine CD23,” *Nature*, 1994.

[143] J. A. Mathews *et al.*, “A potential new target for asthma therapy: A Disintegrin and Metalloprotease 10 (ADAM10) involvement in murine experimental asthma,” *Allergy Eur. J. Allergy Clin. Immunol.*, 2011.

[144] G. Weskamp *et al.*, “ADAM10 is a principal ‘sheddase’ of the low-affinity immunoglobulin E receptor CD23,” *Nat. Immunol.*, vol. 7, no. 12, pp. 1293–1298, Dec. 2006.

[145] G. A. Lemieux *et al.*, “The low affinity IgE receptor (CD23) is cleaved by the

metalloproteinase ADAM10," *J. Biol. Chem.*, vol. 282, no. 20, pp. 14836–14844, May 2007.

[146] D. R. Gibb *et al.*, "ADAM10 is essential for Notch2-dependent marginal zone B cell development and CD23 cleavage in vivo," *J. Exp. Med.*, 2010.

[147] B. J. Sutton and A. M. Davies, "Structure and dynamics of IgE-receptor interactions: FcεRI and CD23/FcεRII," *Immunological Reviews*, vol. 268, no. 1. pp. 222–235, 2015.

[148] N. McCloskey *et al.*, "Soluble CD23 monomers inhibit and oligomers stimulate IGE synthesis in human B cells," *J. Biol. Chem.*, vol. 282, no. 33, pp. 24083–24091, 2007.

[149] M. E. Payet, E. C. Woodward, and D. H. Conrad, "Humoral response suppression observed with CD23 transgenics," *J. Immunol.*, 1999.

[150] M. C. LAMERS and P. YU, "Regulation of IgE Synthesis. Lessons from the Study of IgE Transgenic and CD23-deficient Mice," *Immunol. Rev.*, 1995.

[151] J. Shi *et al.*, "Interaction of the low-affinity receptor CD23/FcεRII lectin domain with the Fcε3-4 fragment of human immunoglobulin E," *Biochemistry*, 1997.

[152] B. Dhaliwal *et al.*, "IgE binds asymmetrically to its B cell receptor CD23," *Sci. Rep.*, vol. 7, 2017.

[153] S. Borthakur *et al.*, "Mapping of the CD23 binding site on immunoglobulin e (IgE) and allosteric control of the IgE-FcεRI interaction," *J. Biol. Chem.*, vol. 287, no. 37, pp. 31457–31461, 2012.

[154] J. P. Aubry, S. Pochon, P. Graber, K. U. Jansen, and J. Y. Bonnefoy, "CD21 is a ligand for CD23 and regulates IgE production," *Nature*, 1992.

[155] D. T. Fearon and R. H. Carter, "The CD19/CR2/TAPA-1 Complex of B Lymphocytes: Linking Natural to Acquired Immunity," *Annu. Rev. Immunol.*, vol. 13, no. 1, pp. 127–149, 1995.

[156] C. Liu, K. Richard, M. Wiggins, X. Zhu, D. H. Conrad, and W. Song, "CD23 can negatively regulate B-cell receptor signaling," *Sci. Rep.*, 2016.

[157] A. M. Cooper *et al.*, "Soluble CD23 Controls IgE Synthesis and Homeostasis in Human B Cells," *J. Immunol.*, 2012.

[158] A. Stief, G. Texido, G. Sansig, H. Eibel, G. Le Gros, and H. van der Putten, "Mice deficient in CD23 reveal its modulatory role in IgE production but no role in T and B cell development.," *J. Immunol.*, vol. 152, no. 7, 1994.

[159] H. Luo, H. Hofstetter, J. Banchereau, and G. Delespesse, "Cross-linking of CD23 antigen by its natural ligand (IgE) or by anti-CD23 antibody prevents B lymphocyte proliferation and differentiation," *J. Immunol.*, 1991.

[160] E. Sherr, E. Macy, H. Kimata, M. Gilly, and A. Saxon, "Binding the low affinity FcεR on B cells suppresses ongoing human IgE synthesis," *J. Immunol.*, 1989.

[161] M. Fellmann, P. Buschor, S. Röthlisberger, F. Zellweger, and M. Vogel, "High affinity

targeting of CD23 inhibits IgE synthesis in human B cells," *Immun. Inflamm. Dis.*, 2015.

[162] R. G. Hibbert *et al.*, "The structure of human CD23 and its interactions with IgE and CD21," *J. Exp. Med.*, vol. 202, no. 6, pp. 751–760, 2005.

[163] S. W. Cho, M. A. Kilmon, E. J. Studer, H. Van Der Putten, and D. H. Conrad, "B cell activation and Ig, especially IgE, production is inhibited by high CD23 levels in vivo and in vitro," *Cell. Immunol.*, 1997.

[164] S. Morita, T. Kojima, and T. Kitamura, "Plat-E: An efficient and stable system for transient packaging of retroviruses," *Gene Ther.*, 2000.

[165] G. Klein, B. Giovanella, A. Westman, J. S. Stehlin, and D. Mumford, "An EBV-genome-negative cell line established from an American burkitt lymphoma; receptor characteristics. EBV infectibility and permanent conversion into EBV-positive sublines by in vitro infection," *Intervirology*, 1975.

[166] K. Weber and M. Osborn, "The reliability of molecular weight determinations by dodecyl sulfate-polyacrylamide gel electrophoresis.," *J. Biol. Chem.*, 1969.

[167] H. Towbin, T. Staehelin, and J. Gordon, "Electrophoretic transfer of proteins from polyacrylamide gels to nitrocellulose sheets: Procedure and some applications," *Proc. Natl. Acad. Sci. U. S. A.*, 1979.

[168] M. Reth, "Antigen receptors on B lymphocytes," *Annual Review of Immunology*. 1992.

[169] B. Dhaliwal *et al.*, "Crystal structure of IgE bound to its B-cell receptor CD23 reveals a mechanism of reciprocal allosteric inhibition with high affinity receptor FcεRI.," *Proc. Natl. Acad. Sci. U. S. A.*, vol. 109, no. 31, pp. 12686–91, 2012.

[170] J. S. He, S. Narayanan, S. Subramaniam, W. Q. Ho, J. J. Lafaille, and M. A. C. De Lafaille, "Biology of ige production: Ige cell differentiation and the memory of ige responses," *Curr. Top. Microbiol. Immunol.*, 2015.

[171] Z. Yang, B. M. Sullivan, and C. D. C. Allen, "Fluorescent In Vivo Detection Reveals that IgE+ B Cells Are Restrained by an Intrinsic Cell Fate Predisposition," *Immunity*, vol. 36, no. 5, pp. 857–872, 2012.

[172] D. Vercelli, B. Helm, P. Marsh, E. Padlan, R. S. Geha, and H. Gould, "The B-cell binding site on human immunoglobulin E," *Nature*, vol. 338, no. 6217, pp. 649–651, 1989.

[173] B. A. Wurzburg, S. C. Garman, and T. S. Jardetzky, "Structure of the human IgE-Fc Cε3-Cε4 reveals conformational flexibility in the antibody effector domains," *Immunity*, vol. 13, no. 3, pp. 375–385, Sep. 2000.

[174] M. D. Holdom *et al.*, "Conformational changes in IgE contribute to its uniquely slow dissociation rate from receptor FcIRI," *Nat. Struct. Mol. Biol.*, vol. 18, no. 5, 2011.

[175] S. C. Garman, B. A. Wurzburg, S. S. Tarchevskaya, J. P. Klnet, and T. S. Jardetzky,

"Structure of the Fc fragment of human IgE bound to its high-affinity receptor FcεRIα," *Nature*, vol. 406, no. 6793, pp. 259–266, Jul. 2000.

[176] T. Kurosaki and S. Tsukada, "BLNK: Connecting Syk and Btk to calcium signals," *Immunity*. 2000.

[177] H. Park *et al.*, "Regulation of Btk function by a major autophosphorylation site within the SH3 domain," *Immunity*, 1996.

[178] D. J. Rawlings *et al.*, "Activation of BTK by a phosphorylation mechanism initiated by SRC family kinases," *Science (80-.).*, 1996.

[179] A. Cherukuri *et al.*, "The Tetraspanin CD81 Is Necessary for Partitioning of Coligated CD19/CD21-B Cell Antigen Receptor Complexes into Signaling-Active Lipid Rafts," *J. Immunol.*, 2004.

[180] M. Maďarová *et al.*, "Identification of new phosphorylation sites of CD23 in B-cells of patients with chronic lymphocytic leukemia," *Leuk. Res.*, 2018.

[181] F. Ramadani *et al.*, "Ontogeny of human IgE-expressing B cells and plasma cells," *Allergy Eur. J. Allergy Clin. Immunol.*, vol. 72, no. 1, pp. 66–76, 2017.

[182] A. Karnowski, G. Achatz-Straussberger, C. Klockenbusch, G. Achatz, and M. C. Lamers, "Inefficient processing of mRNA for the membrane form of IgE is a genetic mechanism to limit recruitment of IgE-secreting cells," *Eur. J. Immunol.*, 2006.

[183] Z. Yang, B. M. Sullivan, and C. D. C. Allen, "Fluorescent In Vivo Detection Reveals that IgE+ B Cells Are Restrained by an Intrinsic Cell Fate Predisposition," *Immunity*, 2012.

[184] A. Radbruch *et al.*, "Competence and competition: The challenge of becoming a long-lived plasma cell," *Nature Reviews Immunology*, vol. 6, no. 10. Nature Publishing Group, pp. 741–750, 15-Oct-2006.

[185] J. Stavnezer and C. E. Schrader, "Mismatch repair converts AID-instigated nicks to double-strand breaks for antibody class-switch recombination," *Trends Genet.*, 2006.

VII Appendix

VII.1 Abbreviations

A	Alanine or Adenine
ADAM10	Disintegrin and metalloproteinase 10
ADCC	Antibody-dependent cell-mediated cytoxicity
Ag	Antigen
AID	Activation-induced cytidine deaminase
AP	Affinity purification
APCs	Antige-presenting cells
BCR	B cell antigen receptor
BER	Base exicison repair
Btk	Bruton tyrosine kinase
C	Cysteine or Cytosine
CD	Cluster of differentiation
CD40L	CD40 ligand
CDRs	Complementary-determining regions
CLM	Cross-linking model
C-region	Constangt
CSR	Class-switch recombination
DAG	Diacylglycerol
ddH2O	Double distilled water
EB	EcoBlast (Ecotropic receptor and blasticidin resistance)
EMPD	Extracellular membrane-proximal domain
ER	Endoplasmic reticulum
ERK	Extracellular signal regulated kinase
$F(ab')_2$	Dimer of antigen binding fragment
FACS	Fluorescence activated cell sorting
FcεR	Fc epsilon receptor
FDCs	Follicular dendritic cells
Fig.	Figure
G	Glycine or Guanine

GC	Germinal center
GFP	Green fluorescent protein
GRP	Guanyl nucleotide-releasing protein
GST	Glutathione S-transferase
H	Histidine
HC	Heavy chain
HRP	Horse radish peroxidase
I	Isoleucine
IC	Immune complex
Ig(s)	Immunoglobulin(s)
IgH	Immunoglobulin heavy chain
IgL	Immunoglobulin light chain
Igα	Immunoglobulin alpha
Igβ	Immunoglobulin beta
IP3	Inositol-1,4,5,-triphosphate
IP3R	Inositol-1,4,5,-triphosphate receptor
IRES	Internal ribosome entry site
ITAM	Immunoreceptor tyrosine-based activation motif
K	Lysine
kDa	Kilo Dalton
KO	knockout
L	Leucine
LPS	Lipopolysaccharides
LTA	Lipoteichoic acids
MAPK	Mitogen activated protein kinase
MEK	Mitogen-activated protein kinase kinase
MER	Mismatch repair
mIg	Membrane immunoglobulin
NFAT	Nuclear factor or activated T cells
NF-κB	Nuclear factor kappa of activated B cells
NHEJ	Non-homologous end-joining
NK cells	Natural killer cells
NP-40	Nonidet P-40 or octylphenoxy-polyethoxyethanol
PAMPS	Pathogen-associated molecular pattern

PBS	Phosphate buffered saline
PGS	Peptidoglycan
phospho	Phosphorylation
PI3K	Phosphoinositide 3-kinase
PIP2	Phosphatidyl-inositol-4,5-bisphosphate
PKC	Protein kinase C
PLC-γ2	Phospholipase C-γ2
PRRs	Pattern recognition receptors
PTKs	Protein tyrosine kinase
pY	Phospho-tyrosine
R	Arginine
Rag	Recombination activating gene
RasGRP	Ras guanine nucleotide release protein
RFP	Red fluorescent protein
RT	Room temperature
S	Serine
SH2	Src homology 2 domain
SH3	Src homology 3 domain
SLP-65	Src homology 2 domain containing protein of 65 kDa
S-regions	Switch regions
ssDNA	Single strand DNA
STAT6	Signal transducer & activator of transcription 6
Syk	Spleen tyrosine kinase
Sε	IgE switch region
T	Threonine or Thymine
TM	transmembrane
U	Uracil
V-domain	Variable domain
V(D)J	Variable (V), Diversity (D), Joining (J) gene segments of the Ig heavy chain or Ig light chain
WT	Wild-type
Y	Tyrosine
YA	Tyrosine to Alanine mutation
α	Anti

λLC	Lambda light chain
εm	Membrane immunoglobulin E
εms / mIgE-S	Membrane immunoglobulin E short isoform
εml / mIgE-L	Membrane immunoglobulin E long isoform
μm	Membrane immunoglobulin M

VII.2 List of Figures

VII.3 List of Tables